QUANTIFYING WHISKING BEHAVIOUR AND ITS NEURAL ENCODING DURING ACTIVE SOMATOSENSATION

A thesis submitted to the University of Manchester
for the degree of Doctor of Philosophy
in the Faculty of Biology, Medicine and Health

2020

Andrea J. Colins Rodriguez
Division of Neuroscience & Experimental Psychology in the School of Biological Sciences

Contents

Word count 36120

List of Tables

List of Figures

The University of Manchester

Andrea J. Colins Rodriguez
Doctor of Philosophy
Quantifying whisking behaviour and its neural encoding during active somatosensation
June 19, 2020

A key problem in neuroscience is to understand what inputs enter a sensory system and how they are encoded. The somatosensory system is fundamentally an active system, however, due to experimental constraints to measure tactile organ behaviour, the literature has focused on the study of anaesthetised animals, suppressing the active components of somatosensation. Therefore, these questions remain largely unanswered for this system, hence, this study was conducted in the mouse whisker system. Specifically, this project aimed to accurately describe mouse whisking behaviour and characterise how mechanical inputs are represented in barrel cortex in awake, behaving mice.

To this end, Chapter 2 describes the development of a method to track whisker shape and kinematics in three dimensions from awake, behaving animals. Whiskers were simultaneously recorded with high-speed video cameras from two vantage points. The whisker tracker algorithm automatically reconstructed 3D whisker information directly from the 'stereo' video data, tracking multiple whiskers in parallel with a low error rate. The output of the tracker was used to produce a 3D description of each tracked whisker, including its 3D orientation and 3D shape, as well as bending-related mechanical forces.

Chapter 3 details the development of a computational model (GLM) to predict neural activity in the barrel cortex in awake, behaving mice from whisker contacts and mechanical sensory inputs as bending and twisting moment. To this end, extracellular recordings from layer 5 obtained during a tactile detection task were used to characterise the sensory inputs using the method developed in Chapter 2. Recorded units conformed a heterogenous population showing sensitivity to touch or one of the mechanical variables. The results suggested that changes in both bending and twisting moments are encoded in cortical neurons, providing a mechanosensory basis for somatosensation during active touch.

In Chapter 4, the features of sensory adaptation which can be observed during active sensation were investigated. For this, extracellular recordings from cortical neurons obtained during a detection task (Chapter 3) were analysed and the simultaneous whisking behaviour was described using the method developed in Chapter 2. Single and multi-unit activity was sensitive to whisker contacts, whose responses were modulated by both behaviour dynamics and neural adaptation. Stimulus-Specific Adaptation was observed for whisker identity, and more weakly for bending direction. These results suggest that encoding of behaviourally relevant stimuli are modulated by sensory adaptation and its effects can be studied and measured in awake, behaving animals.

In conclusion, these results show that a comprehensive analysis of sensorimotor behaviour is critical to understand neural activity and shed light on the dynamic computations performed in barrel cortex in awake, behaving animals.

Declaration

No portion of the work referred to in the thesis has been submitted in support of an application for another degree or qualification of this or any other university or other institute of learning.

Copyright Statement

Acknowledgements

First I would like to thank my mom and the dog for being my family.

I thank Felipe for being my roommate, travel companion and good moral support. And I thank to Roberto for being my best friend for what it seems has been forever.

I would like to express my gratitude to the members of the lab for their encouragement and support throughout this project: Anna Gray, Asia Ercan, Matt Burgess, Luka Gantar, Mat Evans, Dario Campagner and especially to Michaela Loft, not only for her good company but because her recordings made my project possible.

I am also very grateful for working with Rasmus Petersen, who has been a great supervisor. I have learnt a lot. My grateful thanks are also extended to Miguel Maravall and Mark Humphries for their insightful comments and discussions regarding my project.

Finally, I acknowledge funding from CONICYT Becas Chile under Contract No. 72170371.

Chapter 1

Introduction

1.1 General Overview

A key problem in sensory neuroscience is to understand what sensory variables are encoded in the brain and how they are encoded. The somatosensory system is particularly interesting in this regard since it is predominantly an active sense, in other words, the subject can move their sensory organs to gather information (Prescott & Dürr, 2016; C. C. Petersen, 2019). In the last few decades, the whisker system has become a canonical model for somatosensation (Diamond et al., 2008; C. C. Petersen, 2019). However, what sensory inputs are encoded in behaving animals remain unclear, among other reasons, due to the lack of available tools to measure sensory inputs and neural activity simultaneously and accurately. This thesis focused on developing tools to estimate sensory inputs entering the whisker system in awake, behaving animals and asked how these sensory inputs are encoded in the mouse somatosensory cortex.

A fundamental step for understanding sensory coding is to measure accurately and describe sensory stimuli entering the system. In primarily passive sensory systems, such as the auditory and visual systems, the stimuli can be defined as a change in the environment, therefore can be described independently of the subject behaviour.

In contrast, in a predominantly active sense as the somatosensory system, the subject can control their sensory receptors to extract information from the environment, making the sensory inputs depend on, changes in the environment and the subject's behaviour. This brings two main challenges for the study of the somatosensory system. First, measuring sensory inputs involves the measurements of animal behaviour,

in particular, of tactile sensors (e.g whiskers) behaviour. Second, since sensory inputs depend on behaviour, each presentation of the same stimulus (e.g same surface contacting the whiskers) induces an unique sensory experience. Each experience produces different sensory inputs, triggering different responses to the same stimulus (surface), which in turn hinder the understanding of sensory encoding.

The whisker system is a highly powerful system for the study of somatosensation due to several experimental advantages, such as, in the primary somatosensory cortex (S1), whisker sensory inputs are processed in modules that map to individual whiskers on the whisker pad. These modules are known as *barrels*, giving the barrel cortex its name (Woolsey & Van der Loos, 1970). Additionally, as whiskers are external tactile sensors, then instantaneous sensory inputs can be quantified by imaging the whiskers and describing their physical properties (Knutsen et al., 2008; Birdwell et al., 2007). Since it is an interesting model, sensory pathways and circuits within the whisker system are well characterised and genetic tools are available to record and tease the role of these circuits apart (Diamond et al., 2008; Auffret et al., 2018; Campagner et al., 2018).

Although the barrel cortex has been studied for decades, the bulk of the literature has been developed in anaesthetised animals, suppressing the active components of whisking behaviour. This allows the application of highly controlled stimuli and facilitates the recording of neural responses. Only in the last decade have studies started incorporating animal behaviour thanks to the technological advances in imaging and whisker tracking tools (O'Connor, Peron, et al., 2010; Hires et al., 2015; Campagner et al., 2016; Bush et al., 2016; Severson et al., 2017). However, these techniques have been restricted to the analysis of whisker kinematics and mechanics in the horizontal plane, limiting what sensory inputs can be measured, the accuracy of these measurements, what behaviours can be described and what cognitive tasks can be investigated. So far, only pioneer studies have described kinematic and mechanical inputs to the whisker system in 3D in awake, behaving animals (Knutsen et al., 2008; Huet et al., 2015; Huet & Hartmann, 2016). However, there are no automatic methods available to quantify these inputs from behaving animals, therefore, how mechanical and kinematic variables behave during active somatosensation remain partially understood. As a result, if and how these variables are encoded in the somatosensory cortex is still

largely unanswered.

This thesis investigated how to quantify sensory inputs of the whisker system in awake behaving animals and its respective encoding in barrel cortex. First a method was developed to measure whisker shape and kinematic in 3D (Chapter 2), then it was used to identify what sensory inputs are encoded in the barrel cortex (Chapter 3), describing how the encoding of sensory input is modulated by sensory adaptation in awake behaving, animals (Chapter 4).

This chapter provides an overview of whisking behaviour and how to measure it, reviewing the mechanical and kinematical properties of the whisker and how we can derive the sensory inputs entering the whisker system. Then, the general characteristics of the whisker system and the neural coding properties of the barrel cortex are discussed. Finally, how sensory adaptation can impact somatosensory coding in the whisker system and how it has been studied so far are reviewed.

1.2 Whisking behaviour

Mice and rats are tunnel-dwelling animals. Due to their poor vision, they rely on their whiskers to collect tactile information about their nearby environment (Vincent, 1912; Diamond et al., 2008). Especially, rats and mice depend on their whiskers for a variety of behavioural tasks, from simple perceptual tasks like object detection and texture discrimination to complex social behaviours as courting or fighting (O'Connor, Peron, et al., 2010; G. Carvell & Simons, 1990; Wolfe et al., 2011). Here I will focus on how tasks in the first category have aided to understand somatosensation in the whisker system.

Whiskers in the mouse whisker pad are stereotypically arranged in a grid five rows (named A-E along the dorsoventral axis) and between 4 to 7 columns (numbered along the rostrocaudal axis), conforming a group of about 33 whiskers per side (Van Der Loos et al., 1984). Mice actively move their whiskers back and forth in a behaviour termed "whisking" (W. Welker, 1964). Whisking periods are typically bouts of rhythmic whisker movements lasting a few seconds with frequencies ranging between 5 and 25 Hz (Prescott et al., 2016).

The whisking cycle requires the coordinated action of multiple muscles in the

whisker pad (Dörfl, 1982) (Figure 1.1.A). Two main groups of muscles produce whisker movements: extrinsic and intrinsic muscles. Four extrinsic muscles attach the whisker base to the skull, while intrinsic muscles form "slings" around the whisker base and join whiskers in the same row (Dörfl, 1982; F. G. Barth et al., 2013). The coordinated action of these muscles allows rats and mice to translate and rotate their whiskers. Whisker rotations can be decomposed into rotations around the dorsoventral axis (azimuth angle, Figure 1.1.B), rotations around the rostrocaudal axis (elevation angle, Figure 1.1.C) and rotations around the whisker's own axis (roll angle, Figure 1.1.D) (Towal et al., 2011; Knutsen et al., 2008). The latter is also known as twisting. Both rats and mice can twist their whiskers, and in both species, this movement is mediated by oblique intrinsic muscles (Haidarliu et al., 2017). For convention, the cycle starts with the whisker in a retracted position. The mystacial pad is pulled forward by the extrinsic *m. nasalis* muscle to protract the whisker. Then the whisker is rotated further forward by the contraction of the sling muscles associated with each follicle. Finally, the whisker returns to its retracted position due to the relaxation of the protractor muscles and the activation of *m. nasolabialis* and *m. maxillolabialis* (Berg, 2002; Hill et al., 2008). During whisking, mice and rats not only move their whiskers but coordinately move their head, nose and mouth to explore their surroundings (Towal & Hartmann, 2006; Mitchinson et al., 2007).

Beyond the intuition that whiskers act as tactile sensors, the ethological functions of vibrissa have not been completely described. In other words, the complete range of behaviours that whiskers contribute to and how animals use their whiskers in each context is not completely understood. In the case of rats and mice, both species can actively control whisker movement, that is, they both whisk and solve tactile behavioural tasks using active whisking (Kleinfeld et al., 2006; Prescott et al., 2016; Diamond & Arabzadeh, 2013). Studies involving lesions or removal of the whiskers or critical structures in the whisker sensory pathway have found considerable deficits in the performance of natural rat behaviours, such as locomotion, maintaining equilibrium, predation, maze learning, swimming and fighting. During these behaviours, animals use their whiskers in multiple ways that may or may not involve whisker touch (Gustafson & Felbain-Keramidas, 1977; Ahl, 1986; Prescott et al., 2016). During whisking, whiskers can aid to detect both the direction and the

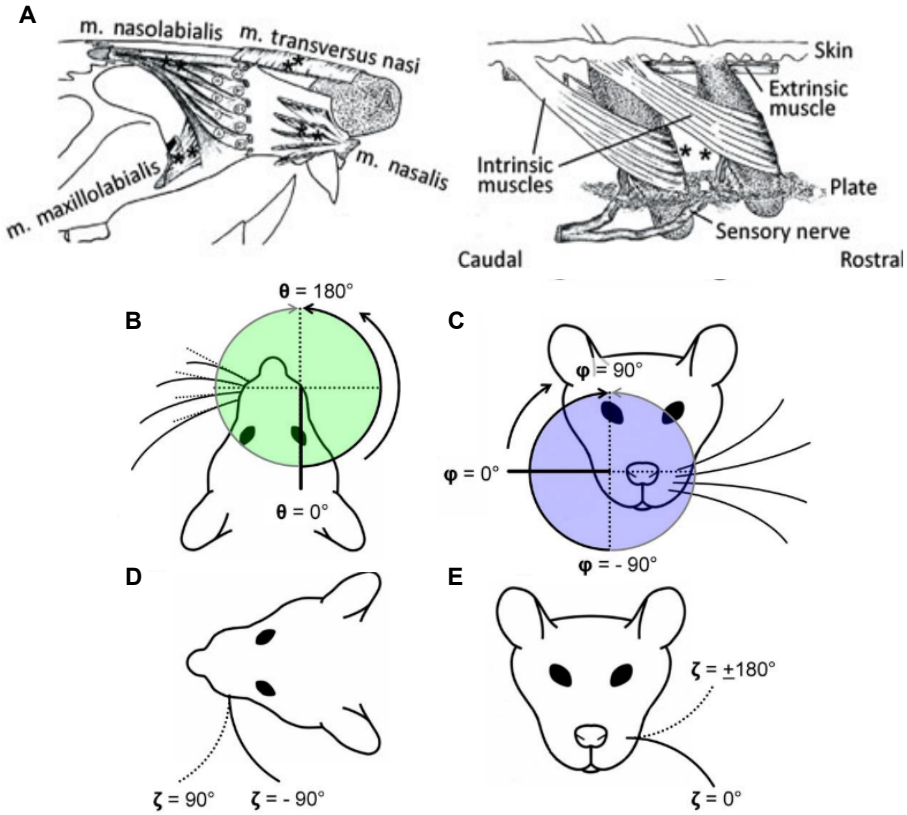

Figure 1.1: Whisker musculature and movement. A) Schematic of extrinsic muscles (left) and intrinsic muscles (right) around the whisker follicle. Adapted from (F. G. Barth et al., 2013), which in turn was adapted from (Dörfl, 1982). B,C,D) Definition of whisker rotations. B) Azimuth or horizontal angle. C) Elevation or vertical angle. D) Roll or twist angle. Adapted from (Towal et al., 2011)

speed of wind (Y. S. W. Yu et al., 2016; Y. S. Yu et al., 2019). However, the most relevant cues for the animal about its surroundings appear when the whiskers encounter objects (M. J. Z. Hartmann, 2011; Grant et al., 2009). Whisker contacts cause whisker deflections that signal the animal firstly that an object or surface is within whiskers' reach (object detection), and characteristics of the location and identity of the object, such as texture and shape. Therefore, loss of whisker tactile sensitivity presumably explains the disruption in some of the behaviours mentioned above (predating, maze learning, etc.). For these reasons, the bulk of the study of somatosensation in behaving animals has focused on analysing exactly these kinds of elemental touch behaviours, dividing them into three types of tasks: Object detection, object localization and texture discrimination.

Object detection is the simplest behavioural task, it can be solved with a single whisker and has been widely applied to study neural phenomena in the somatosensory

system (Hires et al., 2015; Campagner et al., 2016; H. Yang et al., 2015; Kwon et al., 2016).

Object localization tasks have shown that mice are capable of discriminating object location to at least 6° of resolution using multiple whiskers and 15 ° of resolution with a single whisker (Mehta et al., 2007; O'Connor, Clack, et al., 2010; Cheung et al., 2019). Although the sensorimotor bases of object localization remain unclear, this task has given insights about how mice can form strategies to solve behavioural tasks (O'Connor, Clack, et al., 2010; Campagner et al., 2019). Interestingly, it has been shown that mice can develop a behavioural strategy to simplify the task and solve it as a detection task. O'Connor et al. (2010a) showed that in a two-position localization task, where the mouse was rewarded when it reported the presence of a pole in an anterior position, the mouse tended to whisk around the rewarded position and avoid the unrewarded position. In this way, the mouse only needed to detect the pole touching the whiskers instead of scanning a large area with its whiskers and comparing the position of the objects.

Texture discrimination tasks are more complex than object detection and localization. There are three hypotheses regarding the sensory inputs that aid rodents to discriminate between textures: First, the mean speed hypothesis proposes the temporal profile of whisker velocity could produce kinematic signatures for each texture. This way, rough surfaces would trigger greater overall whisker speeds than smooth textures, helping the animal to differentiate between them (Arabzadeh et al., 2005).

The differential resonance theory is based on the hypothesis that is the amplitude of the whisker vibrations produced by different textures which are encoded by the system and help texture discrimination (Neimark et al., 2003). The most supported hypothesis is the so-called "slip-stick" hypothesis. Slip-sticks are brief, high-velocity, high-acceleration whisker movements triggered by the contact between the whisker and a surface. It has been reported that these events drive spikes in the somatosensory cortex (Wolfe et al., 2008; Jadhav et al., 2009; Isett et al., 2018). To solve this controversy, it is a fundamental requirement to develop tools that describe whisker movement in detail (in all directions) and to count with a biomechanical model that describes the mechanical inputs at the base of the whiskers during slip-stick events. Biomechanical models developed for the whisker system so far are detailed in the next

section.

It has been shown that mice can differentiate between coarsely different textures with a single whisker. However, their performance and acuity improve when they use more whiskers (Krupa et al., 2001; G. E. Carvell & Simons, 1995; Morita et al., 2011).

1.2.1 Measuring whisking behaviour

Although mice do whisk while immobile, whisking properties such as frequency, amplitude, the average position of the whiskers are coupled with locomotion features. This, in turn, depend on the exploratory behaviour of the animal at that moment (Sofroniew et al., 2014). Therefore, to completely understand how whisking is represented in the brain, it is necessary not only to consider whisking movements as an isolated phenomenon, but to integrally capture the behaviour of the animal and comprehend what the aim of the behaviour is (Tinbergen, 1951).

Thanks to technological developments in the last fifty years, videography has become a powerful tool for the study of animal behaviour, including whisking behaviour (W. Welker, 1964; O'Connor, Peron, et al., 2010; Hires et al., 2015; Campagner et al., 2018). Recording whisking behaviour presents particular challenges: First, whiskers are small, thin objects. Mice whiskers length varies between 7 and 30 mm. Their base is 70-90 μm diameter and their tips can be 2-5 μm diameter (Ibrahim & Wright, 1975). Hence, whisker imaging requires high spatial resolution. Second, whiskers can reach speeds of 55,000°/s (Bale et al., 2015), requiring also high temporal resolutions. Third, during natural exploratory behaviour, mice can run easily at speeds of 30 cm/s (Sofroniew et al., 2014), adding to the complex movements produced by the whiskers. Fourth, mice present about 30 whiskers on each side of their faces, making extraordinarily difficult to identify individual whiskers properties. And fifth, whiskers are three-dimensional objects that move and deform in 3D (Knutsen et al., 2008; Huet et al., 2015). These challenges have been overcome by imaging the whiskers using high-speed videography of the whiskers, simplifying experimental conditions and limiting the behaviours that can be examined.

A step further into the study of whisking behaviour is its quantification, known as whisker tracking. In the last two decades, many whisker tracking software programs

have been developed. Whisker tracking of freely moving animals provides measurements of sensory stimuli and motor actions, involving measurements of whisker movements, the head/body position and gait (Knutsen et al., 2005; Voigts et al., 2008; Perkon et al., 2011; Gillespie et al., 2019). Although studies of whisker behaviour performed in freely moving animals with intact whisker pad have shed light on areas of animal behaviour and motor control (Mitchinson et al., 2007; Grant et al., 2009; Mitchinson & Prescott, 2013), their coarse measurements are unfitted for the analysis of the input signals that drive the whisker system.

Commonly, a simpler approach has been adopted to study the sensory inputs of the whisker system and how they are processed. This approach consists of a head-fixed animal trained to solve a behavioural task which can be solved with a single whisker (O'Connor, Peron, et al., 2010; Hires et al., 2015; Campagner et al., 2016; Severson et al., 2017; Campagner et al., 2019). Importantly, the task only requires the animal to collect information in the horizontal plane, then the recording of whisking behaviour can be performed with one camera from above (or below) the animal. Whisker tracker packages have been developed specifically for these experimental conditions, seeking to describe both whisker movement and shape of individual whiskers (Clack et al., 2012; Bale et al., 2015).

It is important to note that although rats and mice are widely used as models for somatosensation, and they share many characteristics, there are a few differences between these two species. Concerning quantifying their whisker behaviour, a key difference between these species is their size and, consequently, the size of their whiskers. Whiskers in rats are on average twice as long and thick as mouse whiskers (Ibrahim & Wright, 1975). In other words, to track mouse whiskers requires higher-resolution and more precision than tracking rat whiskers. This difference in length/thickness also impacts the mechanical properties of rat and mouse whiskers, which are discussed in the following section.

1.3 Whisker biomechanics

In order to identify the sensory inputs to the whisker system, it is elemental to describe the physical properties of the whisker and the mechanics and kinematic signals

transmitted to its follicle. Since it is not feasible to measure the mechanical inputs within the follicle in-vivo, biomechanical modelling of the whiskers has become a fundamental tool for their estimation. Due to the complexity and diversity of whisking behaviours, several mathematical models have been developed to characterise whisker mechanics in different contexts. Here I will describe the main physical properties of rodent whiskers and the biomechanical models that have contributed to understanding which sensory inputs are encoded by the whisker system.

Physical properties of the whiskers. Whiskers are thin, long objects, which base are anchored to the whisker follicle. Although whiskers can be considered a type of hair, whiskers are specialised somatosensory organs. They are easily distinguishable from hair since whiskers are longer, thicker and their follicle is heavily innervated (Melaragno & Montagna, 1953; Voges et al., 2012; Ebara et al., 2002). Rodents whisker shaft consists of a tapered (almost conical) structure with a hollow medulla near its base (Voges et al., 2012). Since whiskers do not possess mechanoreceptors along their shaft, all sensory information has to be transmitted to the whisker base in order to reach the mechanoreceptors within the follicle. The whisker follicle contains a blood sinus which is densely innervated with several kinds of mechanoreceptors and nerve endings (Ebara et al., 2002).

Due to its composition and diameter, both rat and mouse whiskers bend and twist when contacting an object as a result of the forces and moment exerted on the whisker (Pammer et al., 2013; Huet et al., 2015; Campagner et al., 2018). On the other hand, during noncontact periods (e.g during whisking), the proximal segment of rat whiskers have been observed to be well approximated by a rigid quadratic curve (Knutsen et al., 2008; Quist et al., 2014). In mice, the validity of this approximation has not been tested. In both scenarios, to quantify the sensory inputs entering the follicle it is critical to determine mechanical and kinematical properties of the whisker and how they are transmitted to the follicle.

Neurons in the periphery of the whisker systems tend to be silent when the whiskers are immobile. Their firing activity increase when the mouse whisks and increase, even more, when the whiskers contact an object (Leiser & Moxon, 2007). Whisking and whisker contacts are different mechanical scenarios, in other words, the forces and

moments reaching the follicle are different (Quist et al., 2014). So far, the modelling of both scenarios and their respective neural encoding has been approached almost independently.

1.3.1 Whisking

Whisking and the whisking cycle has been widely characterised by whisker kinematics, in other words, by properties of whisker motion (Knutsen et al., 2008; Zuo et al., 2011; Lottem et al., 2015; A. E. Yang & Hartmann, 2016). Given the tools for recording and tracking the whiskers, whisking kinematic has been mainly reduced to the movements in the horizontal plane. Especially, most analyses have measured the azimuth (or horizontal) angle, defined between by the whisker and the rostrocaudal axis, and its temporal derivatives (Wolfe et al., 2008; Zuo et al., 2011; Lottem et al., 2015).

Rodents can actively control kinematic parameters of whisking, such as the middle position of whisking (setpoint) and the amplitude of whisking (Towal & Hartmann, 2006; Grant et al., 2009; O'Connor, Clack, et al., 2010; Sofroniew et al., 2014). Additionally, they can produce asymmetric whisking, choosing different setpoints or amplitudes for each side of their faces (Towal & Hartmann, 2006; Sofroniew et al., 2014).

There is a series of candidates forces for driving mechanotransduction during whisking. First, the muscles exerting forces on the follicle and the whisker pad during the whisking cycle could be driving mechanotransduction (Hill et al., 2008). Second, engorgement of blood sinus within the follicle likely varies within the whisking cycle, modulating follicle stiffness (Blythe Towal et al., 2012). Third, whisker's mass could produce inertial effects, resisting to being translated (inertial force) or rotated (inertial moment) during the whisking cycle (Quist et al., 2014). Fourth, tissue within the follicle is viscoelastic. It resists both displacement and velocity potentially exerting spring and damper forces respetively (Severson et al., 2017).

During whisking, using a few simplifications, it is possible to estimate the mechanical variables at the whisker base based on kinematic parameters. If a rigid bar rotates around an axis, the moment (M) applied to rotate the whisker is equal to the product between the angular acceleration (α) and the moment of inertia of the bar

(I) (M. Hartmann, 2016). Because rat whiskers show little deformation during whisking (Knutsen et al., 2008; Quist et al., 2014), the moment at the whisker base can be approximated by a kinematic parameter as angular acceleration during whisking. Although it has not been shown that mouse whiskers are rigid during whisking, some studies have used this approximation in whisking mice. More specifically, it has been shown that neural activity of some neurons in the mouse whisker system can be accurately predicted by acceleration and its temporal derivative, suggesting that M and its rate of change ($\dot{M}$) are sensory inputs encoded in the whisker system (Campagner et al., 2016; Severson et al., 2017).

Other recordings of neural activity in the rat and mouse whisker system have reported that kinematic properties of whisking, such as whisking amplitude, velocity, movement direction or phase are encoded in the whisker system (Leiser & Moxon, 2007; Khatri, Bermejo, et al., 2009; Wallach et al., 2016; Severson et al., 2017). However, it is unclear exactly how these variables are related to mechanical inputs drive mechanoreception within the follicle. Therefore a combination of accurate measurements of the mechanical signals at the whisker base and their respective neural responses are needed.

1.3.2 Whisker contacts

One of the advantages of using the whisker system as a model for somatosensation is that the signals received by the nervous system can be described by characterising the whisker instantaneous shape and movement. In particular, all mechanical signals received by the follicle can be characterised by three forces and three moments at the whisker base, one for each dimension (Huet et al., 2015; M. Hartmann, 2016).

Thanks to biomechanical modelling we know that the mechanical forces transmitted to the follicle during contacts can be derived from whisker geometry (Birdwell et al., 2007; Pammer et al., 2013; Huet et al., 2015). As a consequence, the mechanical forces can be estimated non-invasively from awake, behaving animals using whisker tracking tools. Here I will detail how to measure the mechanical variables at the whisker base from whisker videography, as well as the assumptions and limitations of the biomechanical model.

Although whiskers are 3D objects and they can move and bend in a 3D space (Bermejo

et al., 2002; Knutsen et al., 2008), the bulk of the biomechanical modelling of whisker contacts has been developed in 2D (Birdwell et al., 2007; Quist & Hartmann, 2012; Pammer et al., 2013). This is mainly due to the challenges that represent to record and measure mechanical variables affecting the follicle in 3D. Only in recent years, a few works have attempted to quantify kinematic and mechanical variables considering 3D modelling of the whiskers (Huet et al., 2015; A. E. Yang & Hartmann, 2016; Huet et al., 2017). For this reason, the rest of this section will describe first whisker mechanics and kinematics in 3D, and posteriorly, their approximation from a 2D whisker representation.

3D description When the whisker is imaged overhead, whisker kinematics have been typically characterized by the azimuth angle, which describes the rotation about the vertical (dorsoventral) axis, and its temporal derivatives. A complete characterization of whisker kinematics, however, requires three angles to describe the 3D position of the whiskers and its changes over time (Knutsen et al., 2008): Azimuth angle, elevation angle and roll angle. The elevation describes the whisker rotation about the horizontal (anterior-posterior) axis. The roll, or whisker orientation, represents the angle of rotation of the whisker around its own axis.

All mechanical signals at the whisker base can be written in terms of three forces and three moments in a whisker-centred coordinate system (Huet et al., 2015). The coordinate system in Figure 1.2.A originates at the base of the whisker, and therefore, it moves with the whisker. The x axis is defined as the tangent (its first derivative) at the whisker base, y points to the increasing curvature (or second derivative) of the whisker, and z is the cross product between the x and y axis.

Figure 1.2.B shows a schematic of the forces and moments generated at the base of the whisker during whisker deflection in 3D. Any force exerted on the whisker has three components, one for each axis (F_x, F_y and F_z). Two moments (M_z and M_y) describe how the whisker bends while a rotational force is applied. They constitute the bending moment magnitude as:

$$M_b = \sqrt{M_z^2 + M_y^2} \tag{1.1}$$

and the bending moment direction as:

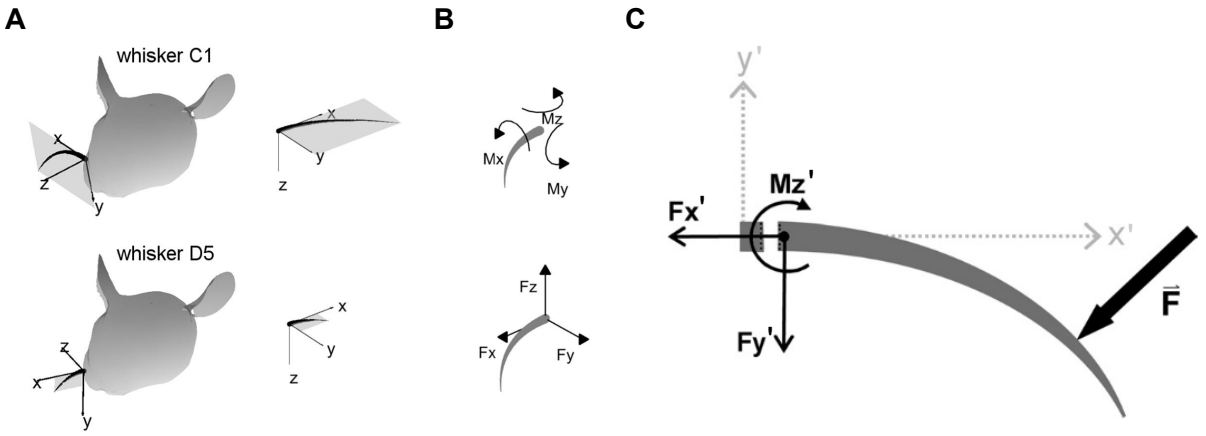

Figure 1.2: Whisker mechanics description in 3D and 2D. A) Whisker-centred coordinate system for 3D whisker mechanics description. Each whisker has its coordinate system which originates at the whisker base. x axis is defined as the tangent at the whisker base, y points to the increasing curvature, and z is the cross product between the x and y axes. B) Mechanical signals at the whisker base: In the general case, three moments (top) and three forces (bottom) can affect the whisker base. Adapted from (A. E. Yang & Hartmann, 2016). C) 2-dimensional description of whisker mechanics. This description assumes that the intrinsic curvature of the whisker lies on the $x' - y'$ plane and that the whisker rotates only on the $x' - y'$ plane. The force exerted normal to the whisker (F) produces two reaction forces and one reaction moment: F'_x or axial force, F'_y or lateral force and M'_z or the bending moment. Adapted from (Quist & Hartmann, 2012).

$$M_d = atan\left(\frac{M_z}{M_y}\right) \tag{1.2}$$

A third moment, known as torsional (or twisting) moment (M_x) can be quantified, which twists the whisker around its own axis (x).

In this scenario, the whisker has been modelled as a cantilevered beam (Birdwell et al., 2007). This model, derived from Euler elasticity theory, assumes that at every moment in time the forces exerted on the whisker are at equilibrium. If a force is exerted at a single point along the whisker and normal to the whisker (F), the model establishes a linear relationship between the change in curvature ($\Delta\kappa_{3D}$) of the beam and the moment (M_b) produced by the load to the whisker at the point s along the whisker:

$$\Delta\kappa_{3D}(s) = \frac{M_b(s)}{EI(s)} \tag{1.3}$$

where $\Delta\kappa_{3D}$ is the change in intrinsic curvature of the whisker at the point s, E represents Young's modulus and I is the area moment of inertia of the whisker (Etnier, 2003; Huet et al., 2015). If the whisker is modelled as a cone, then the moment of inertia is defined as:

$$I(s) = \frac{\pi r(s)^4}{4} \tag{1.4}$$

where $r(s)$ indicates the radius of the whisker at point s.

For torsional changes,

$$\Delta\phi(s) = \frac{\tau(s)ds}{GJ(s)} \tag{1.5}$$

where $\Delta\phi(s)$ represents the change in the angle of the point s around its own shaft, τ is the applied torsion, G is the shear modulus and J is the polar moment of inertia (Etnier, 2003; Huet et al., 2015). If the whisker is modelled as a cone, then the polar area of inertia is:

$$J(s) = \frac{\pi r(s)^4}{2} \tag{1.6}$$

2D description A two-dimensional description of the whisker considers two simplifications from the 3D scenario regarding whisker movement and whisker orientation. First, the whisker movement is limited to one plane, for instance, the horizontal plane. Second, the whisker is oriented so that its intrinsic curvature is completely contained in the same plane of movement. Figure 1.2.C depicts an apparatus that complies with these constraints. Here the whisker is mounted in the apparatus, in which the whisker base is rigidly attached to a post.

In this scenario, a force is exerted at a single point along the whisker and normal to the whisker tangent (F). This way, when the load is applied to the whisker, all changes in the whisker's shape will be captured in the $x'-y'$ plane and the whisker can only rotate in this same plane. In a general 3D scenario, the whisker base is subject to three reaction forces and three moments during a contact, however, in this simplified setup, this set of variables is reduced to two forces and one moment: an axial force (F'_x) along the whisker axis. A force with a positive sign would pull the whisker out of the follicle, while a force with a negative sign would push the whisker into the follicle. A lateral force (F'_y) with a positive sign if it points in the y' direction and a negative sign if it points in the opposite direction. And a bending moment (M'_z) that resists the rotation of the whisker around the z' axis due to the applied force F (Quist & Hartmann, 2012).

This description of the whisker can be defined in the 3D scenario as follows: if an object exerts a force in the $x-y$ plane, normal to the whisker, then the bending moment is equivalent to M_z given that the M_y component is zero. The lateral force corresponds to F_y and the axial force to F_x.

If we apply the quasi-static model for a cantilevered beam to this scenario, for any perpendicular force applied to the whisker, the bending moment M_b is defined as:

$$\Delta\kappa_h(s) = \frac{M_b(s)}{EI(s)} \tag{1.7}$$

Here E represents Young's modulus, I area moment of inertia at the point s and $\Delta\kappa_h(s)$ represent the difference between the apparent horizontal curvature of the whisker during and before contact.

Intuitively, the curvature at any point s can be understood as the inverse of the radius of the circle (r_c) best fitted the segments around the point s. The curvature at any point (s) of a 2D curve can be computed as:

$$\kappa_h(s) = \frac{1}{r_c(s)} = \frac{|x'(s)y''(s) - y'(s)x''(s)|}{\left(x'^2 + y'^2\right)^{3/2}} \tag{1.8}$$

where a' represents the derivative of a respect to s and $|a|$ indicates the absolute value.

The linear relationship between curvature and the bending moment establishes a direct way of estimating the moment at the base of the whisker by defining the geometry of the whisker, which in turn can be extracted from video recordings of the whiskers using the right experimental conditions. To do this, several works have implemented experimental setups where a head-fixed animal performs a task so that whisker movements are contained in the horizontal plane (O'Connor, Clack, et al., 2010; Sofroniew et al., 2014; Campagner et al., 2016; Bush et al., 2016; Severson et al., 2017; Haidarliu et al., 2017; Campagner et al., 2019). In this way, the $x'-y'$ plane defined above closely matches the horizontal plane and the movement and shape of the whiskers can be recorded with a single camera from the top (or below) the animal's head.

Due to its simplicity, this framework has been broadly adopted to outline whisker mechanics underlying active touch and how neural responses to touch can be understood in terms of whisker mechanics. From these studies it has been shown that κ_h

magnitude increase considerably during touch, suggesting that is a relevant mechanical input to the whisker follicle. Even more, these studies propose that M_b and its rate of change $\dot{M}_b$ at the base of the whisker are good predictors of the neural responses in the whisker system (Campagner et al., 2016; Bush et al., 2016; Severson et al., 2017).

Although the cantilevered beam model is a powerful tool to describe whisker mechanics during touch, this model makes two assumptions that need to be considered: First, it is a quasi-static model, which means that assumes that at each moment in time the forces are balanced in a steady state. Second, it assumes that the whisker and the object form a rigid connection at the point of contact at all times, in other words, the whisker does not slide, and thus, friction is ignored. These assumptions limit the capacity of the model, in particular, it cannot account for dynamic properties observed during active contacts, for example, transient events, resonance and slip-sticks events (Huet & Hartmann, 2016).

During the whisking cycle, whiskers roll around their own axis. When whiskers are imaged in the horizontal plane, this can be observed as a change in the apparent horizontal curvature. However, in rats, there are no significant changes in the intrinsic curvature of the whisker during whisking (Knutsen et al., 2008; Haidarliu et al., 2017). This example shows that using a 2D description of the whisker can be misleading since the estimates of kinematic and mechanical variables are coupled. Similarly, during touches whiskers can bend and twist. If touches are imaged only from the horizontal view, both twisting and bending moments are merged into the estimation of changes in κ_h (Huet et al., 2015; Lucianna et al., 2016). To disentangle these two moments it is fundamental to recover whisker shape and position in 3D.

Very few studies have described whisker kinematics or/and mechanics in 3D during active somatosensation (Knutsen et al., 2008; Huet et al., 2015; Huet & Hartmann, 2016). Huet et al. (2015) showed that, during touch, a 2D whisker description can offer a good proxy of bending moment, axial and lateral force in some cases. Although traces for these variables present similar forms over time, they also show that the 2D approximation can overstate the magnitude of these mechanical variables. This is due to changes in whisker orientation during touch can inflate the apparent changes in whisker shape. Even in the cases where the 2D description was a good approximation of the 3D case, the 2D description completely omits the force corresponding to

the vertical axis (F_z), bending in the vertical plane (M_y) and the twisting moment (M_x), which can reach the same order of magnitude that the total bending moment (M_b). However, no systematic analysis has characterised how often and in what conditions the 2D description is a good approximation of the 3D scenario during active somatosensation. The relationship between mechanical variables, such as bending and twisting moments, and the relationship between mechanical and kinematic variables such as whisker orientation and the bending moments, during active touch remain unclear.

In Chapter 2, I develop a method to automatically track multiple whiskers in 3D from high-speed videography recordings, offering a complete kinematic description. In Chapter 3, I took advantage of this method to estimate the twisting and bending moment during whisking behaviour and show how they drive the activity of barrel cortex in awake, behaving animals.

1.4 The whisker system

Over the last 50 years, the whisker system has become one of the most powerful models to study sensory processing and the somatosensory system. One of the main reasons for this is the presence of the barrel cortex, which is a somatotopic representation of the vibrissae on the mystacial pad (Woolsey & Van der Loos, 1970). The barrel cortex consists of an array of histologically and electrophysiologically distinct regions in layer 4 (L4) of the primary somatosensory cortex (S1), known as barrels (Woolsey & Van der Loos, 1970). Each barrel corresponds and mirrors the position of a whisker on the mystacial pad (the principal whisker) (Woolsey & Van der Loos, 1970; C. Welker & Woolsey, 1974). The extensions of the barrels to the rest of the layers in S1 are known as a functional organization called barrel columns (Simons, 1978).

The tactile information processed in barrel cortex is obtained in the whisker follicles and transmitted through the somatosensory pathway (Diamond et al., 2008). The most direct pathway can be divided, in ascending order, into five stages: follicle, trigeminal ganglion, brainstem, thalamus and cortex. Similarly to barrel cortex, the brainstem and the thalamus present topographic maps mirroring the whisker pad, which are known as “barrelettes” and “barreloids” respectively (Van Der Loos, 1976; Ma, 1991).

The modular structure of the whisker system throughout its pathway has made it the most powerful model for experimental and theoretical studies of somatosensation. Jointly, as discussed in the previous section, the fact that instantaneous sensory inputs can be quantified by imaging the whiskers and describing their geometrical properties, facilitate the understanding of the sensory inputs of the system (Knutsen et al., 2008; Birdwell et al., 2007).

To understand neural processing in the barrel cortex, it is vital first to understand the inputs to the whisker system and its processing before arriving at the cortex. Although some information from the physical input is preserved through the pathway, each stage represents or process this information in different ways (Bale & Maravall, 2018). Because the mechanical inputs at the whisker base are challenging to measure directly, many studies have analysed the neural activity of the whisker system in terms of kinematic, controllable parameters. Only in the last decade, the mechanical framework for whisker contacts has been introduced to understand whisker based sensation (see section 1.3). Therefore, here I will describe the most relevant physiological features of each stage, the kind of stimuli that have been studied and their respective representation in each stage of the pathway.

Whisker follicle. As mentioned in above, whiskers are made of keratin and are, therefore, inert. Thus, tactile sensitivity depends on the whisker follicle innervation. Each whisker is innervated by two types of nerves, which are classified according to the portion of the follicle that they innervate: deep and superficial nerves (Figure 1.3). While deep nerves mostly contain large diameter myelinated fibres, superficial nerves contain small diameter unmyelinated fibres. There are several types of mechanoreceptors and nerve endings that can be found within the whisker follicle (Ebara et al., 2002). Although the localization of each type of mechanoreceptor has been studied in recent years (Ebara et al., 2002; Tonomura et al., 2015; Severson et al., 2017; Furuta et al., 2020), the understanding of the cellular basis of mechanotransduction is limited. One of the crucial challenges when relating mechanoreceptor responses to mechanical whisker inputs is to measure the whisker inputs accurately. All studies regarding the mechanosensory basis of mechanoreceptor responses (or their identified primary afferents) have simplified this problem to the study of 2D stimulation. The

main mechanoreceptors within the follicle and their response properties identified so far are outlined below (Figure 1.3):

- Merkel cells: To date, Merkel cells are the best-described mechanoreceptors in the context of somatosensation by whiskers. The majority of this type of cells are located at the level of the ring sinus. Additionally, a small portion of these cells is located in the caudal part of the rete ridge collar. Severson et al. showed that in mice, this type of mechanoreceptors encode both, active touch and self-motion, due to their sensitivity to the increment of the bending moment (M_z) and its rate of change (Severson et al., 2017). However, as they imaged whiskers exclusively in the horizontal plane, their estimation of M_z corresponds to a combination of M_z and the twisting moment (M_x). In anaesthetised rats, Merkel cells respond preferentially to the angle of deflection of the whisker (Furuta et al., 2020).

- Lanceolate and reticular endings: Two types of Lanceolate endings can be found within the whisker follicle, which are classified according to their orientation respect to the whisker shaft: circular and longitudinal endings (Ebara et al., 2002). Similarly to Merkel cells, Lanceolate endings respond preferentially to the angle of deflection of the whisker (Furuta et al., 2020). More importantly, Furuta et al. showed that the responses primary afferent corresponding to Lanceolate endings could be moderately well predicted by a combination of the rate of change of axial force ($\dot{F}_x$) and the rate of change of the bending moment ($\dot{M}_b$). However, their experimental approach had the caveat of trimming the whisker so short that it was almost straight. Therefore, the twisting moment could not possibly contribute to the neural responses.

- Club-like endings: This type of endings are only found within the ringwulst. Therefore, it has been suggested that they sense mechanical aspects related to the movement of the ringwulst within the follicle (Tonomura et al., 2015). As lanceolate endings, club-like endings respond preferentially to the angle of deflection of the whisker and their afferents' response can be relatively well predicted by $\dot{M}_b$ and $\dot{F}_x$ (Furuta et al., 2020).

- Ruffini-like endings: They are widely distributed in the uppermost portion of the follicle (Ebara et al., 2002). However, no direct association has been established

between their responses and the whisker mechanical stimuli.

- Free nerve endings: Free nerve endings are widely distributed within the whisker follicle. Mechanoreceptive nerve endings have been suggested to be sensitive to the strain in the tissue (Mitchinson et al., 2004; Lottem & Azouz, 2011; Severson et al., 2017).

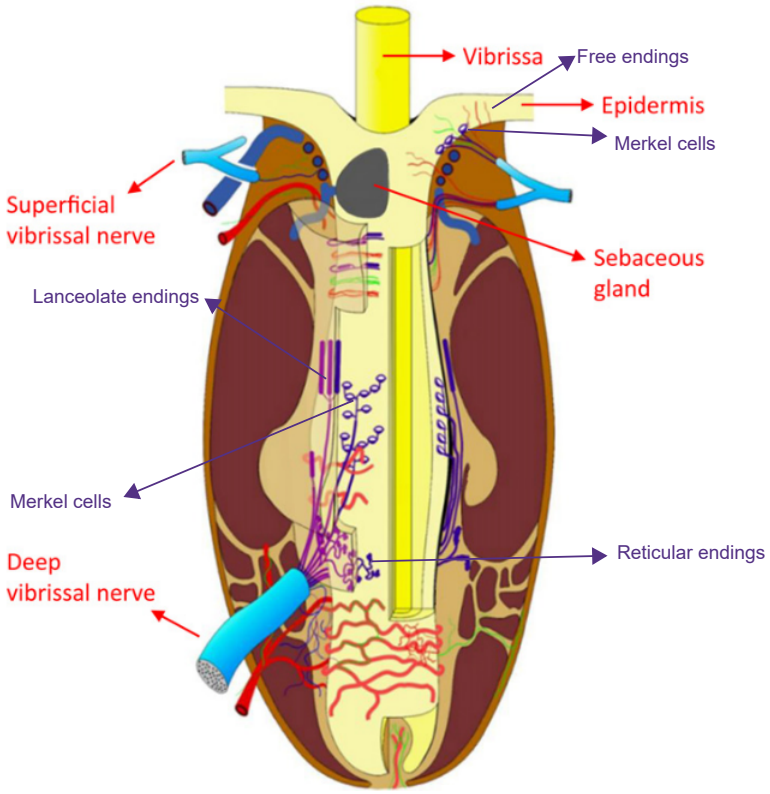

Figure 1.3: Schematic of whisker follicle structure and innervation (for a rat or mouse). Adapted from (Diamond & Arabzadeh, 2013)

Trigeminal ganglion. Neurons in the Trigeminal ganglion (TG) are pseudounipolar, in other words, the cells body present a single axon which divided into two branches. Some of these neurons are primary whisker neurons (PWN). For these set of neurons, their peripheral branch innervates a single whisker follicle, while the central branch ends in the trigeminal nuclei in the brainstem (Torvik, 1956; Clarke & Bowsher, 1962). Unlike cortex, the trigeminal ganglion does not present a topographic map of the whisker pad. Only a weak correlation between the dorsoventral position of the PWNs within TG and the whisker that innervate has been observed instead (Leiser & Moxon, 2006).

Electrophysiological recordings in anaesthetised animals have shown that PWNs respond to whisker deflection, specifically, a combination of whisker position and velocity (Bale et al., 2013). Additionally, most PWNs are selective to the direction of whisker deflection (Lichtenstein et al., 1990; Bale & Petersen, 2009; Storchi et al., 2012). PWN activity is also modulated by the radial distance of the deflection (Szwed et al., 2006).

In awake, behaving animals, 'whisker self-motion' and especially whisker contacts trigger activity in PWNs (Leiser & Moxon, 2007). During active touch exploration, the bending moment is the best predictor of the trigeminal ganglion activity (Campagner et al., 2016; Bush et al., 2016; Severson et al., 2017; Furuta et al., 2020).

Brainstem. Features encoded in the trigeminal ganglion as self-motion and touch are then conveyed to the trigeminal nuclei in the brainstem (Moore et al., 2015). Afferent axons form synapses in multiple nuclei within the complex (Bosman et al., 2011; Evans et al., 2019). The sensory trigeminal nuclei are constituted by two nuclei: Principal (PrV) and spinal (SpV) nucleus. From here there are several synaptic routes to the barrel cortex. The most direct and well-understood pathways are three (see (Bosman et al., 2011) for detailed review): lemniscal, paralemniscal and extralemniscal pathways. In all of them, neurons from the brainstem project to a different area in the thalamus where they form synapses: In the lemniscal pathway, neurons in the principal nucleus project to the ventral posterior medial nucleus (VPMdm) of the thalamus. In the extralemniscal pathway, neurons in the caudal section of the interpolar spinal nucleus project to the ventrolateral domain of the VPM (VPMvl). The paralemniscal pathway arises from the rostral part of the interpolar spinal nucleus, which cells project to the posterior nucleus (POm) and the zona incerta (ZI) of the thalamus.

Neurons in the thalamus then project to different areas and layers of the somatosensory cortex. These pathways are a small fraction of the synaptic routes that can reach the cortex, other more complex pathways can include interaction or even loop architectures with both motor and sensory areas (Bosman et al., 2011).

Thalamus In the thalamus it has been observed that neurons in the lemniscal pathway represent both touch and vibrissa self-motion signals (Nicolelis & Chapin, 1994;

Veinante & Deschênes, 1999; Moore et al., 2015); neurons in the paralemniscal pathway represent whisking signals, and neurons in the extralemniscal pathway represent contact signals (C. Yu et al., 2006).

Similarly to the TG, neurons in the VPm nucleus of thalamus encode the position, velocity and acceleration of the whisker movements. However, neurons usually are sensitive to only one of these variables instead of a combination of features (R. S. Petersen et al., 2008). Direction of whisker deflection also modulate neural responses in VPm (Simons & Carvell, 1989; Timofeeva et al., 2003; Bale & Petersen, 2009).

Cortex Even though barrel cortex was first defined over 40 years ago, the stimulus features that encode and how they are encoded is partially understood. The elementary stimulus features encoded in barrel cortex have been thoroughly studied in anaesthetised animals. In the simplest case, when stimulating the system with single whisker deflections, each barrel process tactile information from its corresponding whisker on the mystacial pad (the principal whisker). However, some neurons within the barrels can also respond, or even prefer stimulation from surrounding whiskers (Simons, 1978; Laboy-Juárez et al., 2019). Similarly to the rest of the pathway, neurons in cortex encode position, velocity, acceleration and direction of whisker deflections in addition to their frequencies (Simons, 1978; Arabzadeh et al., 2003; Ewert et al., 2008) and the interval between repetitive stimulation (Ahissar et al., 2001; Webber & Stanley, 2004).

Multi-whisker stimulation has started to open a new world of possibilities for the study of the barrel cortex. Despite the technological developments that allow the independent stimulation of up to 24 whiskers simultaneously, only elementary properties of multi-whisker integration have been determined (Estebanez et al., 2016). Sequential stimulation of two whiskers can induce a suppresion (Simons, 1985; Simons & Carvell, 1989) or facilitation (Ego-Stengel et al., 2005) of cortical responses depending on spatial and temporal pattern (Ego-Stengel et al., 2005; Laboy-Juárez et al., 2019). Responses to more complex spatiotemporal patterns still need to be investigated.

Responses to sensory stimuli are also critically dependent on the temporal patterns of the stimuli and their statistical properties. Their effects are discussed in detail in the next section.

Thanks to the recent breakthroughs made in tracking whisking behaviour and neural recordings in awake animals, some pioneers works have started to characterise the responses of barrel cortex to natural stimuli in awake, behaving rodents. Yu et al. showed that unlike in previous stages of the ascending pathway, self-motion responses are substantially attenuated in layer 4 of barrel cortex (J. Yu et al., 2016). Additionally, Hires et al. show that touches were a dominant sensorimotor feature encoded in the barrel cortex (Hires et al., 2015), which is consistent with the results obtained in anaesthesia animals. On the other hand, it has been observed that slip-sticks events can drive sparse but precisely timed spikes in layer 4 and 5 of S1 (Jadhav et al., 2009). Interestingly, slip-sticks events have been proposed as a relevant cue for texture discrimination in rodents (Jadhav & Feldman, 2010; Wolfe et al., 2008; Isett et al., 2018). This is supported by the variation in both the rate and magnitude of the slip-sticks between smooth and coarse surfaces (Wolfe et al., 2008; Isett et al., 2018).

In comparison to the previous stage of the pathways, there are three main differences in stimuli encoding in barrel cortex. First, in contrast to the highly reliable encoding observed in other stages, neurons in cortex show substantial variability in response when exposed to identical stimuli (Sachdev et al., 2004; Arabzadeh et al., 2005; C. C. Petersen, 2007). Second, neurons in barrel cortex are more markedly tuned to whisker touch than to self-motion (Hires et al., 2015; J. Yu et al., 2016). Third, neurons here are sensitive to behavioural choice (H. Yang et al., 2015; Kwon et al., 2016).

All these studies have deepened our understanding of how behaviorally relevant stimuli as touch and slip-sticks event can drive cortical activity. However, the mechanosensory basis of these events, and thus, of the activity in barrel cortex is unclear. In particular, how a mechanical descriptor as the bending moment, which is the main driver of neurons in the periphery (Campagner et al., 2016; Bush et al., 2016; Severson et al., 2017; Furuta et al., 2020), can affect cortical is poorly understood. Although indirect evidence has pointed out that this variable could modulate activity in barrel cortex (O'Connor, Peron, et al., 2010; Hires et al., 2015; J. Yu et al., 2016), no study has explicitly tested how much of the responses to whisker stimuli can be understood from the mechanical point of view.

In Chapter 3, I describe how cortical neurons respond to two mechanical variables,

the bending and twisting moment, from multiple whiskers in behaving mice performing a contact detection task.

1.5 Sensory adaptation

Sensory coding aims to understand how sensory stimuli are represented in the brain. The classical approach to understand how stimuli are encoded is based on the assumption that the neural code is stationary. In other words, the rules to translate a stimulus into neural activity do not change over time. However, it has been long observed that these rules possess dynamical properties which depend on stimulus history or context (Adrian, 1928; Simons, 1978; A. L. Fairhall et al., 2001; Maravall et al., 2007; Ollerenshaw et al., 2014). Although changes in the encoding rules can be a product of a variety of physiological causes, all the consequences of a change in neural encoding are commonly referred to as sensory adaptation.

Throughout the years, sensory adaptation has been an evolving term that has been used to report a series of phenomena. In the specific case where neurons are exposed to a constant or repetitive stimulus, a neuron or population response is said to adapt if after time or upon subsequent presentations, the response decreases (Adrian, 1928; Weber & Fairhall, 2019; A. Fairhall, 2014). Other authors refer to adaptation as shifts of neural representation over time after a change in stimulus statistics or context (Weber & Fairhall, 2019; A. Fairhall, 2014). Whereas some authors define adaptation in more general ways as "the accommodation of neuronal responses to ongoing stimulation" (Maravall et al., 2007, 2013).

The first two definitions offer straightforward methods to test and quantify adaptation effects. Each method depends on stimulus history. For a repetitive or maintained stimulus, sensory adaptation can be shown as an attenuation of the neural responses, either in the spike counts or intracellular responses (Khatri et al., 2004; Martin-Cortecero & Nuñez, 2014). The extent of adaptation effects can be measured, for a repetitive stimulus, as the ratio between the responses to later stimulus and the responses to the first stimulus. For a maintained stimulus, this is equivalent to the ratio between the responses to the end and beginning of the stimulus (Khatri et al.,

2004; Martin-Cortecero & Nuñez, 2014). Instead, for scenarios where the stimulus suffers a change in context, adaptation can be shown as a shift in the encoding properties of the stimulus, for instance, a shift in tuning curves or the neurons' receptive field before and after the change in context (Maravall et al., 2007, 2013).

It has long been proposed that sensory adaptation is not only the fatigue of the neurons due to the exposure to a stimulus, but provides both computational and perceptual benefits. For instance, adaptation could help to transmit information of sensory signals more efficiently, matching the coding strategy to the statistic of the stimulus (Maravall et al., 2007; A. Fairhall, 2014). Also, it would minimise energy costs by triggering fewer spikes for repetitive, less informative, stimuli (Weber & Fairhall, 2019). On the perceptual benefits, in the whisker system, adaptation would change the perception of the environment, enhancing the detection of objects in a non-adapted state and facilitating spatial discrimination in adapted neurons (Wang et al., 2010; Ollerenshaw et al., 2014).

Sensory adaptation can be observed in three different aspects of encoding in the whisker system: First, responses to a maintained stimulus, for instance, a maintained whisker deflection, decay over time. This phenomenon has been used to classify neurons as Rapid Adapting neurons and Slowly Adapting neurons according to the speed of the decay of the neural responses. Each type of neuron could aid to encode different properties of the stimulus (Simons, 1985; Lichtenstein et al., 1990; Stüttgen et al., 2006; Lottem & Azouz, 2011). Second, responses to repetitive whisker deflections decrease over time (Simons, 1978, 1985; Khatri et al., 2004; Katz et al., 2006; Wang et al., 2010; Martin-Cortecero & Nuñez, 2014; Musall et al., 2014). Specifically, the responses to each whisker deflection are equal or weaker than the responses to the previous deflection in the stimulus train. Third, responses adapt to stimulus statistics (Maravall et al., 2007; Díaz-Quesada & Maravall, 2008; Maravall et al., 2013), in other words, the input-output function between the stimulus and neural activity is rescaled to match the statistics of the ongoing stimulus. For example, the sensitivity of a neuron to the velocity of whisker deflection is proportional to the standard deviation of the velocity. Therefore, input-output functions of the neuron captured under different velocity distributions (with the same mean value) can be matched normalising them by their respective standard deviation (Maravall et al., 2007). This

type of adaptation could contribute to coding efficiency by maintaining the quantity of information transmitted about a stimulus feature.

To probe how sensory adaptation affects the coding properties of the whisker system, many studies have used the second aspect described above. Although they all use the repetitive stimulus paradigm, the stimulus properties, the delivery of the stimulus and the degree of anaesthesia of the animal vary across experiments, modulating the extent of adaptation effects (Lampl & Katz, 2017). While different experimental conditions have given different insights about sensory adaptation, they obstruct the comparison across studies.

In anaesthetised animals, increasing adaptation effects have been observed along the ascending somatosensory pathway, reaching a peak in barrel cortex (Martin-Cortecero & Nuñez, 2014). Neurons in barrel cortex adapt to repetitive discrete and continuous stimulus (Simons, 1985; Khatri et al., 2004; Musall et al., 2014). The extent of adaptation effects strongly depends on the stimulus frequency. In cortex, small adaptation effects are visible at stimulus frequencies around 1-2 Hz, increasing monotonically up to frequencies of 40 Hz (Khatri et al., 2004). This frequency range encompasses typical whisking frequencies (5-25 Hz for rats and somewhat higher for mice (Berg, 2002; O'Connor, Clack, et al., 2010)), predicting that neurons in barrel cortex should be subject to sensory adaptation in behaving animals.

A particular case of adaptation has been termed Stimulus-Specific Adaptation (SSA), where a neuron adapts to a specific stimulus feature. For instance, neurons in barrel cortex are said to adapt specifically to whisker identity if their responses to stimulation of one whisker are not affected by previous stimulation of another whisker (Katz et al., 2006; Musall et al., 2017). Cortical neurons have also been observed to adapt specifically to the direction of bending, velocity and intensity of deflection in a smaller degree (Khatri, Bruno, & Simons, 2009; Ganmor et al., 2010; Musall et al., 2017).

The extent of adaptation and SSA in barrel cortex is also dependent on location recording, varying substantially throughout the cortical layers. Layer 2/3 and 4 and present robust signs of adaptation to deflection above 2 Hz (Simons, 1978; Chung et al., 2002), while neurons in layer 5/6 show significant adaptation effects from deflections above 1 Hz (Chung et al., 2002; Ahissar et al., 2000). Regarding SSA, puzzling results have been reported. While (Katz et al., 2006) showed that adaptation was highly

specific to whisker identity in layers 2/3 and 4, (Musall et al., 2017) indicates that whisker-specific adaptation effects in layer 4 are significantly smaller than in layer 2/3 and 5/6. The apparent conflicting results can be a product of differences in stimulus intensity or depth of anaesthesia.

Several physiological phenomena could give rise to sensory adaptation effects. Although the precise phenomena that act in each scenario are unclear, three types of mechanisms have been posited as the underlying biological causes of adaptation in barrel cortex: intrinsic, synaptic and network mechanisms. Intrinsic mechanisms correspond to intracellular changes that can give rise to adaptation hallmarks. For instance, it has been shown that membrane hyperpolarization after sustained stimulation accounts for more specific adaptation properties, as adaptation to the stimulus statistics in barrel cortex (Díaz-Quesada & Maravall, 2008). In other sensory pathways and cell types, multiple changes in somatic currents have been proposed to cause adaptation effects, such as, changes in calcium-activated and sodium-activated potassium currents (Sanchez-Vives et al., 2000), changes in M-currents (Constanti & Brown, 1981) and slow recovery of sodium channels (Azouz & Gray, 2000).

Synaptic mechanisms are based on the variations of synaptic inputs that could cause adaptation effects, such as synaptic enhancement of inhibition or depression of excitatory synapses. In the case of adaptation in barrel cortex, the decrease of synaptic inputs from thalamocortical inputs can explain the firing rate attenuation observed after repetitive stimulation of the whiskers (Chung et al., 2002; Katz et al., 2006).

Network mechanisms involve changes in neural circuits that can produce adaptation effects. For instance, it has been proposed that SSA can be caused by the differential activation of sensory pathways. In barrel cortex, for instance, specific adaptation to whisker-identity could be a product of the differential activation of neural populations in the thalamus which are tuned to whisker identity (Whitmire & Stanley, 2016; Lampl & Katz, 2017).

Depth of anaesthesia plays an important role in the extent of adaptation effects. Using electrical stimulation to the whisker pad has shown that adaptation effects are stronger when the animal is in a quiescent state as anaesthesia or awake immobility than in expectant animals (Castro-Alamancos, 2004). In awake rats, it has been

found that adaptation to electrical stimulation of the infraorbital nerve was stronger during awake immobility than during active whisking (Fanselow & Nicolelis, 1999). More recently, it has been shown that adaptation effects decrease in the presence of Acetylcholine (Martin-Cortecero & Nuñez, 2014), which has been reported to increase in cortex upon the presentation of a behaviourally relevant stimulus, presumably increasing the level of attention/arousal (Nuñez et al., 2012; Himmelheber et al., 2000).

Despite the profound computational and perceptual consequences that adaptation may have in the whisker system, it has not been extensively quantified in awake, behaving animals. Studies regarding adaptation in awake animals usually involve either electrical stimulation of the whisker pad (or a nerve) (Fanselow & Nicolelis, 1999; Castro-Alamancos, 2004), or mechanical stimulation of the whisker via a piezoelectric device instead of active sensory inputs generated by the animal (Ollerenshaw et al., 2014; Musall et al., 2014).

Only very few studies have attempted to describe some of the adaptation effects in awake, behaving animals. Including active whisking behaviour when characterising sensory adaptation is challenging because of the lack of control over sensory inputs, which brings two complications: First, because the animals can control their stimuli, sensory inputs need to be quantified measuring whisking behaviour. Second, because whisking behaviour is highly variable, changes in the responses to a stimulus can be caused either by sensory adaptation or a change in whisking behaviour. Some studies have attempted to overcome these challenges by measuring whisking behaviour and neural responses during successive touches that seem to be similar. Intracellular recordings in layer 2/3 and 4 from awake, behaving rodents suggest that most neurons show little adaptation to successive active touches (Crochet et al., 2011; Crochet & Petersen, 2006; Yamashita et al., 2013). However, the criteria to choose these touches are based on kinematical measures obtained from the horizontal plane, instead of mechanical variables that are more likely to drive neural activity. Also, this kind of analyses is only able to show a few (or a single) trials where all touches are alike. Another report shows that in layer 4, neural responses to touch decrease significantly for later touches in a train of successive active touches (Hires et al., 2015). However, a decrease in the strength of the touches was simultaneously observed, making unclear if this effect can be attributed exclusively to sensory adaptation or a mechanical effect.

In Chapter 4, I test if sensory adaption can be observed in mice performing a contact detection task and measure the extent of its effect in the neural coding.

1.6 Aims and chapters' outline

The main goal of this thesis is to quantify rodent whisking behaviour and its encoding in awake, behaving animals. To do this, three aims are outlined corresponding to each result chapter:

- Chapter 2: Quantify whisking behaviour in awake, behaving mice. In this chapter, I developed a method to track multiple whiskers in 3D, I imaged mouse whiskers in behaving animals (head-fixed mice) solving a behavioural task. I implemented the method in Matlab and tracked the imaged whiskers. From the tracking, I am able to quantify the three angles that describe whisker position and kinematics, and the shape of the whisker, from which the bending moment at the whisker base can be estimated.

- Chapter 3: Predict barrel cortex activity in awake, behaving mice from mechanical whisker inputs. Here I extended the whisker tracker developed previously to estimate the two main mechanical variables affecting the whisker during whisking behaviour: bending moment and twisting moment. I tracked the imaged whiskers while the mouse solved a pole detection task and described how these two variables behave during whisking and whisker-contact periods. Additionally, I applied a Generalised Linear Model (GLM) to predict the activity of barrel cortex neurons using touch and mechanical variables as candidate predictors. I found that the recorded neural population was heterogeneous, presenting neurons encoding preferentially the rate of change of the mechanical variables or touch. Behavioural and neural recordings analysed in this chapter are part of the data presented in Chapter 4.

- Chapter 4: Quantify sensory adaptation effects in barrel cortex neurons in awake, behaving mice. I analysed the pole detection task in order to test if sensory adaptation was an observable phenomenon in awake, behaving mice. I showed that neural encoding, as well as whisking behaviour, evolve within trials, shaping

neural activity in barrel cortex. In particular, I found that neural responses to repetitive touch decrease over time, in agreement with the classic definition of sensory adaptation. Additionally, I showed that a portion of neurons in barrel cortex specifically adapt to whisker identity and to a lesser degree to bending direction.

Throughout the project, all methods and analyses were developed and performed considering awake, behaving head-fixed mice for the following reasons: First, mice and rats are the most popular models for the study of somatosensation in the whisker system. However, mice have played a more prominent role in the last decades due to the availability of techniques for genetic manipulation, which is relevant for the long-term research program (Ellenbroek & Youn, 2016; Guo et al., 2014; O'Connor et al., 2013). Second, and directly relevant for this thesis, one of the main physical differences between mice and rats is their size. In particular, tracking whiskers in mice is more challenging than tracking whiskers in rats. Since the mouse whiskers are smaller and thinner, higher spatial resolution is required. Additionally, since mouse whiskers are more pliable, whisker tracking techniques used in rats (such as the use of dye markers (Knutsen et al., 2008; Roy et al., 2011)) cannot be extrapolated to mice. Therefore, if the objective is to create a functional 3D whisker tracker for both rats and mice, it is crucial to validate it first in mice. Finally, head-fixation is a widely used technique for the study of whisker behaviour and the recording of its related neural activity (Bermejo et al., 2002; O'Connor, Clack, et al., 2010; Sofroniew et al., 2014; Campagner et al., 2016, 2019). One of the main caveats with this approach is that the interaction between whisker and head movements is lost. However, head-fixation allows a high degree of stimulus control and monitoring of the animal's movements (Bermejo et al., 2002; Clack et al., 2012; Roy et al., 2011), which is crucial for precise whisker tracking, particularly in 3D.

1.7 Journal format thesis

This thesis is presented in journal format. The rationale to choose this format is based on the availability of the prepared content produced during this thesis: one already published chapter in which I am a joint first author with Rasmus Petersen (Chapter 2);

and two manuscripts (Chapters 3 and 4) to be submitted in the short term where I will be a joint first author with Michaela Loft. Writing the two latter chapters in manuscript format will accelerate their submission and publication.

I have developed a substantial part of the design, research and data analysis of all chapters. More specifically, all chapters involve the analysis of behavioural and electrophysiological recordings of awake, behaving mice during a pole detection task. Animal training, whisker imaging and electrophysiological recordings were performed by Michaela Loft. Behavioural apparatus and task were designed by Ramsus Petersen and Michaela Loft. My contribution to each chapter was:

- Chapter 2: I have collaborated with Rasmus Petersen in the design and implementation of the whisker tracking method. I analysed and curated the behavioural data and participated in the development of the experimental methods.
- Chapter 3: In this chapter, I have designed the research together with Rasmus Petersen. I analysed and curated the behavioural data and electrophysiological recordings. Rasmus Petersen helped me with the implementation of the method to estimate torsion and bending moment.
- Chapter 4: In this chapter, I have designed the research together with Rasmus Petersen and Miguel Maravall. I analysed and curated the behavioural data and electrophysiological recordings.

1.8 Published content

The second chapter of this thesis was published as Petersen R*, Colins Rodriguez A*, Evans M, Campagner D, Loft M. (2020) *A system for tracking whisker kinematics and whisker shape in three dimensions.* PLoS Computational Biology, 16(1):e1007402. Petersen R. and Colins Rodriguez A. are joined first authors on this publication. Example data used in this publication and tutorial is held in Figshare (http://doi.org/10.6084/m9.figshare.9758894.v1). Code is available from Github (https://github.com/PetersenLab/WhiskerMan).

Chapter 2

A system for tracking whisker kinematics and whisker shape in three dimensions

2.1 Abstract

Quantification of behaviour is essential for biology. Since the whisker system is a popular model, it is important to have methods for measuring whisker movements from behaving animals. Here, we developed a high-speed imaging system that measures whisker movements simultaneously from two vantage points. We developed a whisker tracker algorithm that automatically reconstructs 3D whisker information directly from the 'stereo' video data. The tracker is controlled via a Graphical User Interface that also allows user-friendly curation. The algorithm tracks whiskers, by fitting a 3D Bezier curve to the basal section of each target whisker. By using prior knowledge of natural whisker motion and natural whisker shape to constrain the fits and by minimising the number of fitted parameters, the algorithm is able to track multiple whiskers in parallel with low error rate. We used the output of the tracker to produce a 3D description of each tracked whisker, including its 3D orientation and 3D shape, as well as bending-related mechanical force. In conclusion, we present a non-invasive, automatic system to track whiskers in 3D from high-speed video, creating the opportunity for comprehensive 3D analysis of sensorimotor behaviour and its neural basis.

2.2 Introduction

Substantial progress towards the long-standing ambition of measuring "total movements made by the intact animal" (Tinbergen, 1951) is coming from the application of machine vision methods to video recordings of behaving animals (Brown & de Bivort, 2018). Since the whisker system is a major experimental model and since the whiskers are readily imageable (Maravall & Diamond, 2014; Campagner et al., 2018), the whisker system is ideally suited to this endeavour. Tracking the whiskers of mice/rats has already deepened our understanding of active sensation and refined our capacity to relate behaviour to neural mechanisms (Knutsen et al., 2008; O'Connor, Peron, et al., 2010; Hires et al., 2015; Evans et al., 2019; Campagner et al., 2019; Zuo & Diamond, 2019; Campagner et al., 2016; Bale et al., 2015; Bush et al., 2016; Severson et al., 2017). Our aim here was to develop a method to track whisker movements and whisker shape in 3D in behaving mice at millisecond temporal resolution.

Both the movement of whiskers and the mechanical forces of whisker-object contact are 3D. During each whisking cycle, the whisker follicles translate with respect to the head and each whisker rotates in 3D. Although only the horizontal component of this movement is typically measured, whiskers also move vertically (Bermejo et al., 2002) and rotate around their longitudinal axes ("roll")(Knutsen et al., 2008). The mechanical forces of whisker-object contact that are the drivers of neural activity are also 3D. When a mouse 'whisks' against an object, the whiskers bend. Again, although only the horizontal component of bending is typically measured, bending can occur in all directions (Huet et al., 2015). In the trigeminal ganglion, all directions of deflection are represented (Gibson & Welker, 1983; Lichtenstein et al., 1990; Bale & Petersen, 2009; Storchi et al., 2012), indicating that 3D bending information is both encoded and transmitted to the brain.

Starting with the first cinematographic study of whisking by Welker in 1964 (W. Welker, 1964), there is a 50-year history of increasingly sophisticated efforts to measure whisker movement from behaving animals (Campagner et al., 2018). Most studies have measured whisker movement only in the horizontal plane, using either linear, charge-coupled device (CCD) arrays (Bermejo et al., 1998; Wolfe et al., 2008) or high-speed imaging (O'Connor, Clack, et al., 2010; Szwed et al., 2006; Pammer et al., 2013;

Peron et al., 2015). However, horizontal plane imaging provides a direct measurement of only one of the 3 angles that define 3D whisker orientation. Moreover, estimates of whisker bending moment obtained by imaging apparent curvature of a whisker in the horizontal plane (Pammer et al., 2013; Birdwell et al., 2007; Clack et al., 2012) can be contaminated by roll (Knutsen et al., 2008). This is significant since bending moment is a primary driver of contact-related mechanotransduction (Campagner et al., 2016; Bush et al., 2016; Severson et al., 2017). High-speed cameras sufficient to form the basis of a 3D whisker imaging system have long been available: the main bottleneck to achieving 3D whisker tracking has been the computational complexity of the 3D reconstruction problem. A few studies have measured aspects of 3D whisker movement in vivo (Knutsen et al., 2008; Bermejo et al., 2002; Huet et al., 2015; Roy et al., 2011) and ex vivo (Quist & Hartmann, 2012), but no automatic approach has so far been developed that measures both 3D whisker orientation and 3D whisker shape from high-speed video of behaving animals.

Here, we obtained 3D information noninvasively from head-fixed mice using a high-speed imaging system consisting of two cameras, positioned to minimise occlusion, and developed computational methods to reconstruct 3D whisker state. We used the system to track up to 8 whiskers in parallel, and to obtain a 3D description of each whisker, encompassing both its 3D orientation and 3D shape.

2.3 Results

2.3.1 3D Imaging of whisking behaviour

To obtain a video data set with which to develop 3D whisker tracking, we trained head-fixed mice to detect objects with their whiskers (N=6). On each trial, a vertical pole was presented in either an anterior location out of reach of the whiskers ("No-Go trials") or a posterior location within reach ("Go trial"). Mice learned to perform the task accurately (81±17%, mean ± SD over mice) and performed 135±22 trials per daily session. When the pole moved up at the onset of a trial, mice would typically commence exploratory whisking. On Go trials, one or more whiskers typically contacted the pole; on No-Go trials, there was no contact. In this way, we obtained a varied data set, which included episodes of whisking both with and without contact (average behavioural

session 0.5M video frames). We recorded high-speed video of mice using a system of two high-speed cameras (Fig 2.1). One camera imaged whisking in the horizontal plane. The other camera imaged in an off-vertical plane, the orientation of which (25° off coronal, 10° off horizontal) was optimised to minimise occlusion of whiskers against the background of the body of the mouse (Fig 2.1). For brevity, we refer to this second image plane as "vertical".

2.3.2 Reconstructing whiskers in 3D from 2D views

Using the two-camera setup, we imaged mice (1000 frames/s) as they performed the pole detection task. This resulted in a time series of image pairs (horizontal and vertical views): we refer to each such image pair as a 'frame'. Our next aim was to develop an automated algorithm to track multiple whiskers in 3D. For two reasons, we focussed on the basal segment of the whisker shafts. First, during whisker-object contact, whiskers bend and the associated mechanical forces/moments drive mechanoreceptors located in the follicle. Thus, changes in whisker shape at the base of the whisker are intimately related to neural activity in the ascending whisker pathway (Campagner et al., 2016; Severson et al., 2017). Second, tracking only the basal segment (not the whole whisker) reduces the number of parameters required to describe the shape of a whisker. To accurately describe the shape across its entire length requires at least a 5^{th} degree polynomial (Clack et al., 2012) which, in 3D, has 15 parameters. However, the basal segment of a whisker is well-approximated by a quadratic curve (Pammer et al., 2013; Quist & Hartmann, 2012) which, in 3D, has 9 parameters.

The basic computational problem is to reconstruct the 3D coordinates of multiple whiskers from two 2D images. 3D whisker reconstruction is particularly challenging, since whiskers are similar to each other and their images can overlap. The key challenge is the lack of a unique mapping between points across the 2D images. Knutsen *et al.* overcame this by marking the shaft of one whisker with spots of dye (Knutsen et al., 2008). The two images of each dye spot could then be matched and, after camera calibration, their 3D locations reconstructed. This is an elegant solution but there is the possibility, particularly for thin whiskers such as those of a mouse, that application of dye perturbs whisker mechanical properties. In a more recent, non-invasive approach, Huet *et al.* achieved 3D tracking of a single whisker; tracking

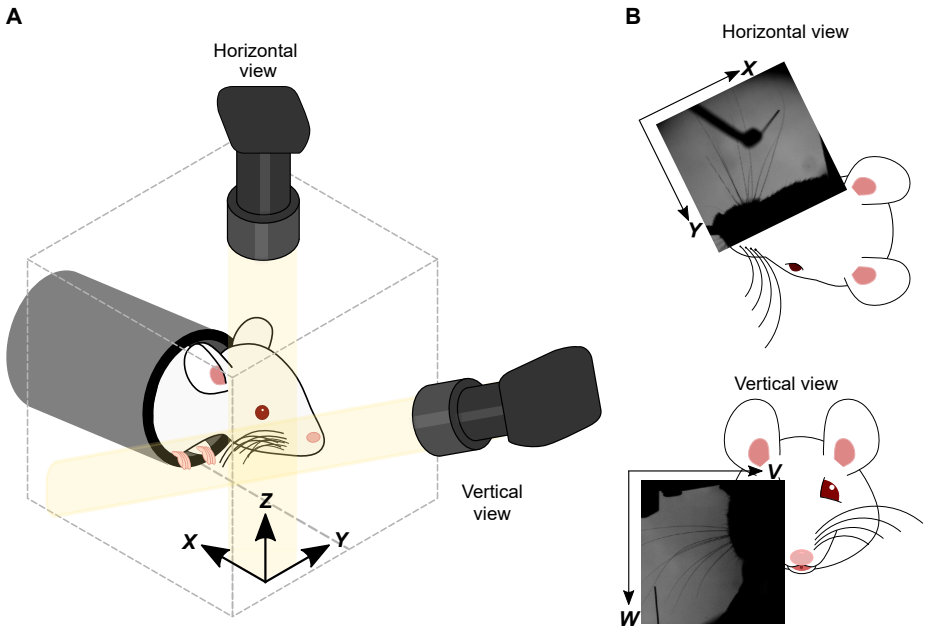

Figure 2.1: Experimental setup for 3D imaging. A) Schematic showing the camera angles and 3D head-centred xyz coordinate frame. B) Horizontal and vertical views, with corresponding 2D coordinate frames.

automatically in one image plane and tracking manually in a second, orthogonal plane (Huet et al., 2015). Since there was only one whisker, coordinates describing the whisker in one plane could be uniquely matched to those in the other plane. However, manual tracking is impractical for large data sets (O'Connor, Clack, et al., 2010; Hires et al., 2015; Campagner et al., 2019, 2016; Severson et al., 2017). In sum, no method currently exists that achieves automatic and non-invasive tracking of multiple whiskers in 3D. Our innovation here was to achieve this by applying constraints expressing prior knowledge of natural whisking to the 3D reconstruction problem. Our whisker tracker describes each target whisker as a 3D Bezier curve (Fig 2.2). This is a parametric curve segment $\boldsymbol{b}(s) = (x(s), y(s), z(s))$, where $0 \leq s \leq 1$ parameterises location along the curve. In our case, $s = 0$ marked the end closest to the whisker base and $s = 1$ marked the end furthest from the base. A Bezier curve is defined by 2 or more control points (Fig 2.2), the number of which controls the complexity of the curve. We used quadratic Bezier curves, each of which has 3 control points since, as noted above, this is the lowest-degree curve that is accurate for our purposes. In this case, the first and last control points lie on the whisker shadow, while the middle point does not necessarily sit on the whisker.

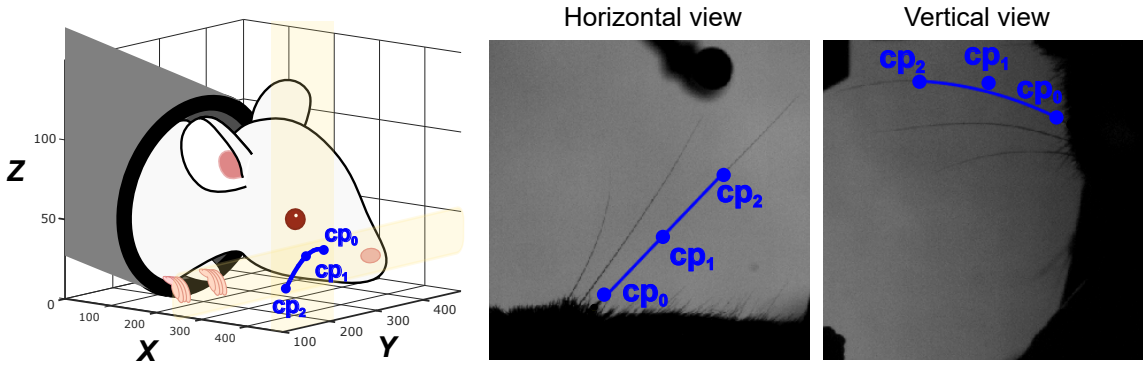

Figure 2.2: Description of whiskers by quadratic 3D Bezier curves. Left: schematic of a 3D Bezier curve representing a whisker (blue line), defined by its three control points $\boldsymbol{cp}_0$, $\boldsymbol{cp}_1$ and $\boldsymbol{cp}_2$ (coloured dots). Middle, right: projection of the 3D Bezier curve, and its control points, onto horizontal and vertical image planes.

2.3.3 Whisker tracking algorithm

The essence of our algorithm was to track one or more target whiskers by fitting 3D Bezier curves to the image data. The core principle was, for each frame, to tune the control points of the Bezier curves so that their projections onto the two image planes matched as closely as possible the images of the basal segments of the target whiskers. The degree of match was quantified by the following cost function (Methods, Equation 2.4):

$$E(f) = E_h(f) + E_v(f) + R_1(f) + R_2(f)$$

Here E_h and E_v (defined in Equations 2.5-2.6) measured the average image intensity (the line integral) along a given Bezier curve projected into the horizontal and vertical image plane respectively; R_1 and R_2 (defined in Equations 2.7-2.8) were regularising terms. Since whiskers imaged as black (low pixel intensity) and background as white (high pixel intensity), E_h and E_v were low when a Bezier curve $\boldsymbol{b}(s)$ coincided with a whisker (Fig 2.2), and at a local minimum with respect to local changes to the positions of the control points, whereas E_h and E_v were high if they coincided with a background region. Thus, a target whisker was tracked by minimising the cost function with respect to the control point positions of the associated Bezier curve. For the first frame of the video, the control points could be either manually selected by the user using computer mouse clicks within the video images, or selected by the automatic initialisation algorithm as detailed in the whisker tracking pipeline section.

It was possible to track multiple whiskers in parallel by taking advantage of prior

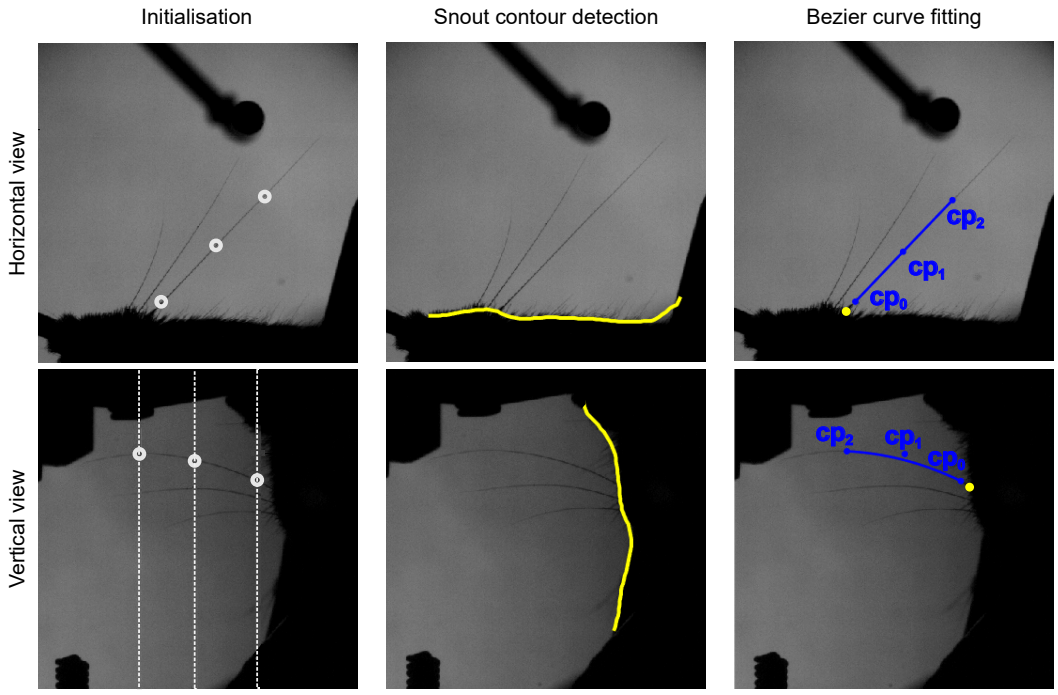

h

Figure 2.3: Whisker tracking pipeline. Left: Initialisation of control points for a given target whisker (see Methods for details). Initial values for control points in horizontal (top, white circles) and vertical views (bottom, white circles). White dotted lines in vertical view represent the range of z values consistent with each of the (x, y) points in horizontal view. Middle: Estimation of snout contour (yellow). Right: Fitting of 3D Bezier curves to image data. Projections of the 3D Bezier curve for one whisker (blue lines) and of its control points (blue dots) are shown in horizontal (top) and vertical (bottom) views. Yellow dots indicate intersections between snout contour and extrapolated Bezier curves.

knowledge of natural whisker motion. First, since whiskers move and deform smoothly over time, the location of a whisker in a given frame was (with sparse exceptions, see below) predictable from that in the previous frames. Thus, by seeding the control point positions of a Bezier curve representing a given whisker using corresponding positions from previous frames (Methods), it was possible to maintain accurate "locking" between each Bezier curve and its target whisker. Second, we used prior knowledge to constrain the cost function. As detailed in Methods, a "temporal contiguity" constraint (R_1) penalised discontinuous, temporal changes in Bezier curves (Methods, Equation 2.7) and a "shape complexity" constraint (R_2) penalised unnaturally complex curve shapes (Methods, Equation 2.8). The full whisker tracking pipeline (Fig 2.3) is detailed in Methods.

2.3.4 Tracking multiple whiskers in 3D

To test the algorithm, we applied it to the image data from our task. We found that we were able to track several whiskers at the same time (Fig 2.4; Movie 1). Fig 2.4.C shows a 12 ms sequence of whisker-pole contact from a mouse where 8 whiskers were intact and the others had been trimmed to the level of the fur (Fig 2.4.A-B). The algorithm successfully tracked changes in both orientation and shape of the 8 whiskers. Different types of motion were tracked: some whiskers bent against the pole whilst others slipped past it (Fig 2.4.D). The outcome of the tracker was a sequence of 3D curve segments, each representing the basal segment of a given whisker in a given frame (Fig 2.4.E).

To assess tracking accuracy, we tracked a randomly selected set of 100 trials (50 go, 50 No-Go) where a mouse was performing the task with 3 whiskers, all others trimmed to the level of the fur. This dataset comprised 350,000 frames. During 'free whisking, changes in whisker position/shape were entirely due to whisking motion, and such changes were smooth as a function of time, so that the temporal contiguity and shape complexity constraints of the cost function (Methods, Equations 2.4 and 2.7) were accurate. Such errors as did occur were mainly due to (1) occlusion and (2) whisker overlap. (1) On occasion, a whisker was occluded against either the mouse's body (ear or cheek) or the experimental apparatus (pole). However, by optimising the view angles of the cameras (see above) and by minimising the image footprint of the apparatus, we minimised these effects. On the No-Go trials, we detected 0.11 occlusion events/whisker per 1000 frames. Since occlusion was rare, such events were dealt with by skipping affected frames and restarting tracking afterwards. (2) On occasion, whiskers overlapped each other in either horizontal or vertical view. Because the tracker applies prior knowledge of natural whisker shape/location, our algorithm was relatively robust to such events. For example, the tracked video sequence illustrated in Fig 2.4 includes overlap between whiskers C1 and D2. However, errors did sometimes occur. The most common overlap error was when a small whisker overlapped a large one to such a degree that the Bezier curve tracking the small whisker locked onto the large whisker. Such events were minimised by trimming all non-target whiskers to the level of the fur. Also, since our software includes capability for manual curation, we were able to rectify these errors when they did occur, by using GUI tools to nudge the control points of the errant Bezier curve back onto its target whisker. The incidence

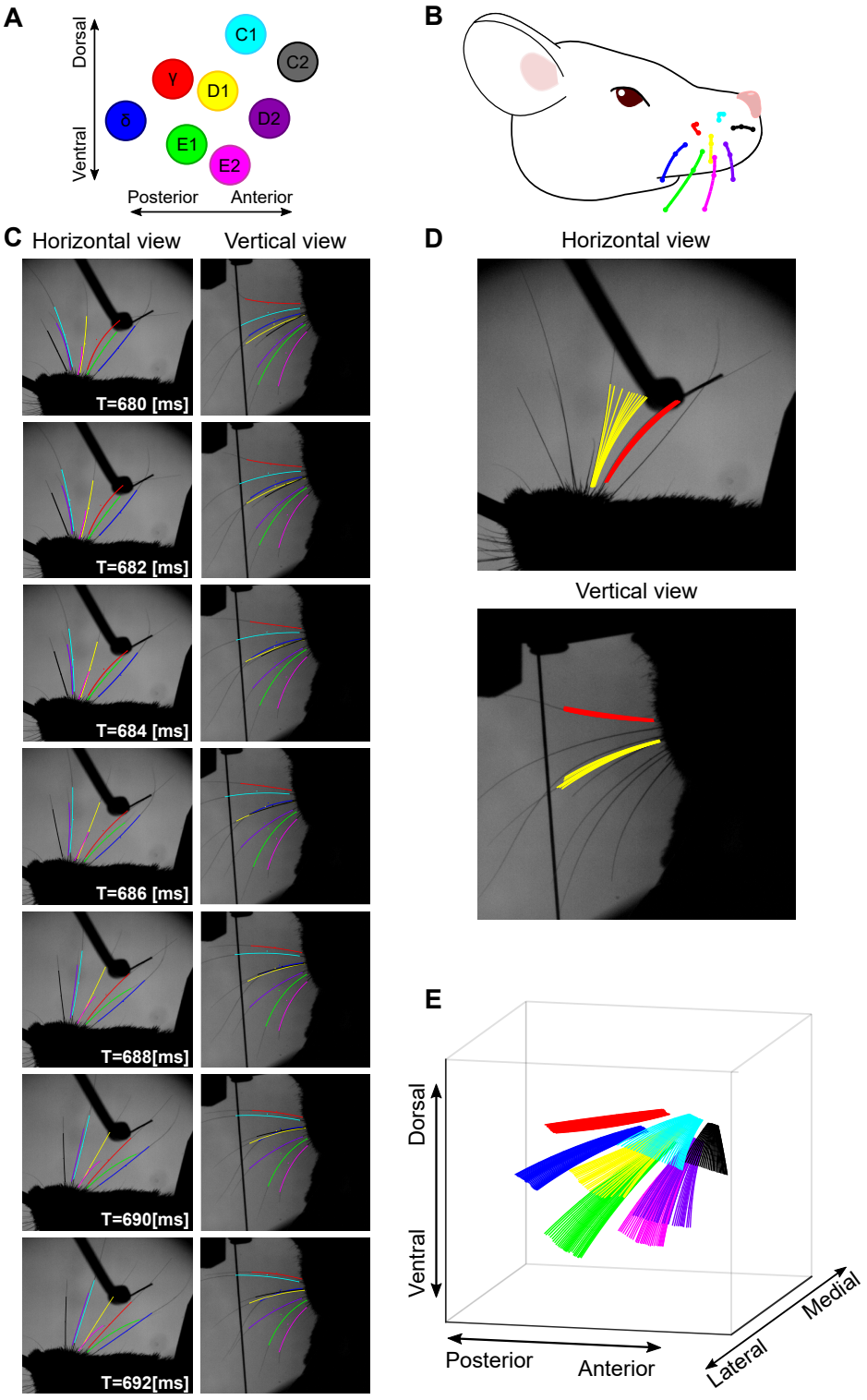

Figure 2.4: Tracking multiple whiskers in 3D. A-B) 8 whiskers were tracked in a 3.5 s video sequence (1000 frames/s). C) A sequence of 12 frames showing Bezier curves for all tracked whiskers, projected into horizontal and vertical views, taken from the example video (Movie 1, Supporting information). Whiskers are colour coded as in panel A. D) Tracking solutions for 2 whiskers (colour coded as in panel A) across 12 frames projected onto horizontal and vertical views. E) 3D tracking solutions for 8 whiskers across a sequence of 30 frames, including the sequence of panel D.

of overlap errors increased with the number of intact whiskers. It depended also on their location: there was typically less overlap within a row of whiskers than across an arc. On No-Go trials of the test data set, there were 0.01 overlap errors/whisker per 1000 frames.

Tracking was more challenging when videos included not only whisking motion but also whisker-object contact. During contact, changes in whisker position/shape from frame to frame were most often smooth and gradual (Fig 2.7, average tip speed: C1 0.71 px/ms, C2 0.72 px/ms) but, occasionally, a whisker slipped off the pole at high speed ('slip event'), generating discontinuous whisker change between adjacent frames (Fig 2.4.D-E). During such slips, tracking errors sometimes occurred, since the tracker's routine for estimating the location of a whisker based on previous frames assumes smooth motion. On Go-trials, high-speed slips occurred in a small fraction of video frames (0.23 slips/whisker per 1000 frames). As above, using the software's GUI curation tools, we were able to correct errors resulting from slips.

2.3.5 Measuring 3D whisker orientation and 3D whisker shape

Having tracked one or more whiskers in a set of videos, the next step was to use the tracking data to estimate 3D whisker kinematics and 3D whisker shape. To this end, we measured the 3D orientation of each whisker (Knutsen et al., 2008; Huet et al., 2015; Quist & Hartmann, 2012) in terms of its azimuth (θ), elevation (φ) and roll (ζ) (Fig 2.5; Methods; Movie 2).

To illustrate the method, we first estimated 3D whisker angles during free whisking, and illustrate results for a mouse with whiskers C1-C3 intact (Fig 2.6). Azimuthal whisker angle was highly correlated across whiskers (whiskers C1-C3, Pearson correlation coefficients ρ = 0.98-0.99), as was elevation (ρ = 0.94-0.99) (Fig 2.6.A). Elevation was highly anti-correlated with azimuth (ρ = -0.89- -0.96; Fig 2.6.B left). Roll angle correlated with azimuth/elevation but, consistent with (Knutsen et al., 2008), the degree of correlation was whisker-dependent (ρ = 0.13-0.80; Fig 2.6.B middle, right). Whisker-object contact perturbed these angle relationships and partially decorrelated the azimuth-elevation relationship (ρ =-0.49- -0.79).

An important feature of video-based whisker tracking is that it allows non-invasive measurement not only of kinematics but also of mechanical forces/moments acting on

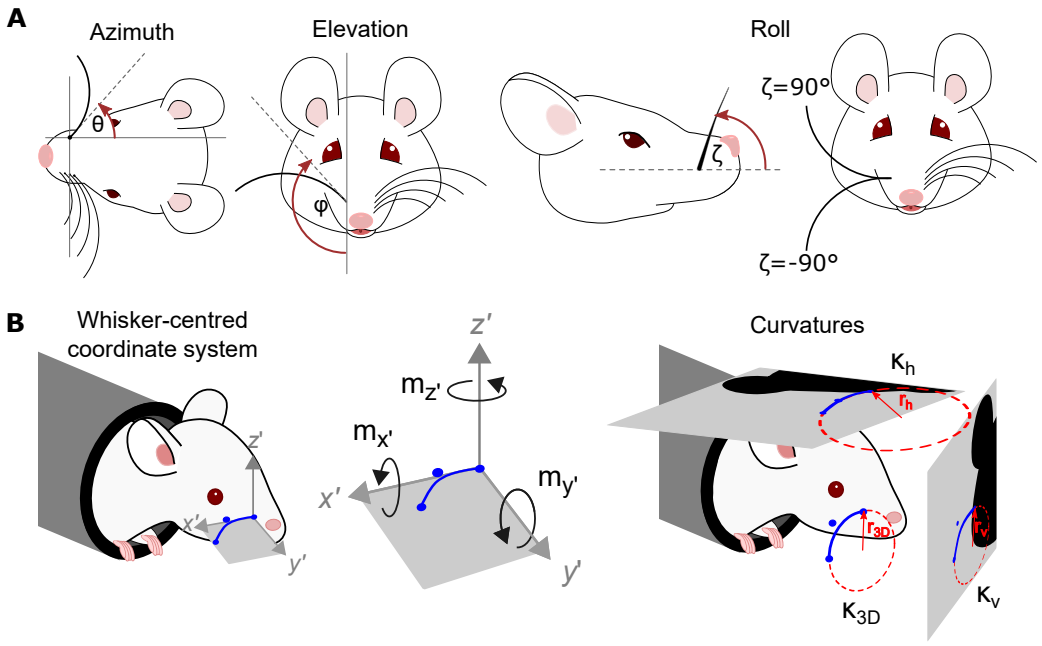

Figure 2.5: Description of a whisker in terms of 3D kinematic and 3D shape parameters. A) Azimuth (θ), elevation (φ) and roll (ζ) angles. These angles are defined with respect to the tangent to the Bezier curve $\boldsymbol{b}(s)$, describing the whisker at $s = 0$. Azimuth describes rotation about the vertical (dorso-ventral) axis through $s = 0$; elevation describes rotation about the horizontal (anterior-posterior) axis through $s = 0$; roll describes rotation about the x' axis, defined in panel B. B) Left. Whisker-centric coordinate frame with origin at $s = 0$ (Equations 2.9-2.11). The x' axis is tangent to $\boldsymbol{b}(s)$ at $s = 0$; the y' axis is the direction in which $\boldsymbol{b}(s)$ curves; the z' axis is orthogonal to the $x' - y'$ plane. Middle. Components of moment in the whisker-centric coordinate frame. Right. 2D and 3D whisker curvature (Equations 2.13-2.15). r_h and r_v denote the radii of the circles that best fit the projection of $\boldsymbol{b}(s)$ into the horizontal and vertical image planes respectively (at a given point s); r_{3D} denotes the radius of the circle that best fits $\boldsymbol{b}(s)$ itself.

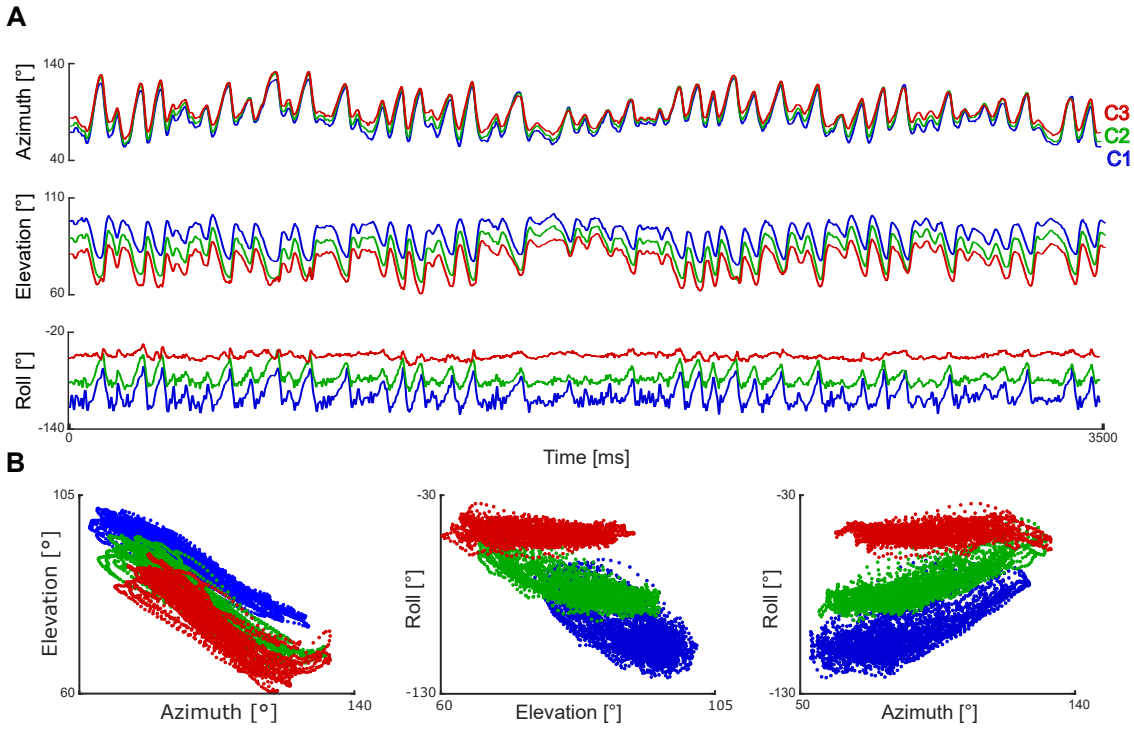

Figure 2.6: 3D whisker kinematics during free whisking. A) Changes in 3D angles for whiskers C1, C2 and C3 during a 3.5 s episode of free whisking. B) Relationships between angles.

the whiskers (Campagner et al., 2018; Huet et al., 2015; Pammer et al., 2013; Birdwell et al., 2007). The physical basis for this is that the shape of a whisker contains information about these mechanical factors. In particular, when a whisker quasi-statically bends against an object, there is a linear relationship between whisker curvature and bending moment. On this basis, studies combining video-based tracking with measurement of neural activity have discovered that bending moment is the best single predictor of mechanoreceptor activity during whisker-object contact (Campagner et al., 2018, 2016; Bush et al., 2016; Severson et al., 2017). However, it should be noted that, in other situations (whisking in the absence of object contact and dynamic situations such as texture exploration and collisions), curvature does not have the same clean, mechanical interpretation (Boubenec et al., 2012; Quist et al., 2014; Yan et al., 2013).

Previous studies have sought to measure the bending moment related to whisker-object contact by imaging in the horizontal plane (O'Connor, Peron, et al., 2010; Hires et al., 2015; Campagner et al., 2019; Zuo & Diamond, 2019; Campagner et al., 2016; Severson et al., 2017; Pammer et al., 2013; Peron et al., 2015). However, there are limitations of the planar imaging approach. First, it senses only the component

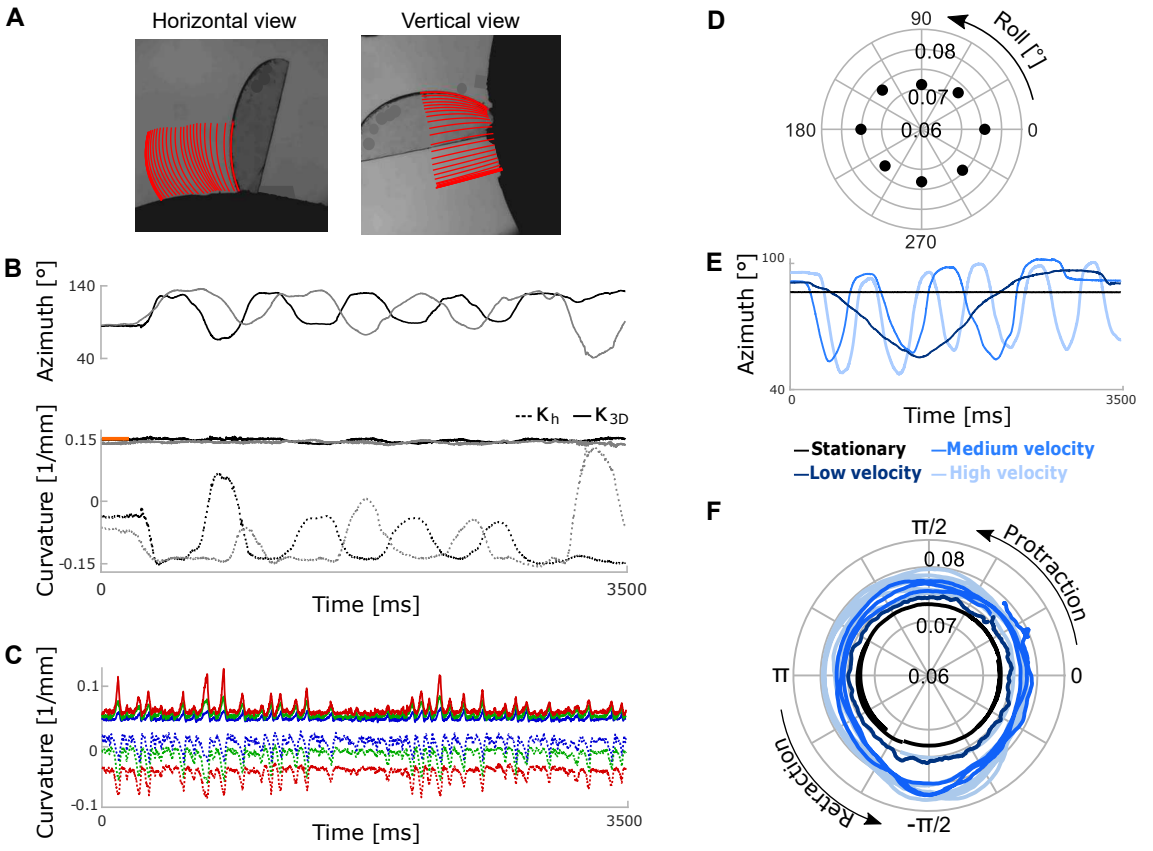

Figure 2.7: Tracking and estimating 3D curvature for a rigid test object (panels A-B), whiskers of a behaving mouse (panel C) and an ex vivo whisker (panels D-F). A) Tracking the edge of a coverslip. The coverslip was mounted, like a lollipop, on a rod; the rod was oriented in the mediolateral direction and rotated around its axis. Red lines indicate tracking results (300 frames, 10 frame intervals, 1000 frames/s). B) Top: Azimuth angle for two trials (black and grey traces). Bottom shows measured curvature: horizontal curvatures (dotted lines), κ_{3D} (solid lines) and true curvature (orange). C) Horizontal and 3D curvatures during free whisking (same trial as Fig 2.6). Solid lines represent κ_{3D} and dotted lines indicate horizontal curvatures for C1-3 (colours coded as in Fig 2.6). Fluctuations in vertical curvature were similar to those in horizontal curvature ($|\rho|>0.49$). D) κ_{3D} for a stationary ex vivo whisker (C3) at different roll angles. E) Azimuth angle for ex vivo trials with simulated whisking at different speeds. F) κ_{3D} as a function of whisking phase.

of bending moment in the horizontal image plane and necessarily misses any out-of-plane bending. Second, since whiskers roll during the whisking cycle, the shape of a whisker, as projected in the horizontal plane can change purely due to roll even during free whisking (Fig 2.7). A benefit of 3D imaging is that it addresses these limitations. First, 3D imaging enables bending in any direction to be measured. Second, it permits the intrinsic shape of a whisker to be teased apart from both its position and angular orientation. We measured the intrinsic shape, which we term κ_{3D}: $\kappa_{3D}(s)$ expresses the 3D curvature at each point s along the whisker shaft and has the key property of being invariant to curve location and to curve orientation (Methods; Equation 2.13).

First, to verify that our system accurately measures 3D curvature we tested whether

it could correctly recover the shape of a rotating, rigid object. To this end, we simulated whisking (motion with both forward-backwards and rolling components) a rigid disk, whose edge had curvature comparable to that of a typical mouse whisker (a 13 mm diameter, glass coverslip), imaged it as described above and tracked its edge (Fig 2.7.A). Due to the rolling motion, curvature in the horizontal and vertical planes, κ_h and κ_v, oscillated strongly (Fig 2.7.B). Despite this, our algorithm correctly recovered that 3D curvature κ_{3D} was constant - fluctuations (SD) in κ_{3D} were 5.6% that of κ_h and 8% that of κ_v - and matched the true curvature of the object (Fig 2.7.B).

However, when we measured $\kappa_{3D}(s)$ of whiskers from behaving mice, we found substantial fluctuations, even during free whisking (Fig 2.7.C): SD of κ_{3D} was 40-91% that of κ_h and 51-68% that of κ_v. This suggests that, in contrast to rat where the proximal segment of the whisker shaft undergoes rigid motion during whisking (Knutsen et al., 2008), during natural whisking, mouse whiskers do not behave as rigid objects. To determine whether this lack of rigidity occurs in the absence of whisker movement ('static') or whether it is dependent on movement ('dynamic'), we first positioned a (stationary) ex vivo mouse whisker (C3) in the apparatus at a series of roll angles, imaged it, tracked it and measured κ_{3D}. Varying roll angle changed κ_{3D} by up to 6% (Fig 2.7.D). Next, we 'whisked' the whisker backwards and forwards in the horizontal plane at different velocities (Fig 2.7.E) and measured κ_{3D} as a function of whisking phase (Fig 2.7.F). We found that κ_{3D} changed by up to 12% over a cycle. This change in κ_{3D} increased linearly with whisking velocity (Fig 2.7.F; $R^2 = 0.95$). Linear extrapolation to average whisking velocity observed during free whisking in mice performing our task (0.78 °/ms) implied a κ_{3D} change of 66% (C3). In comparison, changes in κ_{3D} during free whisking were 56-150% (whiskers C1-C3). Overall, these data indicate that whisker motion during free whisking in mouse is non-rigid and predominantly a dynamic effect.

Estimation of κ_{3D} allowed construction of a simple proxy to the magnitude of the bending moment, which we term $\Delta\kappa_{3D}$ (Methods). This quantity is a generalisation of the corresponding measurement from horizontal plane imaging, referred to here as $\Delta\kappa_h$. Since the mice were whisking against a vertical pole, the predominant changes in curvature were in the horizontal plane and, thus, one might expect minimal benefit

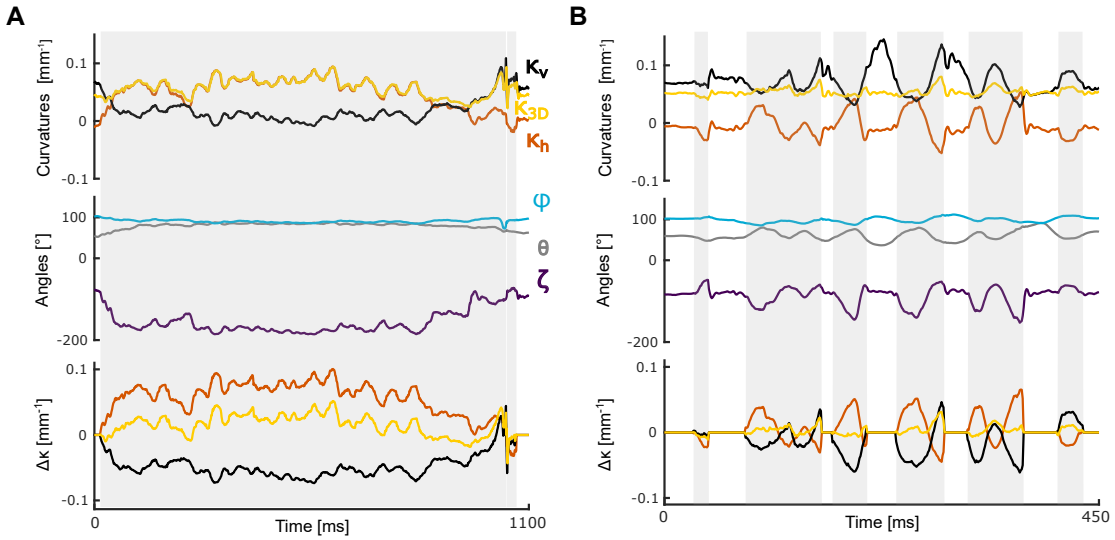

Figure 2.8: Comparison of 2D and 3D curvature as mouse whisks against a pole (whisker C2): curvatures (upper panel), 3D kinematics (middle panel) and curvature change (bottom panel, $\Delta\kappa_{3D}$, $\Delta\kappa_h$, and $\Delta\kappa_v$). A) Contact episode where both movement and bending of the whisker were largely restricted to the horizontal plane. In this case, $\Delta\kappa_{3D}$ and $\Delta\kappa_h$ were highly correlated. Grey shading indicates periods of whisker-pole contact. See Movie 3. B) Example with the same whisker as panel A for contact episode with significant vertical component of whisker motion. See Movie 4.

from the 3D approach. Even here, however, we found $\Delta\kappa_h$ to be markedly contaminated by roll. A simple instance of this effect is shown in Fig 2.8.A (Movie 3). Here, the whisker initially curved downwards (roll angle -90°): whisker-pole contact from time 0-45 ms rolled the whisker in the caudal direction (roll angle -180°) with only minimal change in 3D curvature but with a substantial effect on the curvature projected in the horizontal plane. Thus, $\Delta\kappa_h$ increased by 0.05 mm^{-1}, introducing a marked mismatch between $\Delta\kappa_h$ and $\Delta\kappa_{3D}$ (Fig 2.8.A bottom). A more typical and complex instance of the effect of roll angle is shown in Fig 2.8.B (Movie 4). Here there were large fluctuations in $\Delta\kappa_h$ (e.g., at times 310-370 ms, fifth touch) which almost entirely reflected changes in roll angle in the absence of change to 3D curvature. On average, $\Delta\kappa_h$ explained 44% of the variation in $\Delta\kappa_{3D}$ (touch periods from 47 trials). In this way, 3D imaging permits more accurate measurement of mechanical forces acting on whiskers.

2.4 Discussion

In order to obtain a comprehensive description of 3D whisker movements and 3D whisker-object interactions, we imaged mouse whisking behaviour using a high-speed

'stereo' imaging system. We developed software, first, to fit a 3D curve segment to each of one or more target whiskers and, second, to extract 3D kinematic and shape parameters from them. The new method allows both the 3D orientation (azimuth, elevation and roll) of a whisker and its intrinsic 3D curvature to be measured at millisecond frame rate, during both free whisking and whisker-object contact.

The vast majority of previous work on automatic whisker tracking has focussed on imaging in the horizontal plane (O'Connor, Peron, et al., 2010; Hires et al., 2015; Pammer et al., 2013; Peron et al., 2015; Birdwell et al., 2007; Clack et al., 2012; Boubenec et al., 2012; Wolfe et al., 2008; Szwed et al., 2006; Campagner et al., 2019; Zuo & Diamond, 2019; Campagner et al., 2016; Bale et al., 2015; Bush et al., 2016; Severson et al., 2017). However, as detailed in the Introduction, single-plane imaging necessarily captures only a fraction of the full 3D kinematic and 3D shape parameters that characterise a whisker. The advance here is a system able to extract a full 3D description of both whisker kinematics and whisker shape. The tracking algorithm is automatic (after initialisation) and achieves accurate performance under our typical conditions. The system also includes GUI error correction tools, which allow accuracy to be further improved, and extend the applicability of the system to more challenging situations.

Our work builds on previous advances in 3D whisker tracking in behaving rodents. Methods based on linear CCD arrays and markers provide simple and effective means to measure some aspects of 3D whisker kinematics, but also have limitations. CCD arrays (Bermejo et al., 2002) image whiskers at a single point along the shaft: this method confounds whisker translation with whisker rotation, cannot measure whisker shape and cannot recover roll angle. Also, CCD study of 3D whisking has been limited to one whisker at a time. The approach of marking a whisker with spots of dye (Knutsen et al., 2008; Roy et al., 2011) has been used to recover all 3 orientation angles but has not been used to measure whisker shape changes during object touch. Also, although application of dye marker dots was reported not to disturb rat whisking, mouse whiskers are thinner, less stiff and hence more liable to perturbation. Our method addresses these limitations by leveraging the extra information available from video, and achieves automatic, non-invasive multi-whisker tracking, as well as the ability to recover not only three-angle kinematic information but also information

about whisker shape changes during object contact. The only previous 3D video-based study (Huet et al., 2015) required manual tracking for the vertical view. Our algorithm runs on a standard workstation and the system only requires the addition of a second camera to an existing 2D imaging setup.

The method presented here has some limitations. First, although the error rate was low, the experimental conditions were designed to avoid both extensive object-whisker occlusion (by using a stimulus object with small foot-print) and extensive whisker-whisker overlap (by trimming non-target whiskers). Error rates are likely to be higher in the presence of experimental apparatus where there is more occlusion or if no whisker trimming is carried out. Use of additional cameras provides a potential way to reduce error rates further (and can be incorporated through adding terms analogous to Equations 2.5-2.6 to the cost function of Equation 2.4). Second, our tracker describes the basal segment of the whisker, not the full whisker, since our focus is primarily on elucidating the fundamental mechanical events that drive neural activity in the whisker system. To track a whisker across its entire length, a quadratic curve description is insufficient. One direction for future work is to investigate whether the tracker can be extended to fit higher degree Bezier curves without excessive loss of robustness. Third, our method has been developed for head-fixed mice. This has the advantage that it simplifies the tracking problem. However, it would also be useful to extend the approach to freely moving animals, perhaps by combining whisker tracking with head-body tracking (Vanzella et al., 2019; Knutsen et al., 2005; Hewitt et al., 2018; Pasquet et al., 2016; Voigts et al., 2008; Gyory et al., 2010; Perkon et al., 2011; Nashaat et al., 2017; Gillespie et al., 2019).

In conclusion, although whisker movements are well-known to be 3D, previous, automatic methods for tracking whiskers from high-speed video were limited to the horizontal plane. Here, we obtained 3D information using a two-camera, high-speed imaging system and developed computational methods to reconstruct 3D whisker state from the video data. Our method permits measurement of both 3D whisker kinematics and whisker shape changes at millisecond frame rate from awake, behaving mice. The method can be combined with cellular resolution neural activity measurement and thus has potential to advances our understanding of sensorimotor behaviour and its neural basis.

2.5 Methods

All experimental protocols described in this section were approved by both United Kingdom Home Office national authorities and institutional ethical review. All parameters and variables used in this section are summarised in Table 2.1. All computer code was written in MATLAB (The MathWorks Inc., Natick, MA) and run on a standard workstation (Core i7, 16GB RAM).

2.5.1 Behavioural apparatus

Mice (C57; males; 6 weeks at the time of implant) were implanted with a titanium head-bar as detailed in (Campagner et al., 2016). After surgery, mice were left to recover for at least 5 days before starting water restriction (1.5 ml water/day). Training began 7-10 days after the start of water restriction. Mice were trained and imaged in a dark, sound-proofed enclosure using apparatus adapted from (Campagner et al., 2016). A head-fixed mouse was placed inside a perspex tube, from which its head emerged at one end. The stimulus object was a 0.2 mm diameter, vertical carbon fibre pole which could be translated parallel to the anterior-posterior (AP) or mediolateral (ML) axes of the mouse by a pair of linear stepper motors and rotated in the horizontal plane to 'Go' or 'No-Go' locations by a rotatory stepper motor. To allow vertical movement of the pole into and out of range of the whiskers, the apparatus was mounted on a pneumatic linear slide, powered by compressed air. The apparatus was controlled from MATLAB via a real-time processor. Mouse response was monitored by a lick port located anterior to the mouth. Licks were detected as described in (O'Connor, Clack, et al., 2010). Each lick port consisted of a metal tube connected to a water reservoir via a computer-controlled solenoid valve. Lick port position was monitored using an infrared camera and adjusted using a micromanipulator.

2.5.2 Behavioural task

Head-fixed mice were trained to detect the presence of a metal pole using a single row of whiskers. The animal training contained two stages: first, animals were trained to solve the task with the whisker pad intact. Once they reached 70% of accuracy during one session, whiskers were trimmed to a single row. Mice were then trained

until they again reached 70% accuracy during a session. Usually, animals reached the final learning criterion after three weeks of training. At the point of data acquisition, mice were 10-11 weeks of age. On each trial, the pole was presented either within reach of the whiskers ('Go trial') or out of reach ('No-Go trial'). At the start of each trial, the computer triggered the pole to move up (travel time 100 ms). The pole stayed up for 1 s, before moving down. On Go trials, the correct response was for the mouse to lick a lick port. Correct responses were rewarded by a drop of water (10 μl). Incorrect responses on Go trials (not licking) were punished by timeout (3-5 s). On No-Go trials, the correct response was to refrain from licking and incorrect responses (licking) were punished by timeout and tone (frequency 12 kHz).

2.5.3 High-speed stereo whisker imaging

Whiskers were imaged based on the methods of (Campagner et al., 2016), except that, to provide 3D information, two cameras were used. The whiskers were imaged using two high-speed cameras (Mikrotron LTR2, Unterschleissheim, Germany; 1000 frames/s, 0.4 ms exposure time) via telecentric lenses (Edmunds Optics 55-349, Barrington, NJ) as illustrated in Fig 2.1. Illumination for each camera was provided by a high-power infrared LED array (940 nm; Roithner LED 940-66-60, Vienna, Austria) via diffuser and condensing lens. The imaging planes of the two cameras were horizontal (spanning AP and ML axes) and vertical respectively. The field of views were typically 480×480 pixels, with pixel width of 0.047 mm. The two cameras were synchronised by triggering data acquisition off the computer-generated TTL pulse that initiated a trial. Typically, imaging data were acquired in an interval starting 0.5 s before pole onset, ending 1.8 s after pole onset. To provide an independent check that data files from the two cameras came from corresponding trials, an IR LED was positioned in the corner of the field of view of each camera and, starting at pole onset on each trial, flashed a binary sequence that encoded the trial number. Onset of this LED signal also served to verify camera synchrony.

2.5.4 Coordinate frame and calibration

To describe the location of whiskers in 3D, we used a left-handed Cartesian coordinate frame, fixed with respect to the head of the animal (Fig 2.1). The axes were x (AP, with positive x posterior); y (ML, with positive y medial) and z (DV, with positive z dorsal). In standard anatomical convention, the $x-y$ (AP-ML) plane was horizontal; the $x-z$ (AP-DV) plane sagittal and the $y-z$ (ML-DV) plane coronal. The column vector $\boldsymbol{p}^{3D} = (x, y, z)$ denotes a point with coefficients along the x, y and z axes respectively. Throughout, we denote vectors by lower-case bold (e.g., $\boldsymbol{p}$), scalars by lower-case italic (e.g., s) and matrices by upper-case bold (e.g., $\boldsymbol{M}$).

Analogously to stereoscopic vision, our whisker tracker reconstructs 3D whisker location/orientation from images obtained from two viewpoints - horizontal and vertical. Pixel locations in the horizontal image were defined using the x and y axes of the 3D frame (Fig 2.1). Thus, the location of a point $\boldsymbol{p}^H$ in the horizontal image was described by a column vector (x, y). Pixel location $\boldsymbol{p}^V$ in the vertical image was described by a column vector (v, w), defined with respect to axes v and w (Fig 2.1). Due to the orientation of the vertical-view camera detailed above, the v, w coordinate frame was rotated and translated with respect to the x, y, z frame. The relation between the x, y, z and v, w coordinate frames was determined as follows.

With a telecentric lens, only light rays parallel to the optical axis pass through the camera aperture and contribute to the image. In contrast to standard lenses, a telecentric one provides equal magnification at a wide range of object-lens distances and forms an orthogonal projection, facilitating the reconstruction of 3D objects (Li & Tian, 2013). Since the imaging was done with telecentric lenses, the mappings from 3D to the two image planes were described as orthogonal projections. The projections of a 3D point $\boldsymbol{p}^{3D}$ onto a 2D point $\boldsymbol{p}^H$ in the horizontal image plane and a 2D point $\boldsymbol{p}^V$ in the vertical plane were:

$$\boldsymbol{p}^H = \boldsymbol{H}\boldsymbol{p}^{3D} + \boldsymbol{h} \tag{2.1}$$

$$\boldsymbol{p}^V = \boldsymbol{V}\boldsymbol{p}^{3D} + \boldsymbol{v} \tag{2.2}$$

$\boldsymbol{H}$ and $\boldsymbol{V}$ were 2x3 matrices; $\boldsymbol{h}$ and $\boldsymbol{v}$, 2-element column vectors. The 3D coordinate frame and the horizontal image frame had common x and y axes and a common x, y origin: hence, $\boldsymbol{H}$=[1 0 0; 0 1 0] and $\boldsymbol{h}$=[0;0].

To determine the mapping from 3D to the vertical image plane ($\boldsymbol{V}$ and $\boldsymbol{v}$), we performed the following calibration procedure. Using stepper motors, we moved an object with 2 protruding pins on a 3D path through the region of the behavioural setup where the target whiskers were typically located, and recorded a sequence of 100 corresponding images on each camera. The z location of each pin was known in each image. We then tracked the tips of the 2 pins in each horizontal and vertical image frame to obtain a time series consisting of the (x, y, z) and (v, w) coordinates of each pin tip. Using Equation 2.2, $\boldsymbol{V}$ and $\boldsymbol{v}$ were then estimated by linear regression. The variance of the regression residuals was low ($<$0.1% of total variance for data of Fig 2.6).

2.5.5 Bezier curve framework for whisker tracking

Our aim was to develop 'whisker tracker' software to track the orientation and shape of one or more target whiskers. The whisker tracker described each target whisker segment as a Bezier curve, since these have convenient mathematical properties (Fig 2.2). A Bezier curve is a parametric curve segment $\boldsymbol{b}(s) = (x(s), y(s), z(s))$, where $0 \leq s \leq 1$ parameterises location along the curve segment: in our case, $s = 0$ marked the end closest to the whisker base and $s = 1$ marked the end furthest from the base. The shape, orientation and position of a Bezier curve are determined by its 'control points', the number of which determines the complexity of the curve. We used quadratic Bezier curves, which have 3 control points $\boldsymbol{cp}_i$ where i=0,1,2, each with coordinates (x, y, z). These control points were termed "proximal" ($\boldsymbol{cp}_0$), "middle" ($\boldsymbol{cp}_1$) and "distal" ($\boldsymbol{cp}_2$) according to their distance from the whisker base. $\boldsymbol{cp}_0$ defined the location of the basal end of the whisker segment, $\boldsymbol{cp}_2$ the distal end and $\boldsymbol{cp}_1$ the shape. In terms of these control point parameters, a quadratic Bezier curve $\boldsymbol{b}(s)$ was expressed as:

$$\boldsymbol{b}(s) = \boldsymbol{cp}_0(1-s)^2 + 2\boldsymbol{cp}_1(1-s)s + \boldsymbol{cp}_2 s^2 \tag{2.3}$$

2.5.6 Whisker tracking pipeline

Overview. Whisker tracking was operated via a Graphical User Interface (GUI). The GUI allowed a user to load a pair of corresponding videos (horizontal view and vertical view). The first step was to calibrate, as detailed above. Next, to initialise tracking, target whiskers were specified (automatically or manually) by defining approximate locations for Bezier control points. After initialisation, each video frame was processed automatically, in turn. Tracking direction could be set to be either forwards or backwards in time. First, the contour of the snout was located in both horizontal and vertical views. Second (except in the first frame), initial estimates for the Bezier control points were calculated by linear extrapolation from their locations in the previous frames. Third, each Bezier curve was fitted to the image data by adjusting its control points to minimise the cost function defined below (Equation 2.4). Provided the quality of fit for a given Bezier curve met a minimum threshold, tracking of that curve proceeded automatically to the next frame.

Manual initialisation (Fig 2.3 left panel). When tracking a video for the first time, the first step was to specify the target whiskers. In the first frame of the video, the user employed a graphical user interface (GUI) to select sets of control points, specifying one or more target whiskers. For each target whisker, the user defined approximate locations for control points specifying a curve segment corresponding to the basal segment of the whisker, by making computer-mouse clicks within the video images. For each target whisker, the user first specified (x, y) coordinates for the 3 control points in the horizontal view from proximal to distal. Since the imaging geometry was described by linear equations (Equations 2.1-2.2), each such point corresponded to a line in the vertical view. In the vertical view, the user specified a point (v, w) along each vertical line where it intersected the target whisker. From these (x, y, v, w) data, the z coordinates of the control point estimates were calculated from the calibration equation (Equation 2.2). Once initial values for all 3 control points of a given target whisker were specified, refined estimates were calculated by the fitting procedure described below. The refinement process enhanced the robustness of the algorithm to find similar solutions when initial estimates of the control points are used, for example, when different users initialise the same video. On average, two different initialisations

of the same video changed the estimation of the whisker angles by less than 1% (Azimuth angle = 0.13%, Elevation angle = 0.2%), while whisker curvatures estimation was affected by less than 10% (κ_h = 6.3%,κ_v = 1.6%). In order to obtain a reference value for the length of each curve, the arc length of each Bezier curve was calculated. To obtain a reference value for the distance of the proximal control point from the snout, a second-order polynomial was fitted to the Bezier curve and extrapolated to find its intersection with the snout contour.

Automatic initialisation. Typically, an experiment will result in many videos taken of the same mouse under identical experimental conditions. Once one video was tracked using the manual initialisation procedure described above, other videos could then be initialised automatically through a template-matching approach. To initialise tracking of a new video, the user selected a previously tracked video (via the GUI). For each target whisker from this file, a sample of Bezier curve 'templates' were extracted (typically, the solution in every fifth video frame) and goodness of fit of each sample curve to the first frame of the new video was calculated (using the cost function, Equation 2.4). The lowest cost template was then selected. The template was refined by optimising the fit with respect to translations along both x and z axes (within the range $\pm$5 pixels).

Snout contour detection (Fig 2.3 middle panel). First, to isolate the contour of the snout in a given video frame, fine structure such as the hairs of the fur and the whiskers were removed by median filtering (5×5 pixels, 0.23×0.23 mm) of the images followed by smoothing with a Gaussian filter (SD = 12 pixels, 0.56 mm). Next, the spatial gradient of each filtered image was calculated in a direction approximately normal to the snout contour. This gradient was small, except at the edge of the snout where it had a large peak. In the horizontal image, the snout contour was estimated as a function of the x coordinate by minimising the gradient with respect to y. In the vertical image, the snout contour was estimated as a function of the w coordinate by minimising the gradient with respect to v.

Bezier curve fitting (Fig 2.3 right panel). To achieve 3D tracking, we fitted 3D Bezier curves to the horizontal and vertical view image data by varying the locations of their control points so as to minimise the following cost function. Control points for each target whisker were optimised independently:

$$E(f) = E_h(f) + E_v(f) + R_1(f) + R_2(f) \tag{2.4}$$

Here $E(f)$ is the cost (or mismatch) between the image data of frame f and the Bezier curve $\boldsymbol{b}(f,s) = (x(f,s), y(f,s), z(f,s))$, defined by control points $\boldsymbol{cp}_0(f)$, $\boldsymbol{cp}_1(f)$ and $\boldsymbol{cp}_2(f)$. $E_h(f)$ and $E_v(f)$ quantified how well $\boldsymbol{b}(f,s)$ described, respectively, the horizontal and vertical image data of frame f. $R_1(f)$ and $R_2(f)$ were regularising terms (defined below). In the following, to keep down clutter in the notation, dependence on frame and whisker is omitted except where necessary for clarity.

E_h and E_v were defined as line integrals over the projection of $\boldsymbol{b}(s)$ in the horizontal/vertical images respectively:

$$E_h = \oint_{s=0}^{s=1} ds I_h(x(s), y(s)) \tag{2.5}$$

$$E_v = \oint_{s=0}^{s=1} ds I_v(v(s), w(s)) \tag{2.6}$$

Here: $I_h(x,y)$ was the intensity at point (x,y) in the horizontal view image, calculated by linear interpolation between pixel values and $I_v(v,w)$ the analogous quantity for the vertical view image; $(x(s), y(s))$ was the projection of $\boldsymbol{b}(s)$ in the horizontal view image and $(v(s), w(s))$ its projection in the vertical view image (Equations 2.1 and 2.2).

Except at occasional slip-stick events, whiskers move smoothly and, when imaged at 1000 frames/s, changes in location and shape from frame to frame were usually small, particularly for the basal segment. The regularising term R_1 formalised this prior knowledge of natural whisking behaviour ('temporal contiguity'):

$$R_1(f) = \frac{1}{2}\sigma_1 \sum_{i=0}^{i=2} \left\| \boldsymbol{cp}_i(f) - \widehat{\boldsymbol{cp}}_i(f) \right\|^2 \tag{2.7}$$

Here: $\boldsymbol{cp}_i(f)$ was the location of control point i of the whisker in frame f and $\widehat{\boldsymbol{cp}}_i(f)$ was its location estimated by linear extrapolation based on its location in the previous two frames; σ_1 was a variable gain that the user could set from the GUI.

Additional regularisation was necessary to address degeneracy that could arise when tracking near-straight whiskers. Since a line segment is fully described by the location of its two ends, a straight whisker is fully defined by its proximal and distal

control points – in this case, the middle control point is ill-defined. We found, in such situations, that the middle control point tended to migrate towards the whisker base and to generate high-curvature, unnatural shapes when extrapolating the curve to the snout contour (see above). To address this, we used a second regularising term which penalised deviations of the middle control point away from the midpoint between the proximal and distal control points:

$$R_2(f) = \frac{1}{2}\sigma_2 \left\| \frac{(\boldsymbol{cp}_1(f) - \boldsymbol{cp}_0(f))^T \boldsymbol{q}(f)}{\|\boldsymbol{q}(f)\|} - \frac{1}{2}\|\boldsymbol{q}(f)\| \right\|^2 \tag{2.8}$$

Here $\boldsymbol{q}(f) = \boldsymbol{cp}_2(f) - \boldsymbol{cp}_0(f)$ and σ_2 was a user-adjustable gain. R_2 measured deviation of the component of the middle control point $\boldsymbol{cp}_1(f)$ (relative to $\boldsymbol{cp}_0(f)$) in the direction of $\boldsymbol{cp}_2(f)$ (relative to $\boldsymbol{cp}_0(f)$) away from the midpoint of the $\boldsymbol{cp}_0(f) - \boldsymbol{cp}_2(f)$ line.

Nonlinear cost functions can be difficult to minimise due to local minima. However, in the present case, due to the smooth motion of whiskers referred to above, we expected control point solutions usually to be close to their values in the previous frame. It was therefore effective to use a local search strategy, where the initial value for a given control point was set by extrapolating its values from the previous two frames ($\widehat{\boldsymbol{cp}}_i(f)$), but this also made it possible to track multiple whiskers independently. The cost function (Equation 2.4) was minimised (using MATLAB function 'fminunc') with respect to components of the control points. To counter-act possible drift of $\boldsymbol{b}(s)$ along the whisker shaft over time, or change in the arc-length of $\boldsymbol{b}(s)$ over time, we minimised the cost function with respect to components of $\boldsymbol{cp}_0$ and $\boldsymbol{cp}_2$ normal to $\boldsymbol{b}(s)$ at $s = 0$ and $s = 1$ respectively. This procedure also had the advantage of reducing the number of free parameters from 9 to 7. Furthermore, after convergence in a given frame, both the arc length of $\boldsymbol{b}(s)$ and the distance of $\boldsymbol{cp}_0$ to the snout were normalised to equal their reference values set in the first frame (see above), whilst preserving curve shape.

Error correction. As noted above, tracking of each target whisker proceeded automatically to the next frame, so long as the cost E (Equation 2.4) remained less than a user-defined threshold (adjustable via the GUI). Should the threshold be exceeded, for example when a Bezier curve was 'left behind' by a rapid, discontinuous motion of its target whisker during a slip event, tracking of that whisker ceased. To correct such an error, the GUI had tools allowing the user to nudge control points back onto

the target whisker, and to restart automatic tracking.

2.5.7 Extracting 3D kinematics of the tracked whiskers

The next step was to use the tracking data to estimate 3D whisker kinematics and 3D whisker shape. Since whiskers bend during whisker-object contact, and since this contact-induced whisker bending is a fundamental driver of neural activity (see Introduction), it was important to develop a general procedure for describing 3D whisker motion, applicable to non-rigid whisker movement. We separated changes to the orientation of a quadratic curve from changes to its shape in the following manner.

Formally, we described whisker orientation by the following 'whisker-centred' Cartesian coordinate frame $x'y'z'$, with origin at $s = 0$ (Huet et al., 2015). In contrast to the head-centred coordinate frame xyz, the $x'y'z'$ frame is time-dependent; rotating and translating along with its target whisker. The $x'-$axis is aligned to the longitudinal axis of the whisker (tangent to $\boldsymbol{b}(s)$ at $s = 0$). The y'-axis is orthogonal to the $x'-$axis, such that the $x' - y'$ plane is that within which $\boldsymbol{b}(s)$ curves. The z'-axis is orthogonal to both x' and y' axes. Let $\boldsymbol{i'}$, $\boldsymbol{j'}$ and $\boldsymbol{k'}$ be unit vectors that point in the direction of the x', y' and z' axes respectively:

$$\boldsymbol{i'} = \left. \frac{\frac{d\boldsymbol{b}}{ds}}{\left|\frac{d\boldsymbol{b}}{ds}\right|} \right|_{s=0} \tag{2.9}$$

$$\boldsymbol{j'} = \left. \frac{\frac{d^2\boldsymbol{b}}{ds^2}}{\left|\frac{d^2\boldsymbol{b}}{ds^2}\right|} \right|_{s=0} \tag{2.10}$$

$$\boldsymbol{k'} = \boldsymbol{i'} \times \boldsymbol{j'} \tag{2.11}$$

Here $\boldsymbol{i'} \times \boldsymbol{j'}$ denotes the cross product of vectors $\boldsymbol{i'}$ and $\boldsymbol{j'}$. The orientation of a whisker was then described by the 3D angle of the $x'y'z'$ coordinate frame with respect to the xyz coordinate frame. We translated the frames to have a common origin and then calculated the 3D rotation matrix that rotates the xyz frame to the $x'y'z'$ frame (Goldstein et al., 2002). This rotation can be described as the net effect of an ordered sequence of three elemental rotations with angles θ (azimuth), φ (elevation) and ζ

(roll), and was expressed as a matrix $\boldsymbol{R}(\theta,\varphi,\zeta)$. Azimuth describes rotation in the horizontal $x-y$ plane, about an axis parallel to the z axis through the whisker base; elevation describes rotation in the vertical $x-z$ plane, about an axis parallel to the y axis; roll describes rotation around the axis of the whisker shaft (Fig 2.5). We determined the angles θ,φ,ζ for a given whisker at a given time point by minimising the error function:

$$\sum(\boldsymbol{R}(\theta,\varphi,\zeta)[\boldsymbol{i'j'k'}]-[\boldsymbol{ijk}])^2 \tag{2.12}$$

Here $\boldsymbol{i}$, $\boldsymbol{j}$ and $\boldsymbol{k}$ are column unit vectors parallel to the x, y and z axes and the summation is over all matrix elements.

2.5.8 Extracting 3D shape and bending moment of the tracked whiskers

Having described the orientation of a whisker, the next task was to describe its shape. By 'shape', we intend those geometric properties of a curve that are invariant to its location and orientation. As noted above, we described whiskers by quadratic curve segments, which curve entirely within a plane (geometric torsion $\tau(s)=0$). The intrinsic shape of a quadratic curve is fully described by a curvature function $\kappa_{3D}(s)$ (Marsh, 2006):

$$\kappa_{3D}(s)=\frac{\left|\frac{d\boldsymbol{b}(s)}{ds}\times\frac{d^2\boldsymbol{b}(s)}{ds^2}\right|}{\left|\frac{d\boldsymbol{b}(s)}{ds}\right|^3} \tag{2.13}$$

Here $|\boldsymbol{a}|$ denotes the magnitude (2-norm) of vector $\boldsymbol{a}$. $\kappa_{3D}(s)$ has units of 1/distance and is the reciprocal of the radius of the circle that best fits the curve at point s. We computed planar curvatures as:

$$\kappa_h(s)=\left.\frac{\frac{dx}{ds}\frac{d^2y}{ds^2}-\frac{d^2x}{ds^2}\frac{dy}{ds}}{\left(\left(\frac{dx}{ds}\right)^2+\left(\frac{dy}{ds}\right)^2\right)^{\frac{3}{2}}}\right|_{s=0} \tag{2.14}$$

$$\kappa_v(s) = \left. \frac{\frac{dz}{ds}\frac{d^2y}{ds^2} - \frac{d^2z}{ds^2}\frac{dy}{ds}}{\left(\left(\frac{dz}{ds}\right)^2 + \left(\frac{dy}{ds}\right)^2\right)^{\frac{3}{2}}} \right|_{s=0} \tag{2.15}$$

Here $x(s)$,$y(s)$,$z(s)$ are the components of $\boldsymbol{b}(s)$ in the x, y, z coordinate frame. Note, as detailed in Results, that, in contrast to $\kappa_{3D}(s)$, $\kappa_h(s)$ and $\kappa_v(s)$ are not invariant measures of geometric shape; they depend also on curve orientation.

In whisker-centric coordinates, bending corresponds to changes in shape of $\boldsymbol{b}(s)$ in the $x' - y'$ or $x' - z'$ planes (with, respectively, component $\boldsymbol{m}'_z$ defined in the direction of the positive z' axis and $\boldsymbol{m}'_y$ defined in the directions of the positive y' axis) (Fig 2.5;(A. E. Yang & Hartmann, 2016)). Since $\boldsymbol{b}(s)$ is a quadratic curve, it has zero torsion and its curvature is entirely confined to the $x' - y'$ plane: $\kappa_{3D}(s)$ is the curvature in this plane; the only non-zero component of bending moment is $\boldsymbol{m}'_z$. Applying the standard relation between bending moment about a given axis and curvature in the plane normal to that axis (Birdwell et al., 2007; Quist & Hartmann, 2012), it follows that $\boldsymbol{m}'_z(s)$ is proportional to:

$$\Delta\kappa_{3D}(s) = \kappa_{3D}(f, s) - \kappa_{3D,0}(s) \tag{2.16}$$

where $\kappa_{3D,0}(s)$ is the curvature when the whisker is free from contact and in its resting state. All results presented here were evaluated at $s = 0$.

2.6 Supporting information

Movie 1 : Tracking example of 8 whiskers. Left: horizontal view of the whiskers and tracking superimposed. Colours are shown as in Fig 2.4.A. Axes are shown as in Fig 2.1.B. Middle: Vertical view of the whiskers and tracking superimposed. Right: Bezier curves in the three-dimensional space. Axes are shown as in Fig 2.1.A. https://doi.org/10.1371/journal.pcbi.1007402.s001

Movie 2: Whisker tracking and variables. Top: Horizontal and vertical views with tracking superimposed. Colours are shown as in Fig 2.4.A. Bottom: 3D kinematic and 3D shape parameters: Horizontal angle (Azimuth), vertical angle (Elevation), horizontal and vertical curvature, κ_{3D} and roll for each tracked whisker.

https://doi.org/10.1371/journal.pcbi.1007402.s002

Movie 3: Whisker tracking example of movement restricted to the horizontal plane (Fig 2.8.A). Top from left to right: Horizontal and vertical views with tracking of C2 superimposed. Bezier curve in the whisker centred coordinate frame isolating roll angle (Fig 2.5.A). Comparison of whisker shape over time: Dashed line represents the whisker shape at $t = 0$ ms and solid line represents whisker shape of current frame. Bezier curve was rotated using azimuth, elevation and roll angle to be captured in the two-dimensional plane. Bottom from left to right: Horizontal angle (Azimuth), Vertical angle (Elevation), Roll, horizontal curvature and 3D curvature over time. Colours are shown as in Fig 2.8.A.

https://doi.org/10.1371/journal.pcbi.1007402.s003

Movie 4: Whisker tracking example of movement with significant vertical components (Fig 2.8.B). Top from left to right: Horizontal and vertical views with tracking of C2 superimposed. Bezier curve in the whisker centred coordinate frame isolating roll angle (Fig 2.5.A). Comparison of whisker shape over time: Dashed line represents the whisker shape at $t = 0$ ms and solid line represents whisker shape of current frame. Bezier curve was rotated using azimuth, elevation and roll angle to be captured in the two-dimensional plane. Bottom from left to right: Horizontal angle (Azimuth), Vertical angle (Elevation), Roll, horizontal and 3D curvature over time. Colours are shown as in Fig 2.8.A.

https://doi.org/10.1371/journal.pcbi.1007402.s004

Table 2.1: Parameters and variables summary.

Axes	
x	Anterior-posterior axis, with positive posterior
y	Medio-lateral axis, with positive medial
z	Dorsal-ventral axis, with positive dorsal
v	Medio-lateral axis from the vertical view, with positive medial
w	Dorsal-ventral axis from the vertical view, with positive ventral
x'	Axis ofthe whisker centred coordinated frame described as tangent to the whisker at $s = 0$. Positive indicates toward the tip of the whisker.

y'	Axis ofthe whisker centred coordinated frame defined by the second derivative of the Bezier curve at $s = 0$. Positive indicates $s > 0$
z'	Axis from the whisker centred coordinated frame defined as the cross product between x' and y'
Calibration	
$\boldsymbol{p}^H$	Point in the horizontal plane with coefficients $(x, y)^T$
$\boldsymbol{H}$	Matrix related to mapping between $\boldsymbol{p}^{3D}$ and $\boldsymbol{p}^H$. $\boldsymbol{H} = [100; 010]$
$\boldsymbol{p}^{3D}$	Point with coefficients $(x, y, z)^T$
$\boldsymbol{h}$	Vector related to the mapping between $\boldsymbol{p}^{3D}$ and $\boldsymbol{p}^H$. $\boldsymbol{h} = [0; 0]$
$\boldsymbol{p}^V$	Point in the vertical plane with coefficients $(v, w)^T$
$\boldsymbol{V}$	Matrix related to mapping between $\boldsymbol{p}^{3D}$ and $\boldsymbol{p}^V$. Values of $\boldsymbol{V}$ are fitted during the calibration procedure
$\boldsymbol{v}$	Vector related to the mapping between $\boldsymbol{p}^{3D}$ and $\boldsymbol{p}^V$. Values of $\boldsymbol{v}$ are fitted during the calibration procedure
Bezier curves and fitting process	
$\boldsymbol{b}(s)$	Bezier curve evaluated at s where $0 \leq s \leq 1$
$\boldsymbol{cp}_i$	Control point $i = 0, 1, 2$ with coordinates $(x, y, z)^T$
j	whisker
f	frame
$E_v(f, j)$	Term from objective function (Equation 2.4) related to vertical image
$E_h(f, j)$	Term from objective function (Equation 2.4) related to horizontal image
$I_h(x, y)$	Intensity at the point (x, y) in the horizontal image
$I_v(v, w)$	Intensity at the point (v, w) in the vertical image
R_1	Regularising term from the objective function related to temporal contiguity
R_2	Regularising term from the objective function related to shape complexity
σ_1	Selectable parameter that weights the first regularising factor R_1
σ_2	Selectable parameter that weights the second regularising factor R_2
$\boldsymbol{q}$	Vector related to Equation 2.8
Extraction of kinematic parameters	

$\boldsymbol{i'}$	Unit vector that points in the direction of x'
$\boldsymbol{j'}$	Unit vector that points in the direction of y'
$\boldsymbol{k'}$	Unit vector that points in the direction of z'
ζ	Rotation angle of the whisker respect to x'
θ	Azimuth angle defined as the angle between the x axis and the projection of tangent at the base ofthe whisker in the horizontal plane
φ	Elevation angle defined as the angle between the $-z$ axis and the projection of tangent at the base of the whisker in the vertical image
$\kappa_{3D}(s)$	3D Curvature evaluated at s
$\kappa_h(s)$	Curvature of the projection of the Bezier curve in the horizontal plane evaluated at s
$\kappa_v(s)$	Curvature of the projection of the Bezier curve in the vertical image evaluated at s

Chapter 3

Predicting spikes of Barrel Cortex neurons from sensory data during active sensation

3.1 Abstract

The whisker system is a widely used model to study somatosensation. Nonetheless, the sensory signals represented in the barrel cortex in behaving animals and those features which modulate its neural activity are only partially understood. Previous studies have shown that behaviourally relevant stimuli, such as whisker contacts and slip-stick events, can drive neural activity in the barrel cortex but the underlying mechanical bases of these stimuli, therefore, how mechanical inputs at the whisker base are encoded during active sensation has not been fully elucidated. This study analysed the mechanical inputs that predict neural activity in the barrel cortex in awake, behaving mice via electrophysiological recordings in the barrel cortex and simultaneous 3D imaging of the mouse whiskers during a tactile detection task. Whisker bending and torsion were characterised during non-contact whisking and touch, then a Generalized Linear Model was used to predict the neural activity from mechanical inputs, the bending and twisting moment. The results suggested that neurons in the barrel cortex present heterogeneous sensitivity, encoding either touch or the rate of change in one of the moments. Some neurons did not show any preference for the studied inputs, leaving room for exploration of other sensory variables. The description of the

bending moment together with the twisting moment in awake behaving animals opens new paths for the exploration of the mechanical basis of somatosensation.

3.2 Introduction

Comprehending what sensory inputs are encoded in the brain and how they are represented is a major problem in sensory neuroscience. Somatosensation is predominantly an active sense, meaning that sensory organs can be purposefully moved to gather information (Grant et al., 2009; Mitchinson & Prescott, 2013; Prescott & Dürr, 2016; C. C. Petersen, 2019). Therefore, characterising somatosensory inputs requires a detailed tracking of sensory organs in behaving animals and their instantaneous physical properties. In the whisker system, the quantification of sensory inputs has been reduced to the horizontal plane, however, mice/rats move their whiskers in three dimensions (Knutsen et al., 2008), the mechanical forces of whisker-object contact are in 3D (Huet et al., 2015); and neurons in the whisker system are sensitive to 3D deflections (Simons, 1978; Lichtenstein et al., 1990; Jones, 2004). Here we present a 3D kinematic and mechanical description of the whiskers in awake, behaving mice and characterise how mechanical inputs are represented in the primary somatosensory cortex during active somatosensation.

The whisker system has become a powerful model for somatosensation, among other reasons, due to the modular stimulus representation in the sensory pathway (Vincent, 1912; Van Der Loos, 1976; Diamond et al., 2008; Campagner et al., 2018). The whiskers are represented in a somatotopic map in the primary somatosensory cortex, known as the barrel cortex (Woolsey & Van der Loos, 1970). Although sensory coding in barrel cortex has been extensively analysed, the bulk of these studies have been performed in anaesthetised animals, obliterating active components of somatosensation. Only in the last decade has animal behaviour been incorporated into sensory coding in the whisker system as a result of recent experimental developments in awake recording techniques and whisker tracking methods (O'Connor, Peron, et al., 2010; Hires et al., 2015; Sofroniew et al., 2014; Campagner et al., 2016; Bush et al., 2016; Severson et al., 2017; Isett et al., 2018). In particular, it has been shown that the barrel cortex encodes behaviourally relevant stimuli, such as touches and slip-sticks during active

sensation (Hires et al., 2015; Isett et al., 2018). Even though somatosensory neurons are driven by mechanical inputs (forces and moments), the encoding of such inputs in awake, behaving animals is not fully understood. Broadly, it has been shown that in touch encoding units, neural responses to touch are modulated by touch strength, although the definition of touch strength can vary across studies (Hires et al., 2015; Crochet et al., 2011; Crochet & Petersen, 2006).

Quantifying animal behaviour from video recordings is a computer vision problem itself, and currently, an active field of research (Nashaat et al., 2017; Mathis et al., 2018; Gillespie et al., 2019; R. S. Petersen et al., 2020). Specifically, the complete quantification of whisking behaviour requires the recovery of the whisker shape and movement in three dimensions. Whisker kinematics at the whisker base can be completely described by three angles (one for each axis) indicating whisker position and its temporal derivatives (Knutsen et al., 2008). Mechanical inputs at the whisker base can be completely represented by six variables, with three forces describing how the whisker resists translation (one for each axis), and three moments describing how the whisker shape changes due to the rotation around each axis (Huet et al., 2015; M. Hartmann, 2016). The moments can be summarised into two quantities: two of the moments characterise how the whisker bends, known as the bending moment, while a third moment, twisting moment, describes how the whisker twists around its own axis.

To date, whisker kinematics and mechanics have been mostly estimated by imaging and tracking whiskers in the horizontal plane. From these recordings, the bending moment during touch has been estimated as the apparent change in whisker curvature due to touch (Birdwell et al., 2007; Quist & Hartmann, 2012). This approach has proved to be useful to provide insightful coding properties of the whisker system (Hires et al., 2015; Isett et al., 2018; Zuo & Diamond, 2019). Moreover, studies applying this technique suggest that the bending moment and its rate of change are the main drivers of primary afferent responses (Campagner et al., 2016; Bush et al., 2016; Severson et al., 2017). However, in this approach, the estimate of the bending moment is contaminated by its artefactual correlation with whisker orientation, which obscures the underlying variables driving cortical activity (Knutsen et al., 2008; Huet et al., 2015; R. S. Petersen et al., 2020). More importantly, this approach omits sensory inputs

that are intrinsically in 3D as the twisting moment, therefore, a complete kinematic and mechanical description of the whiskers during active exploration and their effects in somatosensory coding is lacking. Only a couple of studies have previously quantified the complete array of mechanical and kinematic inputs at the base of the whisker in behaving animals (Huet et al., 2015; Huet & Hartmann, 2016). However, if 3D mechanical inputs other than the bending moment are mechanically and behaviourally relevant during active whisking exploration remains unclear.

Building on previous 3D whisker representations (Knutsen et al., 2008; Huet et al., 2015; R. S. Petersen et al., 2020), herein a method is presented to estimate a complete kinematic description of whisker movements and the moments (bending and twisting) at the base of the whiskers in awake, behaving mice. This method was used to outline how the whiskers bend and twist during non-contact whisking and touch, further exploring if and how the mechanical variables (both moments) are encoded in the barrel cortex during active exploration. This strategy to test if any of the moments were encoded by cortical neurons was based on a Generalised Linear Model (GLM), specifically, we determined the accuracy of the prediction of the activity of the cortical neurons from whisker touch and the mechanical variables. GLMs have been shown to provide a simple yet accurate prediction of primary whisker neuron activity in anaesthetised and awake animals (Bale et al., 2013; Campagner et al., 2016; Bush et al., 2016). Additionally, due to the simplicity of GLMs, the parameters have a clear computational interpretation, providing crucial insights into neural encoding in multiple brain areas (Park et al., 2014; Peron et al., 2015; Pillow et al., 2008; Calabrese et al., 2011). A heterogeneous neural population showing units with preferences for whisker touches or the rate of change of one of the moments was demonstrated.

3.3 Results

3.3.1 Measuring whisker mechanical variables in awake, behaving mice

To estimate both bending and twisting moment at the whisker base, whiskers were imaged with two cameras (horizontal and vertical view) as shown in Figure 3.1.A.

Whiskers were tracked using a customised whisker tracking software built upon (R. S. Petersen et al., 2020) and were represented as cubic Bezier curves in a whisker-centred coordinate system where the origin corresponds to the whisker base. The x axis was aligned to the tangent to the Bezier curve at the base of the whisker and the y axis was aligned to the direction of the increasing curvature of the whisker and the z axis is the cross-product of the x and y axes.

Mice (N=2) were trained to solve an object detection task with a single row of whiskers (C1, C2 and C3). In this task, one pole was placed within reach of the whiskers on "Go" trials. If the mouse responded licking the lick-port, the trial was considered a "Hit" and the mouse was rewarded with a water droplet, otherwise, the trial was considered a "Miss" and the mouse was penalised with a time-out period. On "No-Go" trials, the pole was placed out of reach of the whiskers and if the mouse withheld the licking response ("Correct Rejection") they were not rewarded, otherwise ("False alarms") they were penalised with a time-out period plus a tone (Figure 3.1.B). In all sessions, only whiskers C1 and C2 reached the pole, so the mechanical description was focused only on those whiskers.

During contacts, whiskers are subject to two types of moments, bending and twisting. Assuming that the forces exerted on the whisker are balanced at each point in time (i.e a quasi-stationary model), both moments are proportional to geometrical quantities (Huet et al., 2015; Huet & Hartmann, 2016; M. Hartmann, 2016; A. E. Yang & Hartmann, 2016). The bending moment, which summarises the rotation of the whisker around the z and y axes, is proportional to the changes in the curvature of the whisker due to object touch, whereas the twisting moment, which represents the rotation of the whisker around its own axis (x), is proportional to the change in the angle of twisting in an infinitesimal segment of the whisker due to object touch. To estimate these quantities, the geometrical values of curvature (κ_{3D}) and torsion (τ) were computed as detailed in the Methods section. Figure 3.1.C shows a schematic of these geometrical properties for a helical segment. Top panel shows segments of a helix with the same torsion value ($\tau = 0$) and different curvatures, while the bottom panel illustrates segments with the same curvature ($\kappa_{3D} = 0.1$) and different values of torsion. To form an intuition, the 3D curvature (κ_{3D}) is a generalisation of the horizontal curvature (κ_h) commonly measured during whisker tracking. Measuring the 3D

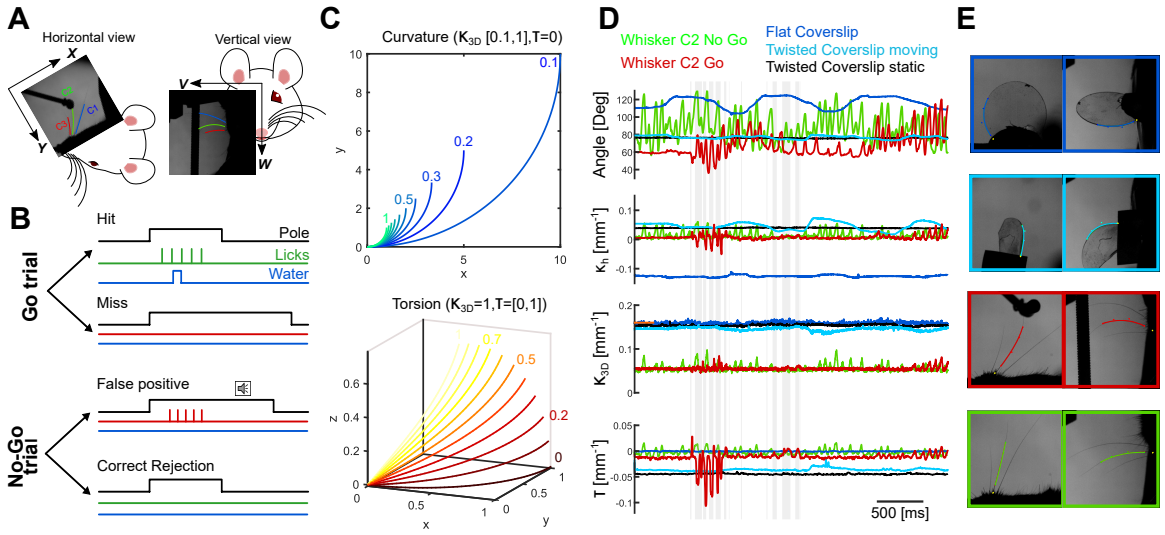

Figure 3.1: Measuring whisker curvature and torsion in awake, behaving mice. A) Experimental setup. Three whiskers from C row (C1, C2 and C3) were imaged with two cameras during the behavioural task. B) Behavioural task schematic. Mice were trained to report the pole's presence within whisker reach (Go trials) by licking a port. On No-Go trials, the pole was moved to a position out of whisker reach and mice should withhold licks. False alarms were penalised with a tone, while Miss trials were penalised with a time-out period. C) Measured mechanical variables schematic. 3D curvature (κ_{3D}) and torsion (τ) were extracted from 3D whisker tracking. Top panel shows a schematic of the segments of a helix with the same torsion ($\tau = 0$) and different curvatures. Bottom panel shows a schematic of helix segments with the same curvature ($\kappa_{3D} = 1$) and different torsions. D) Control measurements. Mechanical variables from three objects were measured using the 3D whisker tracker. A flat coverslip, a twisted coverslip and whisker C2. Variables were measured in different scenarios: Flat coverslip moving (blue), twisted coverslip static (black) and moving (light blue), C2 during No-Go (green) and Go (red) trials. Measured variables from top to bottom: Azimuth angle, horizontal curvature (κ_h), 3D curvature (κ_{3D}) and torsion (τ). The orange line marks the actual coverslip curvature. E) Example video frames from the different objects measured. Colour code corresponds to panel D).

curvature has the advantage of capturing the intrinsic whisker curvature independently of whisker position and orientation (R. S. Petersen et al., 2020), whereas torsion can capture intrinsically 3D deformation of the whisker due to twisting. In particular, the sign of the torsion indicates whether the whisker is twisted clockwise about the x axis (positive) or anticlockwise (negative).

To verify the accuracy of the measurements of curvature and torsion, these variables were estimated for three different objects (Figure 3.1.D): 1) A flat coverslip with known curvature ($\kappa_{3D} = 0.15\,[1/mm]$) and zero torsion (blue line). 2) A twisted coverslip with negative torsion and constant curvature in time (cyan and black lines). 3) Mouse whisker (C2) during Go (red line) and No-Go trials (green line). Figure 3.1.E depicts example video frames from each object imaged. Coverslips were moved in front of the cameras in a whisking-like manner (motion with both forward-backwards and rolling components) to check that the measurements were accurate within the complete field of view. The tracking algorithm could recover the mean values of curvature and torsion of the flat coverslip (averages over time: $\kappa_{3D} = 0.16\,[1/mm]$ and $\tau = -6.7 \cdot 10^{-4}\,[1/mm]$). For the twisted coverslip, a minimal residual structure can be seen in κ and τ when it was translated, which was produced by the shadows that the structure of the coverslip cast when it was perpendicular to the horizontal view. However, estimation from both trials (moving and static object) yielded similar values of torsion and curvatures as expected (averages over time: $\kappa_{3D} = 0.15\,[1/mm]$ and $\tau = -0.04\,[1/mm]$), implying that the values of curvature and torsion were reliably extracted using this method. For whisker measurements, both torsion and curvature changed considerably over time, with the most striking changes of curvature and torsion aligned to touch episodes (grey areas), followed by smaller changes during intensive whisking. The standard deviation of the torsion on the Go trial was 18 times that of the standard deviation of the flat coverslip torsion (blue line), indicating that torsion changes observed in behaving animals are not caused by the noise in the measurements.

The next two sections detail how these two variables (torsion and curvature) change in behaviourally relevant sensory scenarios: non-contact whisking and touch episodes. The final section describes if and how these variables are encoded in the barrel cortex.

3.3.2 Kinematics and whisker shape during non-contact whisking

The whisking cycle is characterised as the protraction and following retraction of the whisker. Whisking kinematics has been commonly described by the horizontal angle (azimuth angle) and its derivatives (Wallach et al., 2016; Campagner et al., 2016; Severson et al., 2017). For rats, the whisker has been considered to be a rigid object during non-contact whisking (Knutsen et al., 2008; Quist et al., 2014; M. Hartmann, 2016). From a mechanical point of view, if a rigid object rotates around one of its axes, then the total moment M can be defined as $M = \alpha I$, where α represents the angular acceleration and I the moment of inertia. Therefore, the total moment at the whisker base can be approximated by a kinematic parameter as angular acceleration (M. Hartmann, 2016; Campagner et al., 2016; Severson et al., 2017). However, recently it was shown that the curvature of mouse whisker can change during whisking (R. S. Petersen et al., 2020), implying that whisking cannot be modelled as rigid-motion. Therefore, kinematics alone is an incomplete description of whisking and changes in whisker shape during whisking need to be characterised. If the whisker is not a rigid object, then α is not well defined and I changes over time. Herein, how the shape of the whisker, specifically its curvature and torsion change within the whisking cycle are analysed.

Whisking episodes were selected from all segments on the Go trials where the pole was out of whisker reach and were defined as segments of at least 300 ms in which the whisking amplitude (extracted from azimuth angle) was at least 5°. Figure 3.2.A shows the azimuth angle, curvature and torsion of whisker C1 and C2 during an example whisking episode.

We then analysed how whisker shape and kinematics changed within the whisker cycle considering that at the beginning of the cycle, the whisker is retracted ($Phase = -\pi$), then it moves forward ($Phase = 0$), finally returning to a retracted position to end the cycle ($Phase = \pi$). Figure 3.2.B shows how both the azimuth and elevation angles evolve during the whisking cycle for whisker C1. In the bottom panel of Figure 3.2.C, a marked difference between the whisker speed during protraction and retraction can be seen. For both angles, the speed reached its maximum during retraction, which is consistent with previous results in awake, behaving mice (G. Carvell

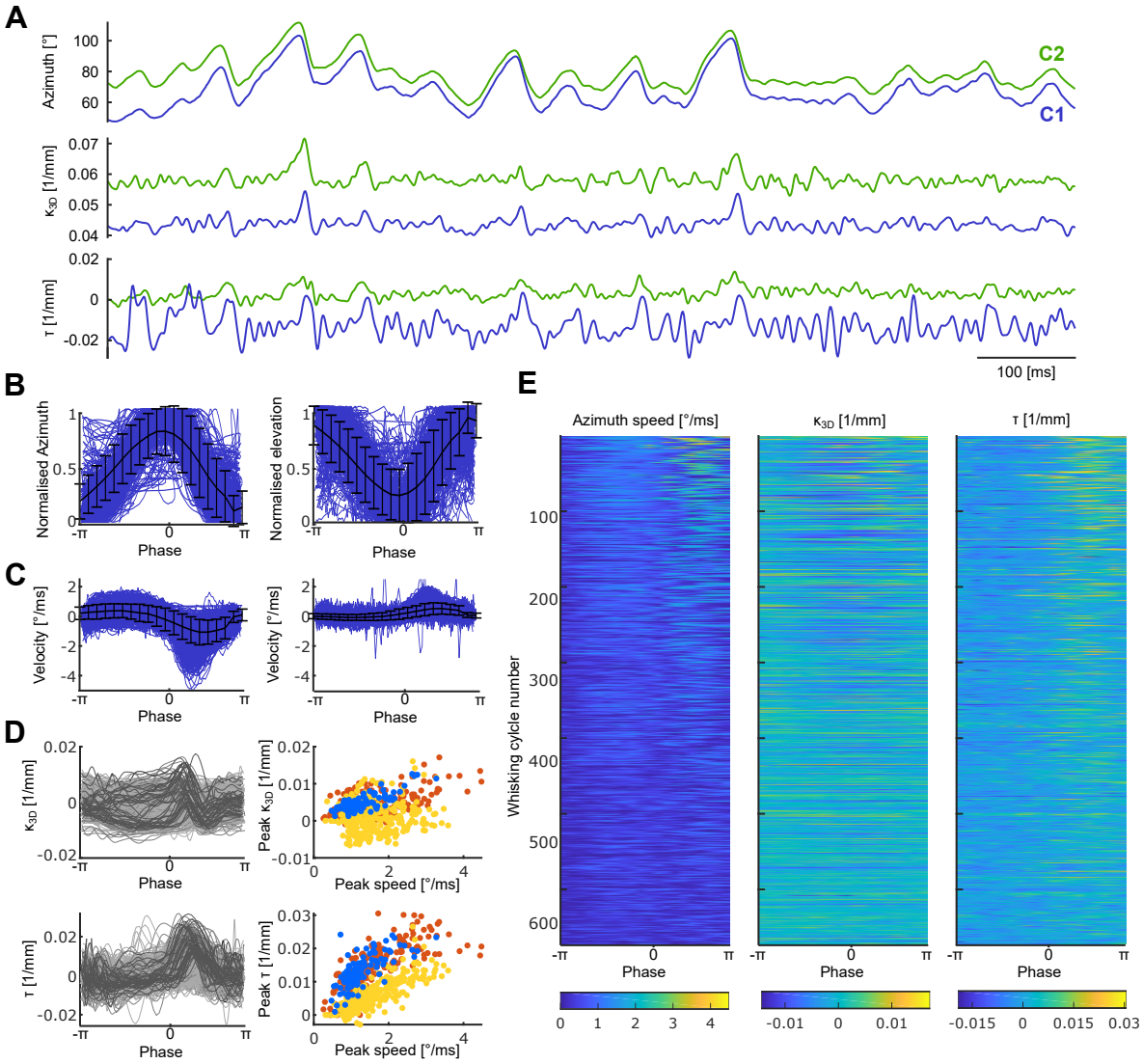

Figure 3.2: Whisker kinematics and shape during non-contact whisking. A) Azimuth angle, curvature and torsion during an example whisking segment. Only whisking cycles from C1 were included for the following panels. Both torsion and curvature were low-pass filtered at 100 Hz and posteriorly corrected by the temporal delay introduced by this process. B) Normalised azimuth and elevation angles within the whisking cycle. Black lines indicate mean and SD across whisks. C) Azimuth (left) and elevation (right) velocities within the whisking cycle. Black lines indicate mean and SD across whisks. D) Changes in mechanical variables within the whisking cycle. Left: curvature (top) and torsion (bottom) within the whisker cycle. Darker shades represent the higher peak speed in the cycle. Right: peak of the mechanical variables within the whisking cycle versus peak speed. Each colour represents a different session. E) Summary of the speed and mechanical variables during the whisker cycles (all sessions). Rows were sorted according to the peak speed of the cycle and only cycles with peaks equal or higher to 1 $°/ms$ were selected for this analysis.

& Simons, 1990; Khatri, Bermejo, et al., 2009).

To analyse the shape of the whisker during whisking, it was first measured κ_{3D} and τ at rest, showing that on average, they presented similar curvatures across animals and session when the whiskers were at rest ($0.046\,[1/mm]$ for C1 and $0.055\,[1/mm]$ for C2). However, the torsion sign depended on the animal. In the coordinate system, the sign of the torsion indicates whether the whisker is twisted clockwise about the x axis (positive) or anticlockwise (negative). For one animal torsion of C2 at rest was $9 \cdot 10^{-3}\,[1/mm]$ for both analysed session, while for the other animal, the torsion for the same whisker was $-13 \cdot 10^{-3}\,[1/mm]$. For C1, the values were more similar across animals, presenting average values of $-10 \cdot 10^{-3}\,[1/mm]$ and $-17 \cdot 10^{-3}\,[1/mm]$ respectively. Therefore, to produce comparable results across animals and sessions, henceforth we define κ_{3D} and τ as the difference between their value at any moment in time and their mean value when the whisker is at rest.

Figure 3.2.D shows how the curvature and torsion change within the whisking cycle. From here it can be seen first that, for at least some of the whisks, there are changes in curvature and torsion. The peak of these increments seemed to be temporally locked to the whisking phase, suggesting that whisker shape depended on the whisking kinematics. To characterise this, the correlation between the peak of the mechanical variables and peak azimuth angle speed was analysed from each whisk. Figure 3.2.D shows a linear relationship between the peak of torsion and speed within each cycle ($\rho = 0.71 - 0.8$ per session). For curvature, there was a less consistent correlation between this variable and the peak speed ($\rho = 0.05 - 0.77$ per session). Figure 3.2.E shows the speed, curvature and torsion profiles according to the peak speed of the whisks, corroborating that the changes in torsion were time-locked to the speed, but also that the amplitude of the changes in torsion depended on the instantaneous speed. In a more general way, these results indicate that at low speeds there were no detectable changes in torsion, however, as the speed increased, the changes in whisker torsion also increased, whereas, a weaker correlation in magnitude and timing was observed for curvature. We then asked if curvature could be better explained by another commonly studied kinematic variable: whisker acceleration. The correlation between the peak of these variables in each whisk was similar to velocity ($\rho = -0.2 - 0.71$ per session), suggesting that acceleration could not explain better

the changes in curvature.

We then performed the same analyses for whisker C2, finding slightly different results. In this case, the correlations between the peak speed and curvature reached $\rho = 0.37 - 0.59$, while the correlation between peak speed and torsion reached $\rho = 0.16 - 0.54$. Therefore, although the results for whisker C1 and C2 were qualitatively similar, there were quantitative differences in the correlations between their shape and speed, suggesting that the correlation between kinematics and the shape of the whisker could be whisker dependent. The variation in the relationship between kinematics and whisker shape could be affected by inertial properties of the whisker, such as its mass, length, thickness, taper, etc.

While the curvature value is always positive due to its geometrical definition, the sign of the torsion indicates whether the whisker is twisted clockwise about the x axis (positive) or anticlockwise (negative). During the whisking cycle, for both whiskers studied here, we observed an increment in curvature and torsion. The increment in curvature indicates that the whiskers were more bent during the retraction phase. When whisker C1 was static, it presented a small negative torsion, however, as shown in Figure 3.2.C, torsion increased during retraction, suggesting a whisker less twisted or even twisted in the opposite direction (clockwise).

Previous studies of whisker kinematics in 3D have shown a high correlation between whisker orientation (or roll angle, ζ) and the horizontal curvature (κ_h) of the whisker during active whisking (Knutsen et al., 2008). Here we found that for both whiskers, the roll angle and curvature were tightly correlated ($\rho = -0.99 - -0.98$), confirming results from previous studies. We then asked if there was a correlation between the changes in horizontal curvature, the torsion and 3D curvature, finding a weak correlation for all combinations: κ_h vs κ_{3D} ($\rho = -0.28 - -0.12$), κ_h vs τ ($\rho = -0.23 - -0.41$), κ_{3D} vs τ ($\rho = 0.21 - 0.35$). This finding suggests that during whisking the changes in curvature observed in the horizontal plane are poorly associated with changes in the intrinsic shape of the whisker and mainly correspond to changes in whisker orientation.

3.3.3 Mechanical variables during active touch

To date, due to experimental constraints, most mechanical descriptions of the whisker during touch have focused on the horizontal plane. Indeed, very few studies have attempted to describe whisker kinematics and mechanics in 3D during active touch (Huet et al., 2015; Huet & Hartmann, 2016). While these works showed that, in an experimental setup like the one presented here, whisker vertical motion and twisting can be observed, no systematic analysis has characterised the relationship between mechanical inputs to the whisker system. In particular, little is known regarding how often and in what conditions the 2D whisker description is a good approximation of the 3D scenario during active somatosensation. The relationship between mechanical variables, such as bending and twisting moments, during active touch remains unclear. Herein, we describe how the bending and twisting moments behave during active touch and compare these inputs to the approximations obtained only from the horizontal plane.

During touch, if assuming only quasi-static effects, the changes in torsion ($\Delta\tau$) are a linear approximation of the twisting moment, while the changes in curvature ($\Delta\kappa_{3D}$) are a linear approximation of the bending moment (Birdwell et al., 2007; Huet et al., 2015; A. E. Yang & Hartmann, 2016). Since both variables depend on the speed of the whisker (Figure 3.2) during non-contact periods, the changes in a variable (e.g. τ) were defined as the difference between the current value of the variable (e.g. τ) and its value when the whisker is static (e.g. τ_0) unless stated otherwise.

Figure 3.3.A shows the changes in torsion and curvature during an example Go trial. The highlighted areas indicate touch periods. Here it can be seen that both variables changed considerably during touch. Figure 3.3.B highlights the touches in an example session and how the magnitude of both variables ($|\tau|$ and $|\kappa_{3D}|$) of whisker C2 evolved during Go trials. The magnitude of both variables was considerably higher within touch than during non-contact episodes. For C2, $|\tau|$ was on average 16 times higher during touch than during non-contact periods, while $|\kappa_{3D}|$ was three times higher during touch periods. Similarly, for C1, $|\tau|$ and $|\kappa_{3D}|$ were on average 8.8 and 4.8 times higher during touch periods respectively.

One of the most common descriptors of touch is its strength. For active whisker touch, strength has been approximated as a change in the whisker speed, or mechanically, as a change in the horizontal curvature at touch onset ($\Delta\kappa_h$) (Zuo et al., 2011;

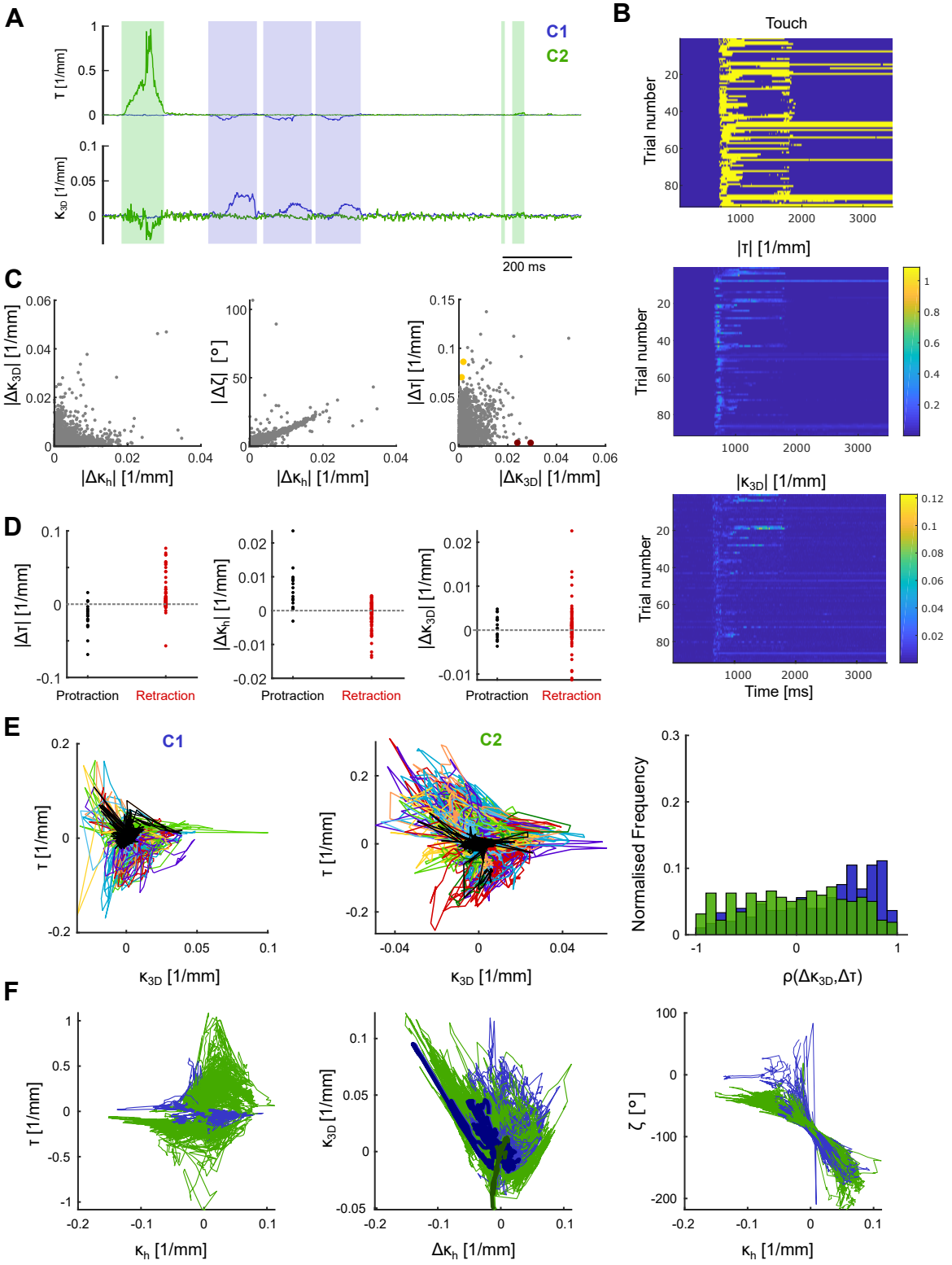

Figure 3.3: Mechanical variables during active touch. A) Mechanical variables during an example Go trial. Touch episodes are highlighted in whisker identity colour code. B) Magnitude of torsion and curvature during Go trials from an example session. Top panel shows touch episodes in yellow and non-contact periods in blue. (Continues on next page)

Figure 3.3: (Continuation) C) The magnitude of change in the variables of interest at touch onset. Coloured dots indicate examples of touches producing mostly changes in only one variable, torsion (yellow) or curvature (red). D) Relationship between the direction of touch and sign of the variables. Change in the mechanical variables at touch onset for protraction (black) and retraction (red) touches. E) Relationship between torsion and curvature during touch divided by whisker identity (left and middle panel). Each coloured line indicates an individual touch, while black lines indicate trajectories during non-contact periods. Right panel shows a histogram of the correlation between the variables during touch for all touches in an example session. F) Relationship between κ_h and torsion, curvature and roll angle during touch for all touches in an example session. Traces with darker shades correspond to touches with a high correlation ($|\rho| > 0.9$) between κ_h and κ_{3D}.

Hires et al., 2015; Campagner et al., 2019). Change in the horizontal curvature is a convenient measurement because, under certain experimental conditions, it is proportional to the bending moment in the horizontal plane (Birdwell et al., 2007; Quist & Hartmann, 2012). This variable presents the caveat that it can change due to factors other than whisking bending, for instance, changes in roll angle during touch can affect the horizontal curvature (R. S. Petersen et al., 2020). Additionally, out-of-plane bending and twisting cannot be captured by this variable. We asked here: if $\Delta\kappa_h$ was a good approximation of $\Delta\kappa_{3D}$ at touch onset and how correlated the magnitude of $\Delta\kappa_{3D}$ and $\Delta\tau$ was at this point of the touch.

Figure 3.3.C shows (left) a weak correlation between the values of $\Delta\kappa_h$ and $\Delta\kappa_{3D}$ at touch onset ($\rho = 0.13$), suggesting that out-of-plane bending was considerable at touch onset, which is consistent with the increments in torsion magnitude observed in Figure 3.3. C and previously reported results (Huet et al., 2015; Huet & Hartmann, 2016). As discussed in the previous section, κ_h accurately captures whisker orientation (ζ) during whisking episodes. During contacts, angle orientation can deviate the approximation of changes in intrinsic whisker curvature $\Delta\kappa_{3D}$ by $\Delta\kappa_h$ (R. S. Petersen et al., 2020). Therefore, we tested if at touch onset, $\Delta\kappa_h$ was still influenced by ζ. Although we found a considerable correlation between $\Delta\kappa_h$ and $\Delta\tau$ ($\rho = 0.43$), the strongest correlation was between $\Delta\kappa_h$ and the changes in roll angle ($\Delta\zeta$) at touch onset ($\rho = 0.78$, middle panel), suggesting that $\Delta\kappa_h$ at touch onset captured mainly changes in the orientation of the whisker rather than changes in whisker shape.

The right panel of Figure 3.3.C shows the magnitude of the changes in torsion ($|\Delta\tau|$) and curvature ($|\Delta\kappa|$) at touch onset. Here, only a weak correlation between the two variables was observed ($\rho = 0.22$), suggesting that every touch had a particular combination of these variables. Moreover, this panel shows that some touches could

trigger changes almost exclusively in one of the two variables (red and yellow dots). In a more general way, this result indicates that active touches were mechanically diverse, while some of them were more affected by the bending moment, others were more affected by the twisting moment.

We then analysed if the sign of the changes in the variables could be related to behaviourally relevant touch properties, such as touch direction, that is, if touch occurred during the protraction or retraction phase (Figure 3.3.D). For this, we manually classified all touches from both whiskers in a session according to touch direction. Touches that presented an unclear direction were discarded from this analysis. We found that the sign of the change of torsion at touch onset was highly associated with touch direction. Specifically, positive changes in torsion (clockwise rotation) suggested a retraction touch, while negative changes (anticlockwise rotation) were associated with protraction touches. Using a binary classifier, the sign of changes in torsion could predict touch direction with an accuracy of 0.74 (left panel). The signs of $\Delta\kappa_h$ and $\Delta\kappa_{3D}$ reached accuracies of 0.6 and 0.58 respectively (middle and right panels).

The sign of the changes in curvature $\Delta\kappa_{3D}$ depends on roll angle (ζ). If the whisker is facing rostrally during a protraction touch, $\Delta\kappa_{3D}$ will be negative, whereas if the whisker is pointed caudally, it will be positive. The roll angle (ζ) is zero when the whisker points rostrally, -90° when it points ventrally and -180 ° when it points caudally. In our experimental setup, 58% of the touches were produced when the whisker had a roll angle between -80 ° and -110°, indicating that the whisker is mainly pointing downward at touch onset, therefore, small changes around -90° in orientation affect the sign of $\Delta\kappa_{3D}$. This indicates that the curvature of the whisker was not contained in the plane of rotation ($x - y$) for most touches, which is a crucial assumption in the approximation of $\Delta\kappa_{3D}$ by $\Delta\kappa_h$. Thus, the orientation of the whisker before contacts explains the poor correlation observed between these variables.

Next, we explored how whisker torsion and curvature were temporally correlated over the complete duration of touches. Figure 3.3.E (left and middle) shows the trajectories of these variables during touch for C1 and C2. Similarly to Figure 3.3.C, it can be seen that there was no strong correlation between the two variables for all touches, rather each touch presented a different (almost unique) combination of torsion and curvature. We did not observe a tendency regarding the signs of the correlation

between the variables (right panel).

Given that the magnitude of $\Delta\kappa_h$ was strongly correlated to changes in roll angle at touch onset, we then explored if the dynamics of κ_h during touch was more correlated to one of the mechanical variables. Figure 3.3.F shows the correlation between κ_h, the mechanical variables and the roll angle. There was a slight to moderate anticorrelation between κ_h and torsion for both whiskers ($\rho_{C1} = -0.52$, $\rho_{C2} = -0.08$ across touches). Although the general correlation between κ_{3D} and κ_h was low ($\rho_{C1} = -0.21$, $\rho_{C2} = -0.07$ across touches), there were a few touches (7%) with an almost linear relationship ($|\rho| > 0.9$, highlighted in dark shades), suggesting that κ_h was a good approximation of the total bending of the whisker in only a small percentage of active touches in these experimental conditions. Given the high correlation between κ_h and roll angle at touch onset, we tested if this correlation was also sustained during touch episodes. The right panel of Figure 3.3.F shows the trajectories of these two variables during touch, showing a clear linear pattern between the variables ($\rho_{C1} = -0.97$, $\rho_{C2} = -0.96$ across touches). These results indicate that κ_h better captured the changes in whisker orientation (roll angle) than changes in bending moment, not only at touch onset but also during touch.

In summary, both torsion and curvature changed during active touches, suggesting that the bending, as well as the twisting moment, characterised active touch. Although these variables were moderately correlated, they could convey different touch features that the animal could exploit to identify behaviourally relevant cues, for example, to categorise between protraction or retraction touches.

3.3.4 Predicting cortical responses from mechanical inputs

Despite the barrel cortex being a powerful model for somatosensation, the vast bulk of its characterisation has been performed in anaesthetised animals. Although this approach has the advantage of highly controlled experimental conditions, it obscures the sensory signals produced during active touch and their processing in awake, behaving animals. Previous studies of barrel cortex in awake, behaving animals have shown that some behaviourally relevant tactile stimuli, such as touch and slip-sticks, are encoded (Jadhav et al., 2009; O'Connor, Peron, et al., 2010; Hires et al., 2015; Peron et al., 2015; J. Yu et al., 2016; Isett et al., 2018). However, the mechanical origins

that drive these phenomena, and in turn the neural activity in the barrel cortex, are poorly understood. Only a few studies have attempted to describe how mechanical inputs at the whisker base drive cortical activity (O'Connor, Peron, et al., 2010; Hires et al., 2015; Peron et al., 2015; J. Yu et al., 2016), all of which have only used two-dimensional whisker imaging, which, as shown in Figure 3.3, produces an incomplete mechanical description of whisker contacts.

In this section, we analyse if and how the 3D mechanical variables, curvature and torsion, are encoded in the barrel cortex. To this end, we tested if the mechanical variables could predict the activity of the recorded units better than touch. From the three recorded sessions, from 2 animals, we selected single- and multi-units recordings (N=21) and applied a GLM to predict neural activity using four different predictors: touch, torsion, curvature and a linear combination of torsion and curvature. We then compared the prediction from the different stimuli. The GLMs were trained and tested using 5-fold cross-validation with two repetitions. A schematic of the implemented GLM is shown in Figure 3.4.A. Neural activity and stimuli were binned to 5 ms resolution. Touch stimuli were represented as two binary time series (one for each whisker) where 1 represented whisker contact and 0 non-contact. Mechanical variables (torsion and curvature) from each whisker were divided into two time series, one considering positive values and other one considering only negative values, giving a total of four time series per mechanical variable.

In the barrel cortex, neural responses to whisker stimulation can be observed between 8 to 30 ms after the stimulus onset (E. Welker et al., 1993; Ahissar et al., 2001; Maravall et al., 2007). To produce comparable models, we set the number of bins of the GLM filters to the same number for all predictors. To set this value, we analysed how the performance of the model in the training and test sets increased with the length of the filters. The performance of the model was defined as the Pearson correlation coefficient between the firing rate of the neurons and the instantaneous firing rate predicted from each model. The instantaneous firing rate corresponds to the output from the nonlinearity step in the GLM (Figure 3.4.A). Both prediction and neural activity were smoothed using a 25 ms boxcar filter. Figure 3.4.B shows the performance of the GLMs according to the length of the filter using torsion as the predictor. Although the performance of the models in training increased significantly

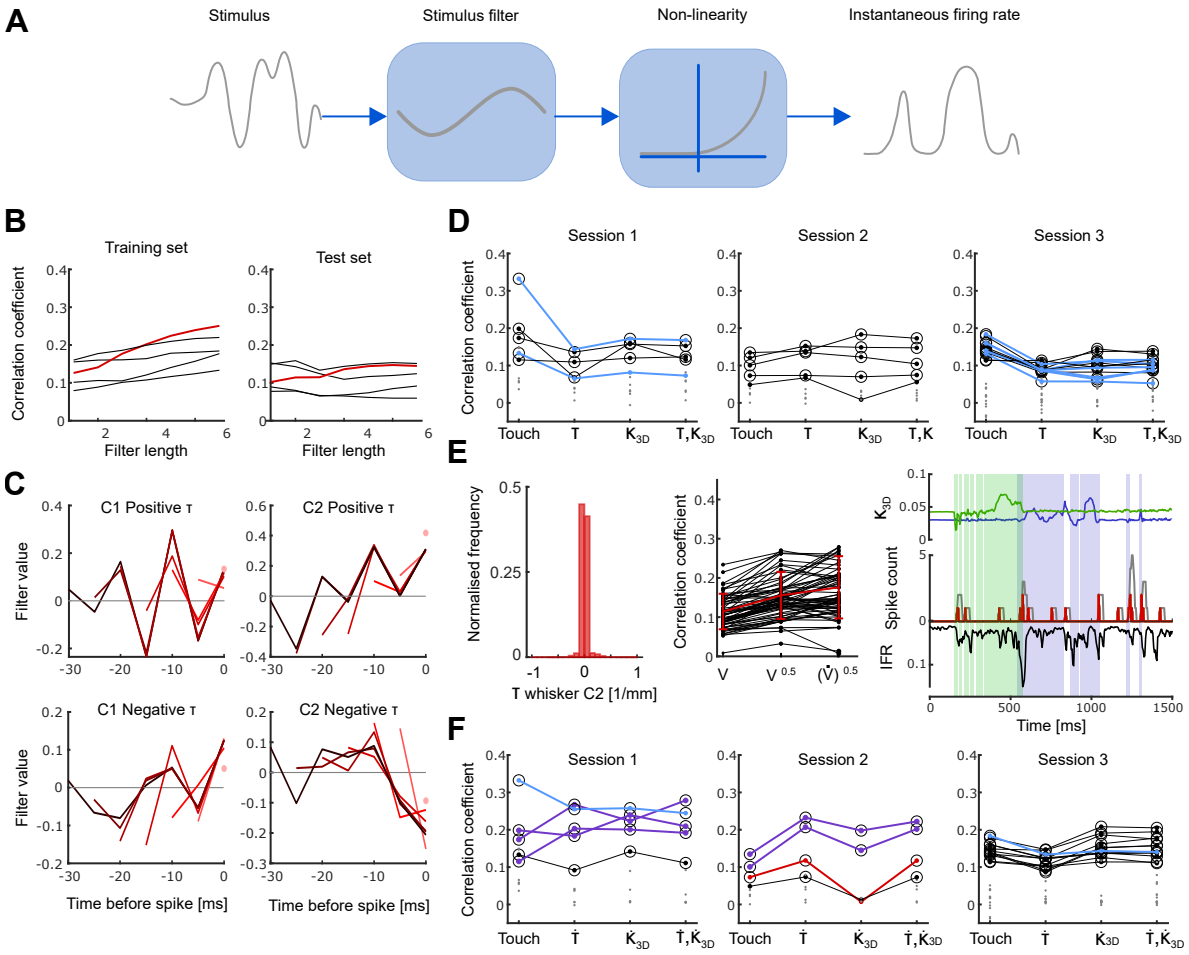

Figure 3.4: Mechanical inputs are encoded in the barrel cortex. A) Schematic of the GLMs used to predict the neural activity. B) Average performance of the models predicting the neural activity from changes in torsion during one session. Performances were evaluated in the training (left) and test (right) sets of the cross-validation process selecting different filter lengths. Each line represents the average across cross-validation repetitions for one unit. C) Torsion filters obtained for one unit selecting different filter length. The selected unit corresponds to the one highlighted in red in panel B). Left panels show filters for whisker C1 and right panels for C2. Top panels show the filter for positive changes in torsion and bottom panels for negative changes in torsion. D) Average performance of the models using touch and mechanical variables as predictors. The performance was defined as the Pearson correlation coefficient between the instantaneous firing rate from the model and neural activity, with both neural activity and model prediction smoothed using a 25 ms causal boxcar filter for the estimation of model performance only. Grey dots indicate chance performance (shuffle test) for each predictor. Black circles indicate units whose performance was significantly different to chance levels. Blue lines indicate units whose responses are best explained by touch. Black lines indicate units whose activity is equally explained by touch and mechanical variables. E) Left: Distribution of τ for C2 during an example session. Middle: Improvement of performance for a mechanical variable when a transformation was applied. Each line represents the average performance of GLM using a mechanical variable as a predictor. V represents any of the mechanical variables, κ_{3D}, τ or both. From left to right: the performance of the models as shown in panel D), then the performance of the model when variables were transformed to root squared and finally when using root square and first temporal derivatives.

Figure 3.4: (Continuation) Right: Prediction of neural activity of an individual unit from an example trial. From top to bottom: Raw curvatures, spike count (red line), filtered spikes (grey line) and prediction (black line) from the GLM for curvature applying both transformations. Correlation coefficient for this trial is $R = 0.37$. F) Analogous to panel D), this time showing performance of the models when the two transformations were applied to the mechanical variables. Blue lines indicate units whose responses are best explained by touch. The red line indicates the unit whose responses are best explained by torsion, blue lines indicate units whose responses are best explained by torsion and curvature, and black lines indicate units whose activity is equally explained by touch and mechanical variables.

for up to 30 ms, the increment was minimal in the test set. Moreover, in some units a decrease of performance was observed for long filters, suggesting overfitting of the model.

The shape of the filters obtained with different filter lengths was also analysed. Figure 3.4.C shows the torsion filters obtained for the unit highlighted in panel B. Here it can be seen that for both whiskers and stimulus signs, the shapes of the filters were consistent across different filter lengths. Also, the magnitude of the filter elements closer to the spike was higher than the ones further away, suggesting that elements closer to the time of spike were more relevant for predicting the neural activity. Therefore, the length of the filters was set at 4 (equivalent to 15 ms) as a compromise between the simplicity of the model and how much temporal information the model can integrate.

An interesting feature of the obtained filters is the considerable magnitude at time $t = 0$, which can occur for a few reasons. First, in the simplest case, when filters have a length equal to 1, the magnitude of the filter is non-zero because there is a correlation between the magnitude predictor and the neural activity. Second, when the filters have more than one element, their magnitude at $t = 0$ corresponds to the bin between 0 and 5 ms before a spike, therefore could be a sign of temporal integration over that bin. In particular, when the filters have two elements and their values have different signs (as in the bottom panels of Figure 3.4.C), it suggests that the filter is capturing the rate of change of the predictor in 10 ms previous to the spike. Third, the values of the filter at time $t = 0$ could be capturing a motor input triggered by whisker-related movements (Musall et al., 2019)

We reasoned that if the mechanical variables were driving neural activity, the prediction of neural activity from the mechanical variables should be more accurate than from a simplified sensory input as touch. Therefore, we compared the performance

of the model using touch as a predictor and the models using mechanical variables. As the touch stimulus is the simplest in terms of the number of variables, and since neurons in the cortex are known to encode touches, we started with the assumption that the recorded units could encode touch, then asking if any of the mechanical variables could predict the neural activity better than touch (Figure 3.4.D). To test this, we compared the performance of touch prediction and the maximum performance obtained within the trio of mechanical variables (torsion, curvature and both). From the three analysed sessions, 8 of the 21 units were best predicted by touch (blue lines, one-tailed two-sample t-test, α=0.05) than any of the mechanical variables. In the rest of the population, there was no significant difference between touch and the selected mechanical variable and no units were better predicted by the mechanical variables than by touch (one-tailed two-sample t-test, α=0.05). In other words, with these models, neurons seemed not to encode either torsion or curvature.

Many factors can play a role in the performance of GLM, for instance, the number of parameters, the sparsity of neural data, the probability distribution of the predictors, the way that the predictors are expressed as input to the model, nonlinearities in the neural code, etc. Two possibilities were tested that could hinder the performance of the models from the mechanical variables: first, that the neural encoding is nonlinear, and second, that the most relevant information of the stimulus is not its magnitude but one of its temporal derivatives.

One of the main assumptions of GLM is that the function that links the stimuli and the neural responses is linear. While this is an accurate assumption for certain neural populations, neural responses - in particular, cortical responses- can be highly nonlinear. If the latter is the case in this neural population, the poor model performance for the mechanical variables might cause the inability of the model to capture nonlinearities of the code. Previous studies have shown that this challenge can be overcome using a feature engineering approach (Benjamin et al., 2017), that is, mathematically transform the stimuli to obtain a new set of features that produce a better performance of the GLM. This approach has been especially successful in central areas such as the cortex (Ahrens, Paninski, & Sahani, 2008; Ahrens, Linden, & Sahani, 2008; Ramirez et al., 2014). To test this hypothesis, we applied three different nonlinear transformations to the mechanical variables and analysed if they improved model performance.

To select which nonlinear transformations to apply to the stimuli, we considered the following: when whiskers are static both torsion and curvature remain constant over time; during whisking and touching, whiskers change in shape, however, as shown in Figure 3.2 and 3.3, the magnitudes of the changes during touch are substantially higher than during whisking, which induced a sparse distribution in both mechanical variables, with a high number of values close to zero and only occasional high non-zero values (Figure 3.4.E, left). This disparity in the values produced exceptionally high responses for strong or sudden touches, which is at odds with the low firing rates usually found in the cortex (Crochet et al., 2011; A. L. Barth & Poulet, 2012). One way to improve the predictions of the models is to apply a nonlinear transformation to the input to avoid creating extremely high responses for strong stimuli. To test this, we tried three sublinear transformations: square root, cubic root and logarithm. From these three functions, the logarithmic transformation did not yield significantly better performance for any of the units and mechanical variables. In contrast, the square and cubic root transformations considerably improved the predictions for many units using the mechanical variables as predictors. Only a slight difference in the improvement of the performances could be observed when using the square or cubic root transformation (28% and 21% improvement across all units and stimuli), favouring the squared root function. It is necessary to note that these sublinear transformations did not counteract the GLM nonlinearity. To assess this, we implemented a version of the GLMs removing the exponential nonlinearity, which yielded considerably poorer results than the original GLMs ($R_{linear} = 0.08$ vs $R_{GLM} = 0.13$) mean across units and stimuli. The right panel of Figure 3.4.E shows that for all units, the average performance of the models was equal or higher when the nonlinear transformation was applied to the torsion and curvature. Moreover, 22% of the evaluations showed a significantly higher prediction when this transformation was used (t-test, $\alpha = 0.05$)

Another possible contributor to model performance is how the temporal patterns in the stimuli are described in the model, that is, in addition to the magnitude of the stimuli, their temporal derivatives could also modulate neural responses. As can be seen in Figure 3.4.B, depending on the whisker identity and the sign of the variable, the filters could cross the zero value one to five times, indicating than this unit is sensitive to the complex temporal patterns of the torsion. Similar patterns were observed in the

filters corresponding to other units and mechanical variables, suggesting a generalised tendency to encode temporal derivatives instead of the absolute magnitude of the variables. Although it is possible to recover GLM filters that can extract temporal derivatives from the stimuli, the firing rates predicted from these estimated velocities heavily depend on the nonlinearity of the model. For example, nonlinearity symmetric with respect to the Y axis (e.g. parabolic curve) would yield high firing rates for high magnitudes of the velocity, independent of its sign. In contrast, an exponential function (as used here) would yield a high firing rate only for one sign of the velocity, therefore, the prediction in the second case would be inaccurate for half of the stimulus presentations. To avoid this scenario, one could explicitly estimate stimulus velocity and divide it into two time series according to their sign, thereby, creating two different filters for stimulus velocity (one for each sign), which would weigh the different velocity signs according to the relationship with the neural responses.

To test if temporal derivatives were encoded in the population, the models were retrained using the time derivatives of the torsion ($\Delta\dot{\tau}$) and curvature ($\Delta\dot{\kappa}_{3D}$). Figure 3.4.E shows that for most units, using the derivative of the variables improved the prediction of neural activity, with only three of the 63 evaluations presenting a significantly lower performance when using the derivatives (t-test, $\alpha = 0.05$). We also tested if the acceleration of the mechanical variables could improve the model performance, however, this was not the case ($R(V^{0.5}) = 0.18$ vs $R(Acc^{0.5}) = 0.1$).

When the performance of the models from the mechanical variables including both transformations was compared, we observed quite different results to those in Figure 3.4.D. Figure 3.4.F shows that some of the units that before showed no preference for touch or a mechanical variable, were now better predicted by a mechanical variable (purple and red lines). However, for six of the seven units that showed a preference for the mechanical variables, there was no significant difference between the torsion and curvature (purple lines). The red line shows the unit that presented a preference exclusively for changes in torsion. These results suggest that some neurons in the barrel cortex represent the two selected mechanical variables (torsion or curvature), and in turn, the bending and twisting moments. As shown in Figure 3.4.F, including both torsion and curvature in the GLMs did not increase the predictive power of the model, suggesting that the neurons were sensitive to only one of the mechanical variables,

however, with our methodology was not possible to differentiate between them. This could be due to the correlation between the torsion and curvature at touch onset. As shown in Figure 3.3, active touches were mechanically diverse and each touch could present a different combination of torsion and curvature. To effectively determine which of the two variables drives neural activity, it would be necessary to compare the responses to touches mainly affected by changes in torsion to touches mainly affected by changes in curvature. However, in this task, the number of touches with these characteristics was not sufficient to generate conclusive results.

Alternatively, it cannot be disregarded that neurons encode a nonlinear combination of both variables. As observed in Figure 3.4.E, applying the stimuli transformations substantially changed the performance of the models. Accordingly, other transformations of the mechanical variables could potentially describe a nonlinear interaction between the variables that predict cortical activity more accurately.

3.4 Discussion

The whisker system is a powerful model for somatosensation but the mechanical forces that act on the whiskers during active somatosensation or how they are encoded in the barrel cortex remain unclear. Previous studies have shown that the bending moment and its rate of change are the main drivers of primary whisker neurons during touch in awake, behaving animals (Campagner et al., 2016; Bush et al., 2016; Severson et al., 2017). However, these studies have been limited to approximate mechanical inputs from the horizontal plane, thereby omitting intrinsically three-dimensional forces and moments acting on the whisker, for instance, whisker bending in the vertical plane and the twisting moment. Here we described how the approximation of both the bending and twisting moment behave during a pole detection task and how they are encoded in the barrel cortex during active touch.

Although the whisker system has become a canonical model for somatosensation (Diamond et al., 2008; C. C. Petersen, 2019), the vast majority of the literature regarding the barrel cortex has been on anaesthetised animals, thus, the sensory inputs encoded in awake, behaving animals remain unclear. Recent studies have shown

that during active somatosensation, the barrel cortex can encode behaviourally relevant stimuli such as touches and slip-stick events (Jadhav et al., 2009; O'Connor, Peron, et al., 2010; Hires et al., 2015; J. Yu et al., 2016; Isett et al., 2018). However, the mechanosensory inputs that drive the neural activity in behaving mice are partially understood, in part due to the lack of tools available to accurately quantify the mechanical inputs of the whisker system during active somatosensation. Most studies describing whisker mechanical inputs and its encoding in the barrel cortex have pointed out that the bending moment in the horizontal plane is a plausible candidate to drive cortical activity (Hires et al., 2015; Peron et al., 2015; J. Yu et al., 2016). However, 2D whisker tracking has two main caveats: first, it completely omits 3D components of forces and moments, and second, it provides an estimation of the bending moment that is mechanically inaccurate due to the artefactual correlation between whisker curvature and orientation. Only recently an automatic method that describes whisker kinematics and shape in 3D was developed (R. S. Petersen et al., 2020). Using this tool as a base, we quantified the changes in whisker shape in 3D in awake, behaving mice, measuring the whisker curvature and torsion at the base of the whiskers during a tactile detection task.

During whisking, changes in torsion correlated to the instantaneous whisker speed, indicating that mouse whiskers, unlike rat whiskers (Knutsen et al., 2008; Quist et al., 2014), deform during the whisking cycle and in turn present the need to capture these changes in the mechanical modelling of the whisker. Also, these results provide a link between a kinematic parameter (velocity) previously reported to drive neural activity and the whisker shape (Khatri, Bermejo, et al., 2009). Furthermore, changes were observed in the whisker curvature during whisker retraction but the correlation between these changes and whisker speed was weaker than in the case of torsion. Future work in biomechanical modelling should detail how the changes in whisker shape during whisking observed here produce forces and moments at the whisker base.

It should be noted that the correlation between the mechanical and kinematic variables described here is derived from 3D whisker tracking, therefore mechanically accurate. In contrast, some of the previously described correlations between these types of variables are a by-product of the 2D whisker tracking approach. For instance, correlations between the 2D estimation of bending moment and whisker orientation

are an artefact caused by the correlation between the horizontal curvature and whisker orientation (roll angle).

In contrast to classic biomechanical approximations in which the whisker only bends during touch (Birdwell et al., 2007; Quist & Hartmann, 2012), we found that both variables (torsion and curvature) considerably increased their magnitude during touch. This indicates that whiskers not only bend but also twist during active touch in our experimental setup. Although both variables increased in magnitude, their correlation at touch onset and during touch was moderate. This suggests that different touches are mechanically different, some more affected by the torsion, others more affected by curvature, and that torsion and curvature could convey different touch properties. For example, at touch onset, the sign of torsion change is an indicator of the touch direction (protraction versus retraction) but the curvature was poorly correlated to this feature.

During whisking episodes and touch, the horizontal curvature closely matched changes in the whisker orientation (roll angle). A linear correlation between these two variables was previously observed during whisking (Knutsen et al., 2008). In contrast, during touch, changes in the horizontal curvature have been used as an approximation of the bending moment (Birdwell et al., 2007; Quist & Hartmann, 2012). However, there was no correlation between the changes in horizontal curvature and changes in 3D curvature, in other words, between the 2D and 3D approximations of the bending moment. This phenomenon could be due to the orientation of the whisker with respect to the pole in our experimental setup. The linear approximation of the bending moment by the change in curvatures assumes that at the moment of touch, the intrinsic curvature of the whisker is completely contained in the horizontal plane (Birdwell et al., 2007; Quist & Hartmann, 2012). For this, the whiskers need to be oriented pointing rostrally or caudally in our experimental setup but both whiskers (C1 and C2) were mainly pointing ventrally before touch, which defied the assumption of the bending moment approximation.

If the intrinsic curvature is completely contained in the horizontal plane, the bending moment is the main mechanical variable affecting the whisker, while twisting can be neglected (Birdwell et al., 2007; Quist & Hartmann, 2012). The fact that the whiskers point ventrally also has a secondary effect on the mechanical variables transmitted to

the whisker follicle, in particular, the whisker is not only subject to bending but also to twisting. It is important to note that both the experimental setup and the analysed whiskers are a standard paradigm for studying the whisker system (O'Connor, Peron, et al., 2010; O'Connor, Clack, et al., 2010; Peron et al., 2015; Hires et al., 2015; Campagner et al., 2016, 2019), which emphasises the importance of imaging the whiskers and estimating the mechanical variables in 3D in these experimental conditions.

Touch is a known encoded variable in the barrel cortex. Furthermore, studies using 2D whisker imaging have shown that the neural responses to touch are modulated by the strength of the touch (Hires et al., 2015; Sofroniew et al., 2014; Peron et al., 2015). However, the 3D mechanical forces associated with touch encoded in the barrel cortex during active touch are unclear. A population in which some units encoded the bending or the twisting moments at the whisker base was identified in the present study. From these units, only one presented a significant difference in the degree to which the torsion and curvature predicted the firing rate. For this unit, torsion was the stimulus that best predicted the firing rate, whereas the rest of these units encoded only one of the variables rather than a linear combination of both. However, our method did not allow to differentiate between them so it cannot be ruled out that these units encoded a nonlinear combination of torsion and curvature. Future work is required to consider how to decorrelate these variables to define their encoding properties. For instance, designing experimental setups that promote a wide range of torsion and curvature combinations could be achieved by using multiple pole locations or pole orientation (vertical vs horizontal).

It is important to note that while our method could show that some units encoded the bending or the twisting moment, the overall prediction capacity of the models was moderate. This can be attributed to the site of the recordings, layer 5. It has been observed that this layer presents irregular responses to sensory inputs, possibly due to the multiple inputs that this layer receives with unobserved dynamics (Hires et al., 2015). For example, in contrast to layer 4, this layer not only receives thalamocortical inputs but also intracortical inputs, making the prediction of its neural activity from sensory inputs more challenging (Petreanu et al., 2009; Hires et al., 2015).

A relevant factor to clarify how the mechanical variables are encoded in the barrel cortex is the pre-processing of the variables before arriving at the cortex. In contrast

to primary whisker neurons, which directly receive inputs from the follicle, neurons in the barrel cortex receive inputs from many different pathways (Diamond et al., 2008; Bosman et al., 2011). In the first instance, the barrel cortex inputs have been processed in the brainstem and thalamus, which could add nonlinearities to the neural encoding. During ongoing active whisker stimulation, several control loops modulate the neural activity of the barrel cortex over time (Bosman et al., 2011; J. Yu et al., 2016), which in turn could induce temporal differences in the code itself. Key insights in this regard could be gained from a systematic analysis of how torsion and curvature are encoded throughout the ascending pathway.

In summary, these results describe how whisker shape and kinematics behave during active somatosensation and show that both bending and twisting moments are encoded in the barrel cortex during touch episodes in awake, behaving mice. This work shows that a detailed description of whisker shape and whisker kinematics is fundamental to elucidate the mechanical basis of somatosensation.

3.5 Methods

All experimental protocols described in here were approved by both United Kingdom Home Office national authorities and institutional ethical review.

3.5.1 Behavioural apparatus

The whiskers were imaged similarly to (R. S. Petersen et al., 2020) using high-speed cameras (LTR2, Mikrotron, Unterschleissheim, Germany; 1000 frames/s, 0.2 ms exposure time) in both the horizontal and vertical view. Both cameras used telecentric lenses (55-349, Edmunds Optics, Barrington, NJ) and the field of view (480 $\times$ 480 pixels) of the horizontal camera was parallel to the transverse plane, while the field of view of the vertical camera was located to 25° of the sagittal plane and 10° from the transverse plane. The position of the vertical camera was chosen to minimise occlusion between the cheek of the mouse and its whiskers. Mice were head-fixed and positioned inside a Perspex tube (inner diameter 32 mm). Licks were detected as described in (O'Connor, Clack, et al., 2010). The whiskers were free to move at all times and were illuminated from below using an infrared LED array (940 nm, LED

940-66-60, Roither, Vienna, Austria) via a diffused condensed lens.

3.5.2 Surgical procedure and mice training

Mice (C57; males; N=2) were first habituated to the apparatus, then anaesthetised with isoflurane (1.5-2.5% isoflurane by volume in O_2) maintaining a body temperature of 37° using a homeothermic heating system to implant the titanium head-bar. The skull was exposed and the titanium head-bar was attached with dental acrylic. After surgery, mice were left to recover for at least 5 days before starting water restriction (1.5 ml water/day). Training began 7-10 days after the start of water restriction. Water was given as a reward during the training and the mice were trained until they reached more than 70% performance. Subsequently, a craniotomy was performed and sealed with silicone elastomer. Mice were left to recover for 2 or 3 days. Before the beginning of the recording, mice performance was tested to be equal or higher to 70%.

3.5.3 Behavioural task

In each trial, a pole (1.59 mm diameter) was commanded to move to known coordinates in the transverse plane: close to the whiskers on Go trials and far from the whiskers on No-Go trials. The pole was then lifted to the final position in all trials. In Go trials, whiskers could reach the pole only while it was on its final position, with the time that the pole went back to the original position determined by the type and outcome of the trial: if the mouse touched the pole and licked the lick-port (Hit), water was released as a reward and the pole was commanded to stay at the final position for 1 second before returning to the original position. If the mouse did not lick the port (Miss), it was penalised with a time-out (3-5 seconds) and only then the pole was commanded to return to the original position. In No-Go trials, if the mouse did not lick the lick-port (Correct Rejection), the pole was commanded to stay for 2.5 seconds in the final position before returning to the original position, otherwise, the mouse was penalised with a tone and a time-out (3-5 seconds), and the pole was then commanded to return to the original position.

3.5.4 Electrophysiology

Recording. Extracellular recordings from layer 5 of the barrel columns were obtained as follows: Mice were trimmed to three whiskers in C row (C1, C2 and C3) under brief isoflurane anaesthesia. Intrinsic optical imaging was performed to locate the area corresponding to the targeted whisker barrel. During the imaging, the targeted whisker was deflected using a piezoelectric device, then a craniotomy was made at the selected location under isoflurane anaesthesia. The craniotomy was posteriorly filled with silicone elastomer.

Acute implantation of a 16-channel linear silicon probe (2 Shanks, Cambridge NeuroTech, Cambridge, United Kingdom) was performed at the beginning of each session under isoflurane anaesthesia. Mice were left to recover for at least 2 hours before starting the recording session. The mouse was exposed to repeated trials during the session. Data was pre-amplified, collected at a sampling rate of 24.4 kHz, filtered (band-pass filter 300-3000 Hz) and acquired to a hard disk (RZ5, TDT). At the end of the recording session, the microelectrode array was withdrawn, the craniotomy sealed with silicone elastomer, and the mouse returned to its home cage.

Spike sorting. Every shank was sorted independently using JRCLUST (Jun et al., 2017). Units used in posterior analyses must meet the following criteria: 1) the first and second PCA components of the spikes belonging to the units must be well isolated from the noise. 2) Their activity was consistent for 30 or more trials. Segments of the sessions in which electrode spatial drift was observed were discarded. 3) The inter-spike interval presented a low spiking probability during the refractory period (2 ms). To classify neural activity into single- or multi-unit activity, a series of visual tests on the output of the spike sorting algorithm was considered. For a group of spikes to be considered as coming from a single-unit, their waveform should be consistent for most spikes; the amplitude of the waveforms should lie well above the threshold for spike detection; the amplitude of the waveforms should reach a maximum in one of the probe's recording contacts and decrease for neighbouring channels; the inter-spike interval histogram should show no spikes in the first 2 ms as indicative of a refractory period, and in the visualisation in the feature space (first and second principal component), the activity should form a well-isolated, distinct cluster. If a group of spikes did

not meet one or more of the described criteria, it was then considered as a multi-unit recording.

One of the main difficulties at the time of spike sorting the data was the drifting of the probe. As the animal is awake and behaving, the probe can move along the axis of insertion due to movements of the animal, hence, the signals of the units could not be followed for the entire recording. Additionally, some units showed stable activity for dozens of trials but the activity was absent for some or part of the recording. This activity change was not associated with probe drift, therefore, we selected units whose activity could be followed for most of the recording. Activity in the barrel cortex is sparse, so to prevent overfitting of the model units were selected only if they showed at least 250 spikes during the exploratory period.

Whisker tracking. To extract kinematic and mechanical variables, the whiskers in the video recordings were tracked in 3D using a freely available software (R. S. Petersen et al., 2020). To reconstruct the whiskers in 3D, the tracker's algorithm integrates information from the horizontal and vertical view through a point-to-point calibration process, with calibrations performed at the end of each recording session.

We extended the capabilities of the whisker tracker software by (R. S. Petersen et al., 2020) to estimate both the bending and twisting moment of the whiskers. In the original method, the shape of the target whisker was described as a quadratic, three-dimensional Bezier curve $\boldsymbol{b}(s) = (x(s), y(s), z(s))$, where, x, y, z are real space coordinates and $0 \leq s \leq 1$ parameterises location along the curve: $\boldsymbol{b}(s = 0)$ corresponds to the end closest to the whisker base, while $\boldsymbol{b}(s = 1)$ to the end furthest from the base.

Since the tracker provided a quadratic solution, the Bezier curve necessarily has zero geometrical torsion. The solution was refitted as a cubic Bezier curve to estimate torsion and the cubic curve was refitted to match the shadow of the whisker using two constraints: 1) spatial contiguity in which the cubic solution had to be similar to the quadratic solution, and 2) temporal continuity in which the cubic solution in frame f had to be similar to the previously tracked frame $f-1$. These two constraints were weighted in the objective function by two parameters, σ_1 and σ_2 respectively. The value of the parameters was set finding in a trade-off between the accuracy to

represent the whisker shape (improved with low values of both parameters) without introducing considerable levels of noise (improved by high values of both parameters). For all the analysed sessions, the same parameters were used during the cubic tracking. Posteriorly, frames were manually curated when occasional tracking errors occurred.

The intrinsic curvature of any continuous curve parametrised respect to arc length $\boldsymbol{b}(s)$ is described as $\kappa_{3D}(s)$ (Marsh, 2006):

$$\kappa_{3D}(s) = \frac{\left| \frac{d\boldsymbol{b}(s)}{ds} \times \frac{d^2\boldsymbol{b}(s)}{ds^2} \right|}{\left| \frac{d\boldsymbol{b}(s)}{ds} \right|^3} \tag{3.1}$$

Here $|\boldsymbol{a}|$ denotes the magnitude (2-norm) of vector $\boldsymbol{a}$. $\kappa_{3D}(s)$ has units of 1/distance and is the reciprocal of the radius of the circle that best fits the curve at point s.

If a quasi-static model of whisker contact is assumed, in other words, at each moment in time the forces are balanced in a steady state, then the total bending moment (M_b) is described as (Birdwell et al., 2007; Huet et al., 2015):

$$M_b(s) = \Delta\kappa_{3D}(s) EI(s) \tag{3.2}$$

where $\Delta\kappa_{3D}(s)$ corresponds to the difference in curvature at the point s when the whisker, E is Young's modulus and $I(s)$ is the area moment of inertia.

The bending moment magnitude can be decomposed into the bending moments around the z and y axes

$$M_b = \sqrt{M_z^2 + M_y^2} \tag{3.3}$$

Torsion of a continuous curve parameterised respect to arc length ($\boldsymbol{b}(s)$) is defined as (Huet et al., 2015):

$$\Delta\phi(s) = \frac{\tau(s) ds}{GJ(s)} \tag{3.4}$$

Where $\Delta\phi(s)$ represents the change in the angle of the point s around its own axis, τ is the applied torsion, G is the shear modulus, $J(s)$ is the polar area of inertia and ds is a differential segment of s.

In our approach, ϕ is proportional to the geometrical torsion, which is defined as (Marsh, 2006):

$$\tau(s) = \frac{\left(\frac{d\boldsymbol{b}(s)}{ds} \times \frac{d^2\boldsymbol{b}(s)}{ds^2}\right) \cdot \frac{d^3\boldsymbol{b}(s)}{ds^3}}{\left|\frac{d\boldsymbol{b}(s)}{ds} \times \frac{d^2\boldsymbol{b}(s)}{ds^2}\right|^2} \tag{3.5}$$

Both $\Delta\tau(s)$ and $\Delta\kappa(s)$ were defined as the difference between their value at any moment in time and their mean value when the whisker is at rest. These values correspond to the values presented as τ and κ in the results section.

3.5.5 Data analysis

Spike trains from the spike sorting were discretised into 1 ms bins to match the resolution of the video recordings.

Changes in torsion and curvature during whisking. Whisking segments were selected using the following criteria: 1) segments should present at least 300 ms of high-amplitude whisking and 2) high-amplitude whisking was defined as periods when the amplitude was above 5°. To compute amplitude and for subsequent analyses, whisker azimuth angle was filtered within the whisking frequency [5, 30] Hz.

Both torsion and curvature were low-pass filtered at 100 Hz using an ideal filter. Posteriorly, time series were corrected to eliminate the delay introduced by the filtering process.

For panels D and E of Figure 3.2, whisking cycles were selected in which maximum speed was at least $1°/ms$. To produce comparable lengths across whisking cycles, for panel E, variables within the whisking cycle were discretised into 20 bins of the same length.

For panels D and E of Figure 3.2, the torsion and curvature were defined as the difference between their value at any moment in time and their mean value when the whisker was at rest in that trial.

Changes in torsion and curvature during touch. Touches were manually detected with customised software. For these analyses, torsion and curvature were defined as the difference between their value at any moment in time and their mean value when the whisker was at rest in that trial, whereas changes in a variable (e.g. $\Delta\tau$) at touch onset (Figure 3.3.C) were defined as the difference between the mean value of

the variable within the first 5 ms from touch onset and the 5 ms before touch onset. All touches from all session were used to compute the corresponding correlations between the variables.

To estimate the accuracy of the relationship between the sign of the variables and touch direction (Figure 3.3.D), the problem was modelled as a binary classification problem. Protraction touches were defined as positives and retraction touches as negatives. For $\Delta\tau$, if a negative change matched a protraction touch, it was considered a true positive, whereas if a positive change matched a retraction touch, it was considered a true negative. Therefore, the accuracy was the fraction of true negatives plus true positives from the total number of touches evaluated. For $\Delta\kappa_{3D}$ and $\Delta\kappa_h$, this definition was inversed due to the opposite correlation between the variables and touch direction. For this particular analysis, the value of the variables was averaged for up to 20 ms after touch onset and reducing the length of the touch onset segments impoverished the accuracy of the classifier for all variables.

Figure 3.3.E and F show the correlations between the variables from one representative session. Panel E correlations were computed by dividing touches by whisker identity, whereas correlations were estimated pooling all touches in the session in panel F.

Modelling the neural data. To predict spikes in the barrel columns, the GLM was used as a model between the stimuli and the neural responses. Neural responses and stimuli were discretised into 5 ms bins and as torsion and curvature can present positive or negative changes, a rectified input was used for the model, that is, each variable from each whisker was divided into two variables containing exclusively the positive (or negative) values of the variables. Touch episodes were represented as a time series in which each bin could be 1 if the whisker was contacting the pole, or 0 if it was not. The GLM is described by the following equation:

$$y_t = f(\vec{k}_1\vec{x}_1 + \vec{k}_2\vec{x}_2 + b)$$

where the neural response $y_t \in [0, 1]$ is a Poisson random variable, f represents an exponential nonlinearity, $\vec{x}_i$ represents the i stimulus (e.g. touch in whisker i), $\vec{k}_i$ its respective filter and b is a bias parameter.

Parameters were fitted minimising a cost function consisting of the negative maximum likelihood and a regularising term $-\lambda\|\vec{k}\|$. The regularising parameter was set as the value that maximised the evidence of the model, with only the segments of the trials where the pole was within whisker reach used to fit the models. To evaluate the model performance, the Pearson correlation coefficient between the instantaneous firing rate from the model and the firing rate from the neurons was computed. The instantaneous firing rate corresponds to the output of the nonlinearity in the GLM. The neural firing rate and the instantaneous firing rate were smoothed by convolution with a 25 ms boxcar filter exclusively for computing the correlation coefficient. To test whether the results were robust to the smoothing time-scale, the above procedure was repeated for a range of boxcar smoothing filters (1, 5, 25, 50, 100 ms). In all cases, units showed similar preferences (exclusively preferring touch or one of the mechanical variables).

GLM performances were produced by a 5-fold cross-validation procedure with two repetitions, producing ten sets in total, with trials randomly divided into test and training sets. Chance levels were computed by a shuffle test using the same cross-validation process but the spikes were shuffled within each trial. To determine if the Pearson coefficient was above chance probability, a one-tailed two-sample t-test was performed (α=0.05).

Chapter 4

Sensory Adaptation in Barrel Cortex during active sensation

4.1 Abstract

Sensory adaptation is a ubiquitous phenomenon, observed across species and sensory modalities. Adaptation has been extensively studied in anaesthetised animals, disregarding how animal behaviour can shape neural activity in awake behaving animals. Somatosensation is fundamentally an active sense, making animal behaviour a critical driving factor of neural activity. In the somatosensory system, if and how adaptation affects the encoding of behaviourally relevant stimuli is still poorly understood. Here we aim to analyse what features of sensory adaptation can be observed during active touch in awake, behaving mice. For this, we performed electrophysiological recordings in barrel cortex and simultaneous 3D imaging of the mice whiskers during a detection task. We found single and multi-units recordings sensitive to whisker contact, whose responses were modulated by touch behaviour and sensory adaptation during active somatosensation. We show that Stimulus-Specific Adaptation can be observed for whisker identity, and more weakly, for bending direction. These results suggest that encoding of behaviourally relevant stimuli is modulated by sensory adaptation, setting a precedent for the study of adaptation during active sensation.

4.2 Introduction

Sensory adaptation is characterised by the change of the neural representation of a stimulus according to the history or context of the stimulus. For example, the attenuation of neural responses to a repetitive stimulus. It is consistently present across species, sensory modalities and stages of processing (Weber et al., 2019). The classical paradigm to study this phenomenon is to analyse the neural responses under anaesthesia using a repetitive stimulus (Simons, 1978, 1985; Khatri et al., 2004; Katz et al., 2006; Musall et al., 2014). The biggest advantage of this method is the high control over the stimulus, which allows isolating the physiological properties of adaptation. However, this approach completely neglects how behaviour can modulate the neural activity, which is critical in an active sensing modality as the somatosensory system. In this work, we investigated how the dynamics of sensory adaptation and behavioural stimuli shape the neural responses in barrel cortex in awake, behaving mice.

Adaptation in the whisker system occurs at all stages of the sensory pathway, but its effects reach their peak in cortex (Maravall et al., 2013; Martin-Cortecero & Nuñez, 2014). Signs of adaptation can be observed in anesthetised animals at the level of synaptic potentials (Chung et al., 2002; Katz et al., 2006), spikes (Simons, 1978; Khatri et al., 2004; Wang et al., 2010; Musall et al., 2014) and networks (Whitmire & Stanley, 2016). In anaesthetised animals, it has been shown that cortical adaptation is specific to whisker identity. In other words, a repetitive deflection of one whisker decrease responses to subsequent deflections of the same whisker, but has little effect on the responses to subsequent deflections of neighbouring whiskers (Katz et al., 2006; Musall et al., 2017). Additionally, the degree of adaptation in cortical neurons also depends on the frequency, intensity and direction of the stimulus (Khatri et al., 2004; Musall et al., 2014, 2017). All of these parameters are fixed to diminish variability in the neural responses, and therefore, are not representative of the natural whisking behaviour.

Activity in the somatosensory cortex is not only governed by environmental stimuli but elements such as alertness and states of anaesthesia play also a fundamental role (Erchova et al., 2002; Castro-Alamancos, 2004). These elements also affect the extent of adaptation effects. Fanselow and Nicolelis (1999) found that adaptation to

electrical stimulation of the infraorbital nerve was stronger during awake immobility than during active whisking. Additionally, Castro-Alamancos (2004) applied electrical stimulation of the whisker pad to show that adaptation effects are more prominent under quiescent states as anaesthesia or awake immobility than in expectant animals. Both of these results predict that the extent of adaptation effects is larger under quiescent states than during active exploration in expectant animals. However, the extent of adaptation effects during active exploration remains unclear.

Only a few studies have attempted to characterise adaptation effects in the somatosensory cortex during active sensation. From these works, there is no agreement on the extent of adaption effects on barrel cortex. On the one hand, intracellular recordings in layer 2/3 and 4 from awake behaving rodents suggest that most neurons show little adaptation to successive active touches (Crochet et al., 2011; Crochet & Petersen, 2006; Yamashita et al., 2013). However, all these studies only considered successive touches which kinematic properties (e.g. as the horizontal angle) were roughly similar, instead of describing the strength of each touch. Touch strength, or its mechanical estimation the bending moment, have been shown to drive mechanoreceptors and trigeminal ganglion activity (Severson et al., 2017; Campagner et al., 2016; Bush et al., 2016) and modulate cortical responses to touches during active sensation (Hires et al., 2015). On the other hand, in layer 4, neural responses to touch decrease significantly for later touches in a series of successive active touches (Hires et al., 2015). However, it is unclear if this effect can be attributed exclusively to sensory adaptation (Neural Adaptation) or if it is due to systematic changes in whisking behaviour (Behavioural Adaptation), for instance, if touches become weaker over time. Therefore, a need to incorporate a detailed description of whisking behaviour in sensory adaptation studies is present.

Measuring rodent whisking behaviour is challenging because of both, the whiskers size and the speed that whiskers can reach. Only in the last few years, high speed-videography and whisker tracking software have allowed imaging the whiskers and estimate their kinematic and mechanics variables in awake, behaving animals (O'Connor, Clack, et al., 2010; Clack et al., 2012; R. S. Petersen et al., 2020). This, in turn, has helped to relate the behaviourally relevant variables, as whisker contacts, to neural activity (Hires et al., 2015; Campagner et al., 2016; Isett et al., 2018).

Here we studied how adaptation is affected by dynamic behaviour in awake, behaving mice solving a detection task. To this end, we simultaneously recorded activity from single-units and multiunits from barrel cortex and imaged multiple whiskers in 3D while mice performed the task. We found that cortical responses to touch decrease after the first touch of the trials, which can be explained by a combination of Behavioural and Neural Adaptation. In our behavioural task, adaptation is moderately specific to whisker identity, and more weakly, to the direction of bending. The methodology proposed here is potentially extendable to multiple behavioural tasks, setting a precedent for the study of adaptation during active sensation.

4.3 Results

4.3.1 Variability of whisking behaviour

In classical preparations to study adaptation in the whisker system, touches are simulated by repetitive whisker deflections. The parameters of these deflections remain constant within and across trials to isolate the effect of a given variable on the neural activity. To explore to what extent active touches can be considered a sequence of precisely repeated stimuli, we analysed if and how touches changed during whisking behaviour.

Mice (N=3) were trained to solve an object detection task with a single row of whiskers (C1, C2 and C3). In this task, one pole was placed within reach of the whiskers in "Go" trials. If the mouse responded licking the lickport, the trial was considered a "Hit", and the mouse was rewarded with a water droplet. Otherwise, the trial was considered a "Miss", and the mouse was penalised with a time-out period. In "No-Go" trials, the pole was placed out of reach of the whiskers. If the mouse withheld the licking response ("Correct Rejection") they were not rewarded, otherwise ("False alarms") they were penalised with a time-out period plus a tone (Figure 4.1.B).

To describe natural whisking behaviour in 3D, we imaged the whiskers using two high-speed video cameras (1000 frames/s) placed as in Figure 4.1.A. Whiskers were tracked using a customised 3D tracking software (R. S. Petersen et al., 2020). From the tracking, both whisker shape and position were extracted. From whisker shape, the 3D curvature (κ_{3D}) at the base of each whisker was estimated for each frame

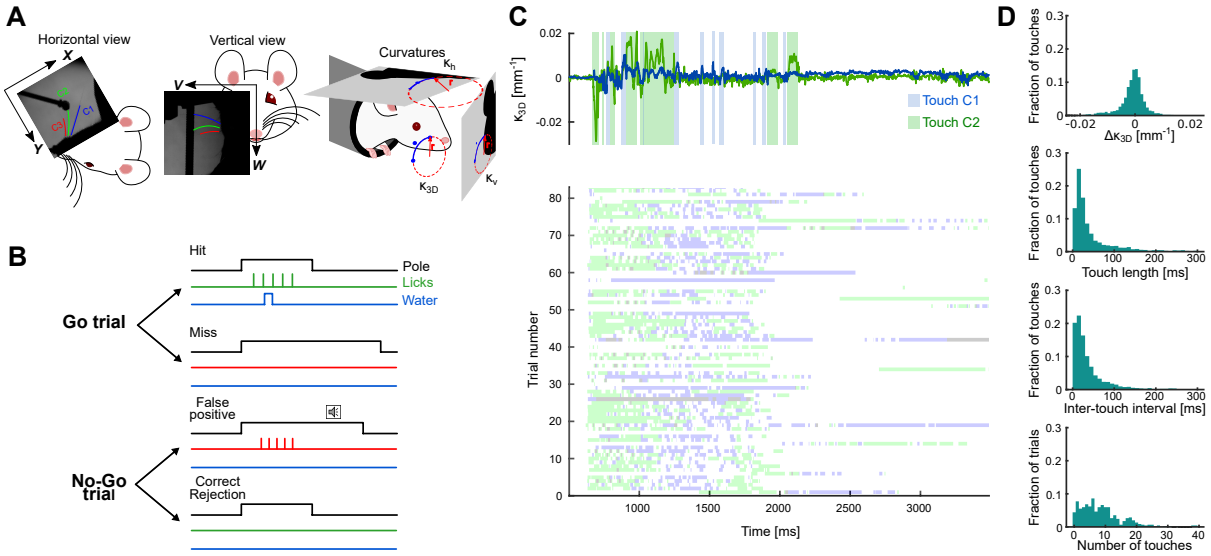

Figure 4.1: Preparation to study adaptation. A) Experimental setup. Three whiskers from C row (C1, C2 and C3) were imaged with two cameras during the behavioural task (left and middle). 3D curvature (κ_{3D}) was extracted from 3D whisker tracking (right). B) Behavioural task schematic. Mice were trained to report the pole's presence within whisker reach (Go trials) by licking a port. On No-Go trials, the pole was moved to a position out of whisker reach and mice should withhold licks. False alarms were penalised with a tone, while Misses were penalised with a time-out period. C) Sources of behavioural variability during active touch. Top: Touches and κ_{3D} from a Go trial example. Down: Contacts periods highlighted for an example session. Only C1 and C2 reached the pole in all sessions. D) Distribution of sources of variability (from top to bottom): Strength of touches ($\Delta\kappa_{3D}$), touch-length, inter-touch interval and number of touches per trial.

(Figure 4.1.A). We estimated the strength of each touch as the change in curvature at the whisker base at touch onset relative to its resting state ($\Delta\kappa_{3D}$). Previously, change in whisker curvature extracted only from the horizontal view ($\Delta\kappa_h$) has been widely used as a proxy for the bending moment (Birdwell et al., 2007; O'Connor, Clack, et al., 2010; Hires et al., 2015; Peron et al., 2015; Campagner et al., 2016; Severson et al., 2017). However, unlike $\Delta\kappa_{3D}$, $\Delta\kappa_h$ is correlated with whisker roll angle during natural behaviour, which distorts the bending moment approximation (R. S. Petersen et al., 2020).

From each recording session, we selected all the "Go" trials for posterior analyses. All touches were manually selected with the help of a customised GUI. We then studied if behavioural variables that can introduce variability in the neural responses to touches changed within and across trials. We call these behavioural variables "sources of variability". For each touch, we computed its strength ($\Delta\kappa_{3D}$) and registered its associated whisker. Upper panel from Figure 4.1.C shows κ_{3D} and touch segments from an example trial, in which C1 and C2 contact the pole multiple times with different

strength. This was a common pattern for all trials, specifically, in all recorded session whiskers C1 and C2 reach the pole in several occasions but there were no contacts from whisker C3 (lower panel). Additionally, the strength of the touches varies within and across trials (Figure 4.1.D), indicating than both whisker identity and the strength are then sources of variability that characterise touches.

A more careful look at Figure 4.1.C and 4.1.D reveals that $\Delta\kappa_{3D}$ not only changes in magnitude but also in sign. The sign of $\Delta\kappa_{3D}$ specifies the bending direction. While positive values indicate the whisker being bent, negative values indicate the whisker being straightened, indicating another source of variability of touches.

Lower panel of Figure 4.1.C shows the contacts periods of both whiskers during one session. This emphasises not only variability within trials but also across trials. From here, it can be observed that for each trial the number of touches, their length and their inter-touch interval vary. Figure 4.1.D shows the distribution of these three variables and touch strength pooling all sessions. Including all the mentioned variables, we could identify at least six parameters that can describe a whisker contact and vary across different touches and trials: whisker identity, touch strength, the direction of bending, touch number within the trial, touch length and inter-touch interval. All of these variables have been shown to modulate the activity barrel cortex activity (Woolsey & Van der Loos, 1970; Axelrad et al., 1976; Khatri et al., 2004; Hires et al., 2015). Therefore, changes on these variables introduced variability on the neural responses, indicating that whisker touches during behaviour greatly differed from the classical stimuli design used to study adaptation. This discrepancy is fundamental to characterise adaptation in behaving animals. First, because classical preparations do not take into account how changes in active whisking behaviour can affect the neural responses to touch, it is unclear how relevant Neural Adaptation effects on the neural responses are in comparison to behavioural effects. Second, because during active sensing both Neural Adaptation and whisking behaviour can modulate neural activity it is necessary to design methods that are able to disentangle these two causes.

In the following sections, to test if we could observe adaptation in behaving animals and characterise its effects, we focused on three main variables that modulate responses to touch in barrel cortex and have been previously studied in terms of sensory adaptation in anaesthetised animals: touch strength, whisker identity and bending direction.

4.3.2 Changes in neural responses to touch within trials

The classical paradigm to study adaptation in the whisker system is to compare the responses to a sequence of identical whisker deflections. In this design, both firing rate and sub-threshold responses gradually decrease during the exposure to a repetitive stimulus (Simons, 1978, 1985; Khatri et al., 2004; Katz et al., 2006). However, under our approach, natural behaviour introduces variability in the properties of the contact, which could obscure adaptation effects. We, therefore, tested if we could still observe an attenuation of firing rate in response to a series of active touches.

Extracellular recordings from barrel cortex were performed simultaneously with 3D whisker imaging. Neural responses were spike-sorted and aligned to touch onset. Figure 4.2.A shows the responses of a neural population recorded in one session. Although the responses seemed to be constant over time when sorted by chronological order, a significant attenuation was observed within trials (Figure 4.2.A). This effect was also observable in individual units (Figure 4.2.B), suggesting that individual units adapted over touches within trials. We will hereafter refer to this phenomenon as firing rate attenuation.

It has been posited that adaptation brings perceptual consequences, such as enhancing acuity and degrading stimulus detectability (Goble & Hollins, 1993; Wang et al., 2010; Ollerenshaw et al., 2014). The later one can be promoted, in a cellular level, by the firing rate attenuation in response to repeated stimuli. Previous research has shown that adaptation degrades the capacity of individual units in barrel cortex to report passive whisker deflections (Wang et al., 2010; Ollerenshaw et al., 2014). To test this in our preparation, we used an ideal observer approach to quantify how well a neuron's activity discriminates between the firing rate at touch onset and during noncontact periods. We divided the touches into first touches of the trials and later touches and produced a histogram of their responses (Figure 4.2.C). Similarly, the activity during noncontact periods was divided into "previous to the first touch" and "inter-touch periods". Accuracy of detecting a touch was measured computing the Area Under the Receiver Operative Curve (AUC) (Figure 4.2.D). For all individual units, the AUC of the first touch was higher than for later touches, suggesting that detectability of touches decreased within trials.

While Figure 4.2.B shows a significant number of spikes before touch onset for

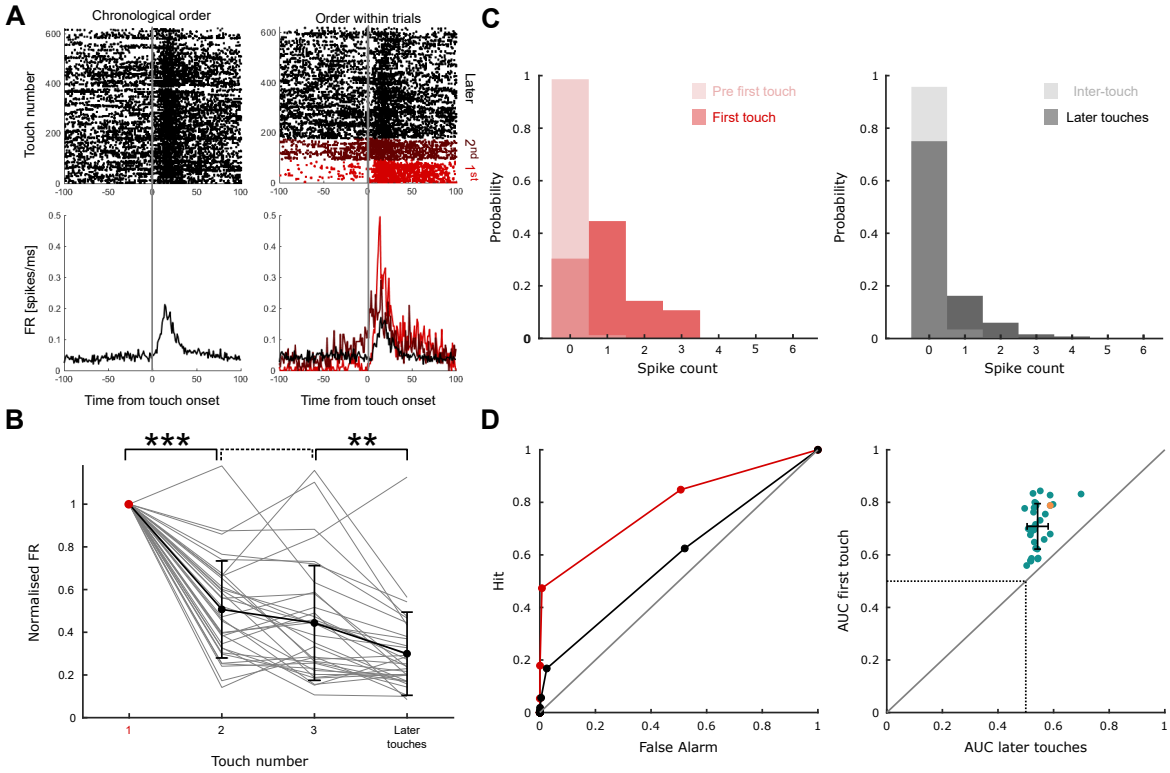

Figure 4.2: Neural responses change within trials. A) Raster plots (top) and PSTHs (bottom) of the neural population (N=7 units) recorded during one session. Left panels show results sorted by chronological order of touches (from the beginning to the end of the recording session), while right panels show the same activity sorted by touch order within trials. B) Firing rate from all selected units by touch order within trials normalised by responses to the first touch (grey lines). Black line represents mean and SD across neurons. C) Distribution of neural responses of an example unit for different events in the trials: First touch, pre-first touch, later touches and inter-touch responses. D) Left: Receiver Operating Characteristic curve (ROC) of touch detection from neural responses shown in C). Diagonal line represents chance performance (where the area under the curve is 0.5). Right: Area Under the ROC curve for first and later touches for all selected units. The highlighted unit corresponds to results shown in C). Black lines represent the mean and SD of the population. Dotted lines represent chance performance. Diagonal line indicates equal detection performance for first and later touches.

later touches, Figure 4.2.C shows that the number of spikes is minimal for inter-touch periods. This discrepancy is a product of the type of responses selected to count the number of spikes. While in Figure 4.2.C the spikes were counted exclusively in segments when none of the whiskers contacted the pole, in Figure 4.2.B, 200 ms segments around all touch onsets were selected. In other words, in Figure 4.2.B segments previous to touch onset can include responses to touches separated by less than 100 ms.

Results from Figure 4.2.B and 4.2.D indicate a reduction in the responses to consecutive, active touches, consistent with previously reported work in awake, behaving

mice (Hires et al., 2015). While these results could be purely a change in the neural representation of the touches (Neural Adaptation), they also could be driven by systematic changes in touch properties within trials (Behavioural Adaptation). Changes in critical behavioural variables could modulate touch responses, which in turn could seem to amplify or reduce adaptation effects. For example, results in Figure 4.2 could be a product of a gradual weakening of the touches within trials.

4.3.3 Behavioural Adaptation

To test if a systematic change in the touch properties within trials can explain the attenuation in the responses to repeated touches, we described how the mechanical and kinematic whisking variables that modulate cortical activity evolved within trials. To this end, we selected a mechanical variable as the bending moment, and a kinematic variable as the displacement at the base of the whisker.

Bending moment is one of the driving variables for the whisker system and is the best predictor of trigeminal ganglion activity during active exploration (Campagner et al., 2016; Bush et al., 2016; Severson et al., 2017). As in the previous section, we measured the change in curvature at the base of the whisker $\Delta\kappa_{3D}$ in the first 5 ms as an estimation of the bending moment.

Kinematic variables as whisker velocity near touch onset have been shown to modulate to cortical activity (Hires et al., 2015). Additionally, in previous adaptation studies, the change in horizontal angle has been used to declare similarity between active touches (Crochet & Petersen, 2006; Crochet et al., 2011; Yamashita et al., 2013). These studies hypothesised that if touches are similar, then any changes in neural responses to touch are purely an effect of Neural Adaptation and not of a change in touch properties. In our setup, whiskers moved in both the horizontal and vertical view when whisking or contacting the pole. We, therefore, summarized these movements as the displacement of the whisker base in the sagittal plane in the first 5 ms since the touch onset (D_b).

Figure 4.3.B shows the tracking solutions for the first 20 ms of the first three touches from an example trial. Changes in the shape and position of the whisker were visible in both planes of view for all three touches. In particular, $\Delta\kappa_{3D}$ decreased considerably over touches, while D_b barely changed. These patterns in behaviour were

highly reliable across trials and sessions. Figure 4.3.C shows that, on average, the magnitude of $\Delta\kappa_{3D}$ was reduced over touches within the same trials. This indicates that touches became weaker after the first touch, and therefore, the apparent sensory adaptation (Figure 4.2) could be a mechanical effect - a consequence of active changes in whisker contact strength during the course of a trial.

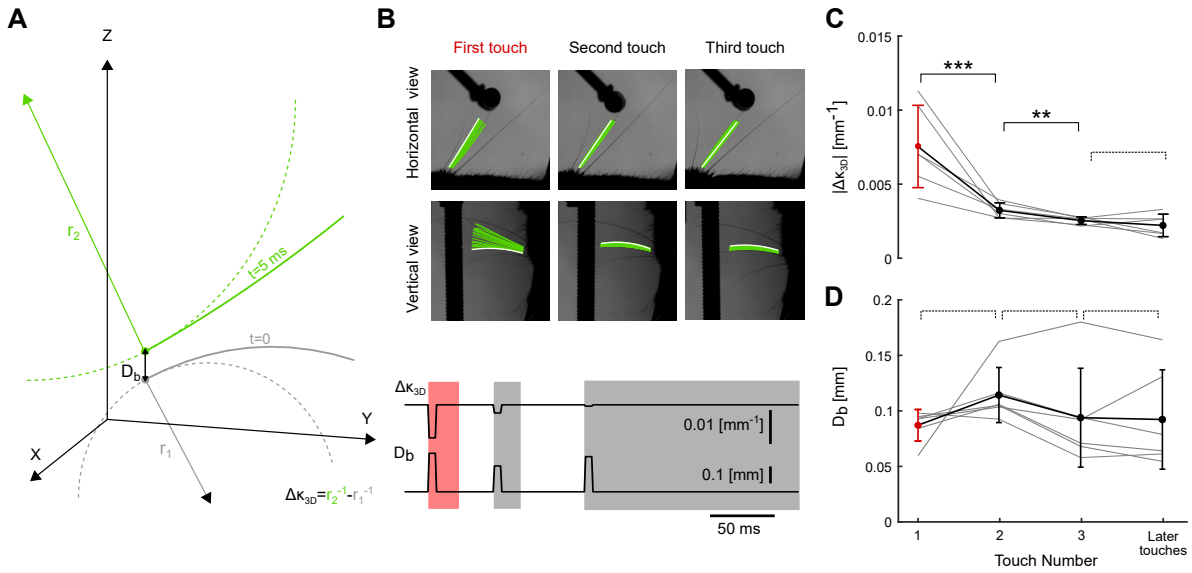

Figure 4.3: Behavioural Adaptation: Strength of whisker contacts decreases within trials. A) Schematic of $\Delta\kappa_{3D}$ and displacement of whisker base (D_b) at touch onset. Solid grey and green lines illustrate whisker at touch onset and after 5 ms respectively. Dashed lines represent circumference to define whisker curvature and arrows indicate the radius of the circumference. B) Single-trial example showing tracking in both views (top), $\Delta\kappa_{3D}$ and D_b (bottom) for the first three touches. Tracking solution at touch onset is highlighted in white, while green lines correspond to the first 20 ms of the touch. $\Delta\kappa_{3D}$ and D_b were computed as the mean of the first 5 ms after touch onset. Shaded areas indicate touch episodes. C) Average $|\Delta\kappa_{3D}|$ at touch onset in all sessions (grey lines). Red and black dots indicate mean across sessions. Bars indicate SD. D) Change of base displacement through touches within trials. Grey lines indicate the mean for each session and black and red dots show the mean across sessions. Bars indicate SD

To analyse if the changes in the mechanical variable $|\Delta\kappa_{3D}|$ were correlated with changes in kinematic variables, we tested if D_b also decreased over time. Figure 4.3.D shows D_b according to the touch number in the trial. In contrast to the change in curvature, no significant differences were found in D_b for subsequent touches. This result indicates that to study sensory adaptation during active touches it is necessary to describe both kinematic and mechanical touch properties to understand the changes in neural responses. Without a careful description of behavioural variables, for example, analysing only whisker kinematics, changes in neural responses could be mistakenly attributed exclusively to Neural Adaptation.

The systematic change in the strength of active touches signals adaptive whisking

behaviour within trials. Behavioural Adaptation in this context could be a product of several reasons. For instance, it could be a task-specific strategy of the mouse to detect the first touches and solve the task quickly or could be part of a more general active control strategy to "minimise impingement" (Mitchinson et al., 2007; Mitchinson & Prescott, 2013).

Behavioural Adaptation within trials observed in Figure 4.3.C could explain at least in part the decline of touch responses observed in Figure 4.2. However, a change in the neural representation of the touches could be simultaneously taking part and producing a decrease in the responses. We test this hypothesis in the next section.

4.3.4 Neural Adaptation

In natural whisking behaviour, mice actively control whisking amplitude, setpoint, velocity, the strength and length of the contact (Towal & Hartmann, 2006; Grant et al., 2009; O'Connor, Clack, et al., 2010; Mitchinson & Prescott, 2013). To test whether firing rate attenuation (Figure 4.2) was caused exclusively by the decrease in the strength of the touches (i.e. Behavioural Adaptation), or Neural Adaptation contributed, we needed to disentangle behavioural and neural components. Neural Adaptation is characterised by a dynamic neural representation of a stimulus (Weber et al., 2019). Usually, the neural representation is history or context-dependent. For example, in the case of history-dependent representations, classical studies illustrate adaptation as a sharpening of receptive fields after the presentation of a repetitive stimulus (Castro-Alamancos, 2004; Khatri et al., 2004; Khatri & Simons, 2007). Adaptation has also been shown as shifts in tuning curves before and after a change in the context of the stimulus (Maravall et al., 2007; Adibi et al., 2013). Here we applied this last approach to our data to assessed if and how the representation of touch strength changed from the first touch of each trial to later touches.

Figure 4.4.A shows responses of an example unit to touch sorted by $\Delta\kappa_{3D}$ (left) and its tuning curves for first and later touches (right). On this unit, touch responses increased approximately linearly with touch strength while decreased with the touch number within the trial, as can be seen in the shift of the tuning curves from first to later touches. The change in the tuning curves showed, firstly, that touch representation was history-dependent, and secondly, that the decay in the touch responses

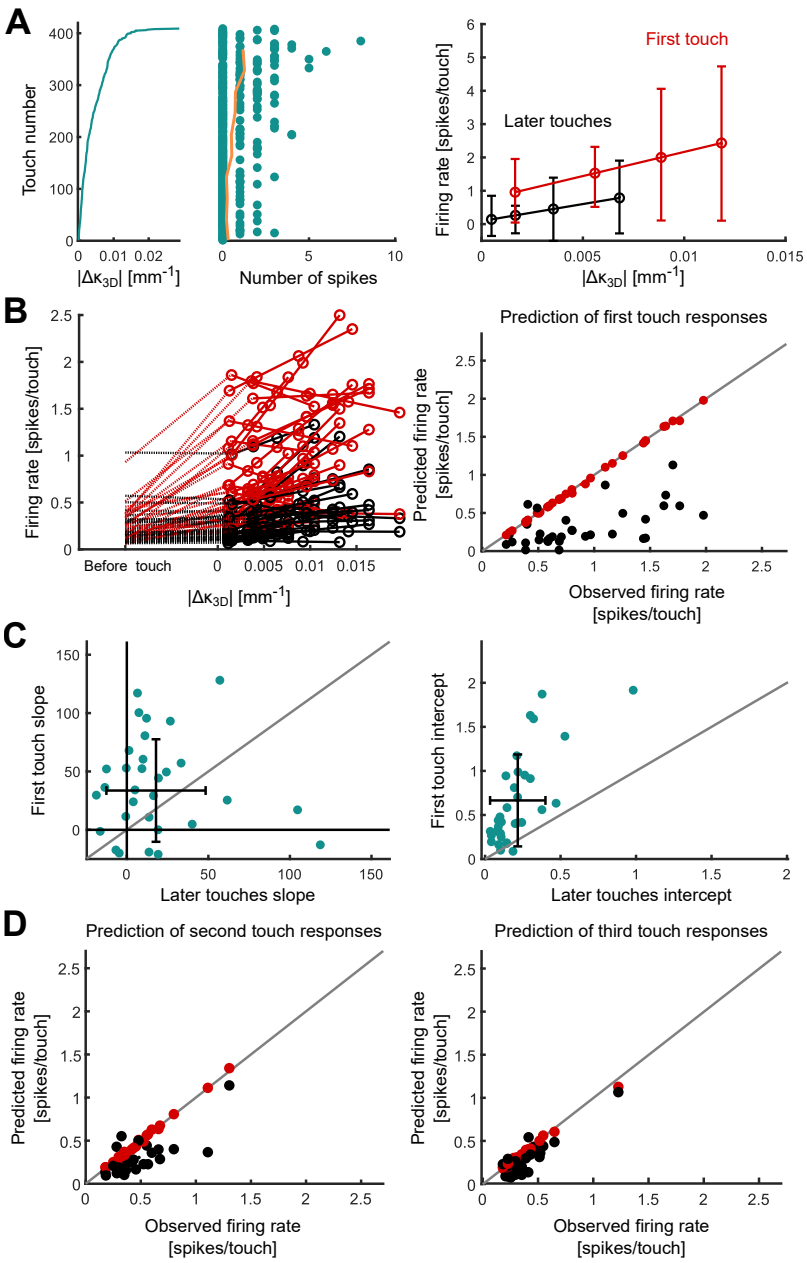

Figure 4.4: Neural Adaptation. A) Left: Touch responses of an individual unit sorted by $\Delta\kappa_{3D}$. Yellow line indicates mean responses across samples (bin size: 40 samples). Right: Tuning curves for first and later touches for the unit on the left panel. B) Left: Tuning curves for first and later touches from all selected units. Responses in the 30 ms segment before first and later touches are shown for comparison. Right: Prediction of responses to the first touch using later touches tuning curves (black circles) and first touch tuning curves (red circles). First touch tuning curves for this panel were fitted all the trials related to the neural activity except for the predicted trial. C) Comparison of tuning curves parameters for first and later touches. Left panel shows slope and right panel shows intercept of tuning curves for all selected units. D) Prediction of responses to second and third touches using later touches (N_{touch} >2 and N_{touch} >3 respectively) tuning curves (black circles) and second and third touches tuning curves (red circles).

was not exclusively a product of the mechanical changes observed in Figure 4.3. In turn, these results indicate that this unit adapted its responses to the strength of the touches. This type of shift in the tuning curves was observable in most units

(Figure 4.4.B, left), suggesting that Neural Adaptation was widely spread across the population.

To quantify the extent of Neural Adaptation, for each unit, we predicted the responses to the first touches using the tuning curve for later touches (black dots in Figure 4.4.B, right). As a control, we compared the first touch responses to the prediction from the tuning curve for the first touches (red dots). For 28 of the 33 units, the prediction of first touch responses was significantly lower than their respective firing rates (two-sample t-test, $\alpha = 0.05$), indicating then that the majority of units were adapting to some level. Although adaptation levels varied considerably across the population, tuning curves for later touches substantially underestimated the responses to the first touch. In particular, prediction of the first touch responses using tuning curves for later touches only reached 44 % (on average across units) of first touch firing rate. Both results confirmed a significant shift in the tuning curves, and then, a substantial part of the response attenuation within trials could be explained by Neural Adaptation.

We then analysed if the change in the tuning curves was a product of a declining tuning to the strength of the touches (the slope of the curve) or product of a change in the sensitivity of the neurons to touch (the intercept). To do this, we compared the slope and the intercept in our regressions for the first and later touches. Figure 4.4.C shows the results for both parameters. The most striking change could be seen in the intercept of the tuning curves, which decreased in 93% of the units for later touches. On the other hand, changes in the slope of the tuning curves were more heterogeneous (Figure 4.4.C, left). Only 63% of the population showed a decrease in this parameter.

Considering that we could observe stronger responses to the first touch of the trials than later touches, we explored if the responses to second and third touches in the trials also presented difference respect to later touches. To this end, we produced tuning curves for second and later touches (N_{touch} >2) and compared their predictions as in panel B (Figure 4.4.D). Tuning curves for later touches predicted on average 67% (across units) of neural responses, suggesting that for the second touch units had not reached the adapted state. We repeated this test for third touches in the trials (later touches were defined as N_{touch} >3) and found that both tuning curves produced more similar results, with later touches tuning curves predicting 75% of the neural responses.

Therefore, we not only observed Neural Adaptation in the recorded population but also, we were able to observe how responses to touch are gradually attenuated due to Neural Adaptation.

As a whole, these results not only confirmed that the sensitivity of neurons to touch decreased within trials, which in turn indicates that neurons were under sensory adaptation during active sensing. But also, they indicated us which units were under Neural Adaptation and gave us an estimation about how strongly each unit was modulated by Behavioural and Neural Adaptation.

4.3.5 Stimulus-Specific Adaptation

Stimulus-Specific Adaptation (hereafter, SSA) is said to be present if a cell attenuates its responses to a repetitive (adaptive) stimulus, but not to a following, different stimulus (test stimulus). Previous works on adaptation in anaesthetised animals have shown that cortical neurons can adapt to specific features of touches, such as velocity, direction and the identity of the whisker producing the contact (Katz et al., 2006; Musall et al., 2014).

Testing SSA during natural whisking behaviour is particularly challenging due to the variability of touches features. To analyse the specificity of adaptation to a variable, we used a method analogous to the oddball paradigm. In a traditional oddball paradigm, the adapting stimuli consist of a series of identical whisker deflections, while the test stimulus presents all the same features that the adapting stimulus has, except for the feature being tested (e.g. whisker identity). If the responses to the test stimulus are stronger than the responses to the last adapting stimulus, then neurons are said to be specifically adapting to the feature. Here, we selected two binary features that can modulate touch responses to test SSA: whisker identity (C1 and C2) and bending direction (negative and positive $\Delta\kappa_{3D}$). As in the classic oddball paradigm, here the touches in the adapting stimuli share the same feature (whisker identity or directionality). However, unlike in the oddball paradigm, all the other touch features can vary, for example, the magnitude of bending, whisker velocity, etc.

To assess the specificity of adaptation to whisker identity, we selected all trials in the session in which at least the first two touches were produced by the same whisker w_1 (C1 or C2) and at least one later touch (3rd or onward) with the other whisker

w_2 (Figure 4.5.A). Touches produced with w_1 were considered as the adapting stimuli, while touches produced with whisker w_2 were considered the test stimulus. Touch episodes in which both whiskers touch the pole simultaneously (overlapping touches) were excluded from this analysis. Figure 4.5.B shows neural responses to touch in the selected trials for one example session. From the 11 units in this session, 3 presented a significantly stronger response for the test stimulus than the last adapting stimulus (orange lines). The increment in firing rate suggested, at least at first sight, that the adaptation is whisker-specific. However, the increment in the neural responses to the test stimulus is not sufficient to declare SSA in behaving animals for two reasons: 1) Neural activity depends on stimulus intensity. In particular, if the test stimulus was stronger than the adapting stimuli, it could simulate the expected SSA effects. To test this, we analysed the magnitude of touch strength ($|\Delta\kappa_{3D}|$) for adapting and test stimuli. Lower panel of Figure 4.5.B shows the average and standard deviation of $|\Delta\kappa_{3D}|$ in the selected trials of the example session. Consistently with the previous behavioural results, the test stimulus was significantly weaker than both adapting stimuli, demonstrating that greater responses to the test stimulus are not a mechanical effect. 2) Tuning to touch strength could be different for different whiskers. For example, if all test touches were produced by the same whisker (e.g. C1), a greater response to w_2 could simply arise if the unit was more sensitive to that particular whisker (C1) than other whiskers.

To isolate the effects of whisker identity adaptation, we produced two tuning curves for touch strength, one for each whisker contacting the pole (C1 and C2). Test stimuli and the first two touches of each trial were excluded to determine these tuning curves. For each test stimulus, we predicted the neural response using the tuning curve for the corresponding whisker (C1 or C2). We then selected all units whose responses to the test touch were significantly higher than the prediction from the respective tuning curve. We found that 25% of the population met this criterion (green lines in the upper panel of Figure 4.5.C), which therefore specifically adapted to whisker identity. For these units, their responses to the test stimulus were comparable or even higher than the predictions from the first touch tuning curve (lower panel Figure 4.5.C), which goes in line with previous results from anaesthetised animals (Katz et al., 2006).

As shown in Figure 4.1.D, behaviour was highly variable from one trial to another.

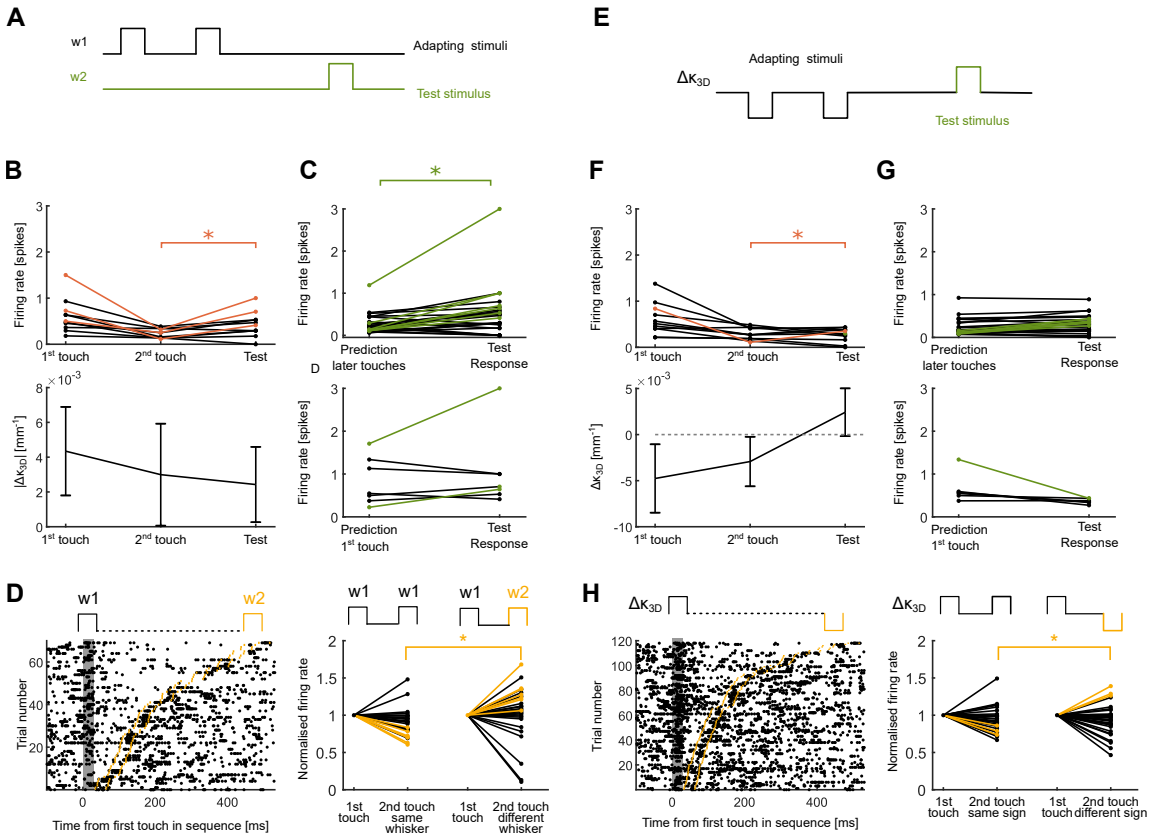

Figure 4.5: Stimulus-specific Adaptation (SSA): whisker identity and bending direction. A) Oddball paradigm schematic. B) Responses to adapting stimuli and test stimulus (top) and mean change in curvature $\Delta\kappa_{3D}$ of corresponding stimuli (below) for an example session. Units whose responses were significantly higher for test stimulus than the second adapting stimulus were highlighted in orange. C) Comparison of predicted activity and neural responses to test stimulus. Top: Responses were predicted using the tuning curves for later touches separated by whisker identity. Units whose responses were significantly higher than their prediction were highlighted in green. Bottom: Responses were predicted using the tuning curves for the first touch shown in Figure 4.4.B. Units whose responses were significantly different than their predictions were highlighted in green. D) Left: Raster of consecutive touches produced by different whiskers sorted by inter-touch time. Grey (first touch) and yellow (second touch) lines show the segments up to 30 ms after touch onsets. These segments were used to quantify the response to touches. Right: Responses to the first and second touches of the sequences. Responses were normalised by the responses to the first touch in the sequence. Units whose responses to the second touch produced by a different whisker were significantly higher than to the same whisker were highlighted in yellow. Sequences that included the first touch of the trial or overlapping touches were excluded from this analysis. E), F), G) and H) show analogous results to A), B), C) and D) respectively but analysing a change in bending direction instead of whisker identity.

As a consequence, the number of trials that met all the criteria to be selected for the SSA test was limited (10±5 per session). A much more common situation was to find successive touches produced by different whiskers. We then assessed how likely to observe a change in the responses every time there was a change in whisker identity was. This test allowed us to study a more representative active behaviour and gain in the number of samples, which in turn increase the statistical power of the test. For

this, we selected all sequences of two successive touches in each session and divided them into 2 groups: Sequences in which both touches were produced by the same whisker (w_1,w_1), and sequences in which there was a change of whisker (w_1,w_2). From these groups, we selected the sequences which the inter-touch time onset was between 30 and 500 ms (Figure 4.5.D). Sequences that included the first touch of the trials or overlapping touches were excluded from this analysis. We found no significant difference in the strength of the touches produced by w_1 and w_2 in any of the sessions. We then compared the responses of the second touch of both groups to the responses to the first touch. Consistently with results in panel C, for 25% units, the amplitudes of the responses to the second touch were higher when were produced by a different whisker, implying that they adapted specifically to whisker identity.

We then repeated these analyses to test whether the direction of bending could also induce SSA. Direction of bending was classified in terms of the sign of κ_{3D} (Figure 4.5.E). Thus positive values κ_{3D} indicate the whisker being bent and negative values being straightened.

Figure 4.5.F shows the responses to the oddball test for the session shown in panel B) and its respective κ_{3D}. For simplicity, the magnitude κ_{3D} was plotted as negative for the adapting stimuli and positive for the test stimulus for this figure. From the upper panel, it stands out that only one unit from the population presents a firing rate significantly higher for the test stimulus. To take into account the strength of the touches in this scenario, we produced two tuning curves for later touches, one for positive values of κ_{3D} and one for negative values. We used these tuning curves to predict the responses to the test touch. In this case, 21% of the population presented stronger responses than the ones predicted for later touches, similar to whisker identity (Figure 4.5.G). For these units, their responses to the test touch were comparable to the prediction produced by the first touch tuning curves, except for two units were the predictions were significantly lower (Figure 4.5.G, lower).

When we compared the responses to sequences with same and different bending direction, only 10% of the units responded more strongly to sequences with different directions. This result suggests that the specificity to bending direction was weaker than for whisker identity.

4.4 Discussion

The classic approach to study sensory adaptation is based on the analysis of neural responses to a highly-controlled, repetitive stimulus applied to an anaesthetised subject. However, this approach is not representative of natural stimuli and their respective processing in awake conditions. Here we studied how adaptation changes the coding properties of barrel cortex neurons in awake, behaving mice. We found that active touch behaviour and sensory adaptation shape the responses of cortical activity.

Mice were trained to report the presence of a pole within whisker reach, which encouraged the mouse to actively whisk to touch the object. Contacts are a known encoded variable in barrel cortex. Furthermore, the strength of the touches modulates the responses of barrel cortex neurons (Hires et al., 2015; Peron et al., 2015; J. Yu et al., 2016). Here, we identified a population of neurons that encode contacts in barrel cortex during active whisking behaviour. Both behaviour and encoding evolved during the course of individual trials, shaping simultaneously cortical responses. To disentangle what causes the changes observed in neural responses to touches, it is necessary: First, to describe in detail the animal behaviour, especially the behavioural variables driving the cortical neurons. In our case, we measured whisking behaviour and its associated mechanical variables as the bending moment. Second, it is necessary to compare the cortical activity in a way that takes into account changes in behaviour. In our case, we compared the tuning curves in different contexts instead of raw neural responses.

Mouse active touch behaviour, and in particular mechanical properties of touch, evolved throughout individual trials, producing strong first contacts and subsequent softer contacts. In the context of our detection task, mice could eventually solve the task by touching the pole once. However, they keep whisking and softly touching the object even after receiving the reward. This pattern of whisking behaviour is consistent with the control strategy called "minimal impingement" (Mitchinson & Prescott, 2013). This control strategy states that freely behaving rodents seek to limit the amount of whisker bending produced by contacts after detecting a touch to carefully explore the object/surface encountered.

In addition to changes in the mechanical properties of touch, neural encoding also

evolved throughout individual trials. Specifically, individual units presented strong responses to the first touch of the trials and gradually decreasing responses for subsequent touches. This is the first time, to our knowledge, that a change in encoding over time has been observed during active somatosensation. More importantly, this observation confirms that sensory adaptation is an observable phenomenon during an active sensing task.

The reduction in the cortical responses to touch after the first touch of the trial induces, as a byproduct, the impairment of individual neurons to detect later touches. A reasonable question to ask is if sensory adaptation can bring any benefit to the representation of sensory stimuli in this context. For instance, if the observed changes in neural encoding could help to represent other features of sensory input after the first touch. Because for the detection task mice only need the first whisker contact, it is difficult to explain with this task what other features are been encoded once the neurons reach an adapted state. Previous works have suggested that adaptation would benefit the encoding of subtle features in the objects (Wang et al., 2010; Ollerenshaw et al., 2014), which goes in line with the minimal-impingement control strategy. Therefore, good tasks to test this hypothesis should encourage the animal to produce multiple touches, for example, evidence accumulation tasks, such as texture discrimination (Zuo & Diamond, 2019).

This last point highlights a possible relationship between whisking behaviour, sensory adaptation and the aim of the behavioural task. Specifically, in a detection task such as the one described here, the animal only needs to contact the object once to solve the task. Therefore, the information gained from the first and later contacts of each trial could be qualitatively different. This, in turn, could affect the encoding of first and later contacts. In particular, a change in the encoding, such as a reduction in the responses to later touches, could be present. If this is true, then the extent of adaptation effects could be enhanced by the aim of the task. To test this hypothesis, it is crucial to measure adaptation effects during other behavioural tasks that encourage the animal to identify a particular feature of the object, for example, distance to the snout, shape or texture.

Our detailed whisker description not only allowed the study of adaptation to touch but also to specific touch features as whisker identity and bending direction. Previous

studies of SSA to these variables in anaesthetised animals shown inconclusive results. Adaptation to whisker identity has been reported to be highly specific in some preparations (Katz et al., 2006), while less specific in others (Musall et al., 2014). Dissimilar results could be due to differences in the stimuli applied or physiological states, such as the strength of anaesthesia (Lampl & Katz, 2017). Here we propose a methodology to test the specificity of this and other variables in awake, behaving mice accounting for differences in the stimuli. Our results show that some neurons in the population adapted specifically to whisker identity and their responses to the test stimulus were comparable to the first touch responses.

In our preparation, mice could solve the task using a single-whisker, therefore multiwhisker integration was not required. However, this methodology could be applied to analyse tactile experiences in which mice need multiple whiskers to solve the behavioural task, such as aperture width discrimination (Krupa et al., 2001) and fine-scale texture discrimination (G. E. Carvell & Simons, 1995). This would shed light in the following questions: if SSA to whisker identity is more prominent in those tasks, how multiwhisker integration can benefit from Neural Adaptation and how mice adapt their behavioural strategies to solve these tasks.

Similarly, we found a group of neurons that adapted to bending direction. Adaptation specificity to this variable, however, appeared to be weaker than for whisker identity. Bending direction was defined in whisker-centred coordinates because during active touch depends on the orientation of the whisker at the moment of touch onset. In preparations where animals are anaesthetised, a similar variable is commonly referred to as direction (or angle) of deflection, which is defined in head-centred coordinates. Directional selectivity has been shown in all stages of the Lemniscal pathway (Bale & Petersen, 2009; Kremer et al., 2011). However, the adaptation of neural responses is weakly or non-specific to this variable (Khatri & Simons, 2007; Musall et al., 2017). Directional selectivity maps have been shown to emerge in late stages of rodents life (Kremer et al., 2011), suggesting that direction selectivity is acquired based on tactile experience. This could, in turn, produce a similar effect in adaptation specificity. Therefore specific adaptation to bending direction could be more prominent in animals trained to solve a behavioural task in which this variable is fundamental to make a decision, for example, discrimination of object's positions, contours or texture.

Although the presence of SSA is indicative of the dependence of cortical responses on previous stimulation, it does not imply a true-deviant detection, in other words, that the change in the response is a product of violations of a rule in the previous stimulus. True-deviant detection has been previously observed in barrel cortex in anesthetised animals (Musall et al., 2017). More specifically, it has been shown that long latency stimulus responses (100-500 ms) show true-deviant detection, while shorter latency (<50 ms) responses do not. However, if true-deviant processing can be observed during active somatosensation remains unclear. Therefore, to assess true-deviant, both short and long latency responses must be exclusively attributed to one stimulus. To guarantee this condition, it is necessary to enforce that the stimuli (i.e., whisker contacts) are temporally separated over long periods, which is not possible in our task.

Although the determination and comparison of the tuning curves in active, behaving animals is more challenging than in controlled conditions, we here presented a simple and insightful method to disentangle how Behavioural and Neural Adaptation modulate cortical activity. The simplicity of the analysis makes it highly applicable to describe adaptation in behaving animals under other experimental conditions. For example, under different behavioural tasks, such as texture discrimination, object localization or gap-crossing tasks.

In summary, our results indicate that sensory adaptation is present in barrel cortex during active somatosensation. Effects of sensory adaptation can be disentangled from effects produced by active touch behaviour thanks to a detailed description of mechanical and kinematical touch features. The methodology presented here opens new paths to characterise sensory adaptation in awake, behaving animals and investigate how this phenomenon affects active perception.

4.5 Methods

All experimental protocols described in here were approved by both United Kingdom Home Office national authorities and institutional ethical review.

4.5.1 Behavioural apparatus

The whiskers were imaged similarly to (R. S. Petersen et al., 2020) using high-speed cameras (LTR2, Mikrotron, Unterschleissheim, Germany; 1000 frames/s, 0.2 ms exposure time) in both the horizontal and vertical view. Both cameras used telecentric lenses (55-349, Edmunds Optics, Barrington, NJ) and the field of view (480 × 480 pixels) of the horizontal camera was parallel to the transverse plane, while the field of view of the vertical camera was located to 25° of the sagittal plane and 10° from the transverse plane. The position of the vertical camera was chosen to minimise occlusion between the cheek of the mouse and its whiskers. Mice were head-fixed and positioned inside a Perspex tube (inner diameter 32 mm). Licks were detected as described in (O'Connor, Clack, et al., 2010). The whiskers were free to move at all times and were illuminated from below using an infrared LED array (940 nm, LED 940-66-60, Roither, Vienna, Austria) via a diffused condensed lens.

4.5.2 Surgical procedure and mice training

Mice (C57; males; N=2) were first habituated to the apparatus, then anaesthetised with isoflurane (1.5-2.5% isoflurane by volume in O_2) maintaining a body temperature of 37° using a homeothermic heating system to implant the titanium head-bar. The skull was exposed and the titanium head-bar was attached with dental acrylic. After surgery, mice were left to recover for at least 5 days before starting water restriction (1.5 ml water/day). Training began 7-10 days after the start of water restriction. Water was given as a reward during the training and the mice were trained until they reached more than 70% performance. Subsequently, a craniotomy was performed and sealed with silicone elastomer. Mice were left to recover for 2 or 3 days. Before the beginning of the recording, mice performance was tested to be equal or higher to 70%.

4.5.3 Behavioural task

In each trial, a pole (1.59 mm diameter) was commanded to move to known coordinates in the transverse plane: close to the whiskers on Go trials and far from the whiskers on No-Go trials. The pole was then lifted to the final position in all trials. In Go trials, whiskers could reach the pole only while it was on its final position, with the time

that the pole went back to the original position determined by the type and outcome of the trial: if the mouse touched the pole and licked the lick-port (Hit), water was released as a reward and the pole was commanded to stay at the final position for 1 second before returning to the original position. If the mouse did not lick the port (Miss), it was penalised with a time-out (3-5 seconds) and only then the pole was commanded to return to the original position. In No-Go trials, if the mouse did not lick the lick-port (Correct Rejection), the pole was commanded to stay for 2.5 seconds in the final position before returning to the original position, otherwise, the mouse was penalised with a tone and a time-out (3-5 seconds), and the pole was then commanded to return to the original position.

4.5.4 Electrophysiology

Recording. Extracellular recordings from layer 5 of the barrel columns were obtained as follows: Mice were trimmed to three whiskers in C row (C1, C2 and C3) under brief isoflurane anaesthesia. Intrinsic optical imaging was performed to locate the area corresponding to the targeted whisker barrel. During the imaging, the targeted whisker was deflected using a piezoelectric device, then a craniotomy was made at the selected location under isoflurane anaesthesia. The craniotomy was posteriorly filled with silicone elastomer.

Acute implantation of a 16-channel linear silicon probe (2 Shanks, Cambridge NeuroTech, Cambridge, United Kingdom) was performed at the beginning of each session under isoflurane anaesthesia. Mice were left to recover for at least 2 hours before starting the recording session. The mouse was exposed to repeated trials during the session. Data was pre-amplified, collected at a sampling rate of 24.4 kHz, filtered (band-pass filter 300-3000 Hz) and acquired to a hard disk (RZ5, TDT). At the end of the recording session, the microelectrode array was withdrawn, the craniotomy sealed with silicone elastomer, and the mouse returned to its home cage.

Spike sorting. Every shank was sorted independently using JRCLUST (Jun et al., 2017). Units used in posterior analyses must meet the following criteria: 1) the first and second PCA components of the spikes belonging to the units must be well isolated from the noise. 2) Their activity was consistent for 30 or more trials. Segments of the

sessions in which electrode spatial drift was observed were discarded. 3) The inter-spike interval presented a low spiking probability during the refractory period (2 ms). To classify neural activity into single- or multi-unit activity, a series of visual tests on the output of the spike sorting algorithm was considered. For a group of spikes to be considered as coming from a single-unit, their waveform should be consistent for most spikes; the amplitude of the waveforms should lie well above the threshold for spike detection; the amplitude of the waveforms should reach a maximum in one of the probe's recording contacts and decrease for neighbouring channels; the inter-spike interval histogram should show no spikes in the first 2 ms as indicative of a refractory period, and in the visualisation in the feature space (first and second principal component), the activity should form a well-isolated, distinct cluster. If a group of spikes did not meet one or more of the described criteria, it was then considered as a multi-unit recording.

4.5.5 Whisker tracking

To extract kinematic and mechanical variables, whiskers in video recordings were tracked in 3D using freely available software (R. S. Petersen et al., 2020). To reconstruct the whiskers in 3D, the tracker's algorithm integrates information from the horizontal and vertical view through a point to point calibration process. Calibrations were performed at the end of each recording session.

The shape of the target whisker was described as a quadratic, three dimensional Bezier curve $\boldsymbol{b}(s) = (x(s), y(s), z(s))$, where, x, y, z are real space coordinates and $0 \leq s \leq 1$ parameterises location along the curve: $\boldsymbol{b}(s = 0)$ corresponds to the end closest to the whisker base, while $\boldsymbol{b}(s = 1)$ to the end furthest from the base.

The intrinsic shape of a quadratic curve is fully described by a curvature function $\kappa_{3D}(s)$ (Marsh, 2006):

$$\kappa_{3D}(s) = \frac{\left| \frac{d\boldsymbol{b}(s)}{ds} \times \frac{d^2\boldsymbol{b}(s)}{ds^2} \right|}{\left| \frac{d\boldsymbol{b}(s)}{ds} \right|^3} \tag{4.1}$$

Here $|\boldsymbol{a}|$ denotes the magnitude (2-norm) of vector $\boldsymbol{a}$. $\kappa_{3D}(s)$ has units of 1/distance and is the reciprocal of the radius of the circle that best fits the curve at point s.

For a quadratic curve, we can apply the standard relationship between bending

moment during contacts ($\boldsymbol{M_z}$) and a change in whisker curvature (Birdwell et al., 2007; Quist & Hartmann, 2012). From here it follows that $\boldsymbol{M_z}$ is proportional to:

$$\Delta\kappa_{3D}(s) = \kappa_{3D}(s) - \kappa_{3D,0}(s) \tag{4.2}$$

where $\kappa_{3D}(s)$ is the curvature of the whisker during contact and $\kappa_{3D,0}(s)$ is the curvature when the whisker is free from contact and in its resting state. All results presented here were evaluated at $s = 0$ and 5 ms after touch onset.

Bezier curves were visually checked to match whisker's shadows and occasional mistakes were manually corrected. Touches were manually detected with the help of a customised software.

4.5.6 Data analysis

Spike trains from the spike sorting were discretised into 1 ms bins to match the resolution of video recordings.

Ideal observer detection performance. For results in Figure 4.2.C and 4.2.D, all selected units responses were defined as spikes from 30 ms non-overlapping segments. For first and later touches, the firing rate was defined as the spikes from touch onset up to 30 ms afterwards. Spontaneous responses (noise) for the first touch were defined as the spikes observed between the beginning of the trials and the first touch. For later touches, the noise was defined as spikes observed while none of the whiskers was contacting the pole while the pole was in reach.

Histograms of the neural activity were produced for each unit. Thresholds were defined as integer numbers between 0 and 20. For each threshold, the hit rate was computed as the area under the touch probability density (first or later) from the threshold until the maximum number of spikes evaluated (20). False alarm rate was calculated as the area under the noise probability density from the threshold until the maximum number of spikes evaluated. These values were used to construct ROC curves, and areas under the ROC curve were used as an estimation of performance.

Tuning curves. The main mechanical variable $\Delta\kappa_{3D}$ was computed as the mean value of κ_{3D} of the 5 ms after each touch onset. Tuning curves were computed using

$\Delta\kappa_{3D}$ absolute value. Tuning curves were constructed as follows: $|\Delta\kappa_{3D}|$ was computed as described above for all the touches in the session. The firing rate for each touch was computed as the sum of the spikes from the touch onset up to 30 milliseconds afterwards. A histogram of $|\Delta\kappa_{3D}|$ values for later touches was produced. The highest 5% of the values were considered outliers. The remaining samples were divided into 4 bins with the same number of samples each. The mean $|\Delta\kappa_{3D}|$ of the samples in each bin was defined as the stimulus value, while the mean of the firing rate in each bin was defined as the response.

To predict the firing rates shown in Figure 4.4.B (right), for each trial, $|\Delta\kappa_{3D}|$ of the first touch was used as an input of the later touches tuning curve. The predicted firing rate for first touches was then averaged across trials. To test the accuracy of the first touch tuning curve, we predicted the activity of first touches using a Leave-one-out cross-validation process. For both comparisons, the measured firing rates are the average unit response across trials between the touch onset and the 30 ms afterwards.

Stimulus-Specific Adaptation. For whisker identity analyses in Figure 4.5.A, B and C, only trials that met the following criteria were selected: First, at least the first two touches were produced by the same whisker. Second, at least one touch was produced with the other whisker after the first two touches. And third, the test touch was not overlapping with a touch from the other whisker. For bending direction analysis (Figure 4.5.E, F and G), analogous criteria were applied: At least to touches with the same direction at the beginning of the trial, at least one later touch in the other direction and the test touch was not overlapping another touch.

For comparison between test touch and later touch responses, we determined two tuning curves for later touches, one for each whisker of bending direction. The tuning curves were obtained fitting all later touches (N_{touch} >2), only test stimuli were excluded.

For comparison between test touch and first touch responses, all first touches and their responses in the session were used to fit the first touch tuning curve. The $|\Delta\kappa_{3D}|$ from each test stimulus was used as input to the tuning curve. The predicted firing rate and the observed responses plotted in Figure 4.5.C and 4.5.G correspond the average prediction across test stimuli.

In the test of the sequences (Figure 4.5.D and Figure 4.5.H), sequences of consecutive non-overlapping touches were selected. Sequences which touch onsets were separated for less than 30 ms were excluded from this test. Sequences were divided into "same whisker sequences" and "different whisker sequences" for whisker identity, and "same direction sequences" and "different direction sequences" for bending direction. Firing rates to the second touch of the sequences were compared to determine the units that presented SSA effect. Units that presented significantly higher rate in the second touch of "different" sequence than for the "same" sequences were considered to be specifically adapting to the selected stimulus (two-sample t-test, $\alpha = 0.05$).

Chapter 5

General Discussion and Conclusions

5.1 General overview

This thesis encompasses the study of active somatosensation in the mouse whisker system. To understand how whisker sensory inputs are represented in the barrel cortex during active sensation, the study aims were: 1) to quantify whisker sensory inputs in awake, behaving animals, 2) characterise the whisker mechanical variables and determine if they are represented in the cortex during active exploration, and 3) describe the main dynamic properties of the barrel cortex neural code during active somatosensation.

Somatosensation is fundamentally an active sense, in other words, animals can move and control their sensory organs to gather information (Prescott & Dürr, 2016; C. C. Petersen, 2019), therefore, it is essential to track the animal's sensory organs and their behaviour to characterise somatosensation. Quantifying animal behaviour is a long-standing ethological problem (Tinbergen, 1951). From a neuroscience perspective, animal behaviour is pivotal to make sense of neural activity in the brain. The lack of tools to accurately measure whisker behaviour has hindered the understanding of active somatosensation, constraining research to either study oversimplified behaviours or producing coarse estimation of the sensory inputs of the whisker system. The present study developed a method to measure whisker shape and kinematics in 3D during active exploration with multiple whiskers, which was then implemented into a whisker tracker software available for the scientific community (Chapter 2).

One of the main aims of sensory neuroscience is to identify the sensory inputs

that drive neural activity. In the whisker system, the physical inputs entering the system can be summarised as kinematic and mechanical inputs. This study provided a complete kinematic description of the whiskers during active exploration of head-fixed animals (Chapter 3). For the first time, the two main mechanical candidates to drive cortical activity during active exploration, the bending and twisting moment, were characterised, showing that these mechanical inputs modulate cortical activity during touch. This indicates that a detailed description of whisker behaviour and its mechanics is fundamental to elucidate the mechanical basis of somatosensation.

A widespread observed phenomenon across sensory systems is the adaptation of neural responses (A. Fairhall, 2014; Weber et al., 2019; Weber & Fairhall, 2019), that is, the fact that the neural code is not static but it adjusts to different contexts. Characterising adaptation in an active sense, as in the whisker system, is challenging because it requires a detailed description of the sensory inputs, the identification of the inputs driving the neural activity and to disentangle how whisking behaviour modulates neural activity from the changes in the neural activity produced by the dynamical aspects of the neural code. A paradigm was presented to study this phenomenon in the whisker system in awake, behaving animals (Chapter 4) and applied in the barrel cortex to show the extent of adaptation effects during active sensation. As a result, this paradigm provides a way to characterise how adaptation effects shape active somatosensation and perception.

The following sections will discuss the main points outlined above, summarising the main criticisms of the study, the challenges to overcome in future studies of active somatosensation and possible directions for future work.

5.2 Quantifying Whisking Behaviour

Quantifying whisking behaviour has deepened our understanding of active sensation and rodent behaviour (Grant et al., 2009; Mitchinson & Prescott, 2013; O'Connor, Clack, et al., 2010). From a neuroscience perspective, defining whisker movements and mechanics is critical to establish the sensory basis of the somatosensory system. Whisker tracking has been typically measured in the horizontal plane (Knutsen et al., 2005; Clack et al., 2012; Gillespie et al., 2019), enabling the estimation of only one

of the three angles that define the whisker position. This approach also allows the estimation of three of the six mechanical variables at the whisker base, the bending moment, axial force and lateral force (Birdwell et al., 2007; Pammer et al., 2013).

In Chapter 2, an experimental method was developed to estimate the three angles that define whisker movement, and in turn, offer a complete kinematic description of the whisker base. Regarding the mechanical variables, this method disentangles the changes in whisker position from changes in whisker shape. Consequently, it provides a more accurate description of the mechanical variables independent of kinematic properties.

This tool not only allows a better description of the whisker kinematic and mechanics but also widens the experimental scenarios that can be analysed, which has been restricted so far to match the conditions set by biomechanical models (Birdwell et al., 2007; Pammer et al., 2013). For instance, several studies aiming to estimate the mechanical variables at the whisker base have designed experimental setups in which the whisker movement and bending are restricted to the horizontal plane (O'Connor, Clack, et al., 2010; Sofroniew et al., 2014; Campagner et al., 2019). The method developed in this study would allow the extension of behavioural tasks to include 3D whisker exploration, for instance, 3D object recognition or discrimination between surfaces' texture. Considering that the proposed method does not require any animal manipulation other than head-fixation, the restrictions for experimental setups designs are only set by the imaging of the whiskers? constraints.

Chapter 3 extended the computational capabilities of the whisker tracker to describe both moments (bending and twisting) from high-speed videography recordings, demonstrating that during active sensation, whiskers not only are subject to bending but to twisting as well (see Chapter 3, Figure 3.3). This implies that the whisker mechanics in these conditions are not exclusively defined by the bending moment, as previously considered (Birdwell et al., 2007; Quist & Hartmann, 2012), but also affected by twisting moment.

Thanks to the exhaustive description of whisker shape and movement, it was determined that the change in horizontal curvature ($\Delta\kappa_h$) in the experimental setup was strongly modulated by whisker orientation (roll angle) rather than whisker bending (see Chapter 3, Figure 3.3). The repercussions of this finding are multiple. First, the

experimental setup was similar to those in several studies using $\Delta\kappa_h$ as a proxy of the bending moment (O'Connor, Peron, et al., 2010; Campagner et al., 2016; Severson et al., 2017; Hires et al., 2015; Campagner et al., 2019). In other words, the estimation of bending moment, and in turn, of the forces at the whisker base could have been contaminated by the roll angle of the whisker. Therefore, future studies aiming to estimate the bending moment should consider this point by either measuring the bending moment in 3D or if imaging the whiskers in the horizontal plane, it is pivotal to comply with the biomechanical modelling assumptions. For instance, if measuring in one plane, the whisker must be oriented in a way that the intrinsic curvature is captured at all times (Quist & Hartmann, 2012).

Taken together, the results of tracking mouse whiskers has provided an insight into the benefits of 3D tracking for both mice and rats. During whisking, mouse and rat whiskers have different mechanical properties, for example, mouse whiskers bend and twist at high whisking speed, therefore 3D tracking is fundamental to describe the whiskers' shape unambiguously. Unlike mouse whiskers, rat whiskers behave as a rigid object during whisking, therefore the shape of rat whiskers can be reconstructed using 2D whisker tracking. However, the 3D tracking of rat whiskers still provides a complete kinematic description (azimuth, elevation and roll angles) that cannot be extracted from 2D tracking. However, during whisker contacts, both mice and rats bend and twist their whiskers, therefore, 3D whisker tracking is crucial to, first, estimate accurately the mechanical variables entering the system, and second, provide a complete kinematical description of the whisker during touch for both species.

Although this method is a critical advance in the description of whisker behaviour and the physical inputs of the whisker system, it has a few limitations. First, its implementation requires the animal to be head-fixed. Head-fixation presents not only advantages to measure whisker behaviour but also to record neural activity. Therefore, to analyse both aspects in freely moving animals, it is necessary to extend the whisker tracking together with neural activity recording methods. In particular, whisker tracking in freely moving animals presents two main challenges: occlusion of the whiskers by the animal's head/body and tracking of animal's head and body. Second, although this method allows tracking of multiple whiskers, it only describes the whiskers from one side of the animal head, restricting the study of bilateral exploration that animals

perform. Another restriction is that the method focuses on recovering the shape at the whisker base, specifically, the whisker is represented as a quadratic (Chapter 2) or a cubic (Chapter 3) Bezier curve. This is appropriate to describe the fundamental mechanical inputs to the whisker system but should be extended to higher-order curves if the entire length of the whisker needs to be studied.

5.3 Whisker kinematics and mechanics during active somatosensation

Whisker kinematics have been widely used as an estimation of physical inputs entering the whisker system (Khatri et al., 2004; Stüttgen et al., 2006; C. C. Petersen, 2007; Maravall et al., 2007; Hires et al., 2015). The bulk of the literature has used whisker position and its derivatives to quantify the strength passive whisker deflections in anesthetised animals (Simons, 1978; Pinto, Brumberg, & Simons, 2000; Maravall et al., 2007; Díaz-Quesada & Maravall, 2008; R. S. Petersen et al., 2008; Bale et al., 2013). In behaving animals, whisker position and angular velocity have been used to approximate the strength of the whisker touch (Crochet et al., 2011; Crochet & Petersen, 2006; Yamashita et al., 2013; Hires et al., 2015), whereas, during active whisking, these variables have been used as a measurement of whisker movement and a proxy of the moment at the whisker base (Khatri, Bermejo, et al., 2009; O'Connor, Peron, et al., 2010; Campagner et al., 2016; Severson et al., 2017). Even though kinematic variables can be correlated to mechanical inputs at the whisker base, they do not explain the basis of mechanotransduction. This way, although kinematic variables can correlate with neural activity, they do not necessarily drive neural responses.

The next section explains how kinematic and mechanical variables are correlated during whisking and whisker contacts, and to what extent geometrical variables are an appropriate representation of mechanical variables.

5.3.1 Non-contact Whisking

A fundamental finding marks the biomechanical modelling of the whisker during non-contact whisking, that is, the 70% most proximal segment of the rat whisker is

rigid (Knutsen et al., 2008; Quist et al., 2014). This fact has been assumed to be similar for mouse whiskers (Campagner et al., 2016; Severson et al., 2017).

If the whisker is assumed to be a rigid object, the moment M at the base can be computed as $M = \alpha I$ were α is the angular acceleration and I represents the moment of inertia (M. Hartmann, 2016). If a neuron is sensitive to the moment, then its activity can be predicted by whisker angular acceleration. Although some neurons throughout the whisker system have been shown to be sensitive to whisker acceleration (Campagner et al., 2016; Severson et al., 2017), other neurons have been shown to be sensitive to velocity, movement direction or particular phases of the whisking cycle (Khatri, Bermejo, et al., 2009; Moore et al., 2015; C. Yu et al., 2006; Crochet & Petersen, 2006; Hires et al., 2015). However, the possible mechanotransduction mechanisms for these last kinematic variables are unclear.

The present study demonstrated that mouse whisker shape changes substantially both in curvature and torsion during whisking. Mouse whiskers are considerable smaller than rat whiskers, which could explain this discrepancy (Ibrahim & Wright, 1975). During whisking, forces and moments at the whisker base are not governed by static effects but by dynamic effects instead (Quist et al., 2014), therefore, the mechanical framework used to describe touch (see section 1.3) cannot be applied to whisking episodes. As a result, the geometrical quantities of torsion and curvature are not necessarily proportional to the twisting and bending moment as during touch. However, changes in shape provide an insight into how the mass distribution of the whisker changes within the whisker cycle, modulating, in turn, the inertial properties (I) of the whisker.

The changes in shape were shown to be phase-locked and their magnitude is proportional to the angular speed (see Chapter 3, Figure 3.2). Previous studies have found primary whisker neurons (PWN) showing a preference for both angular velocities or particular phases of the whisking cycle (Leiser & Moxon, 2007; Khatri, Bermejo, et al., 2009; Severson et al., 2017). Therefore, this study provided a link between the kinematic parameters represented in the whisker system and the whisker shape. Future studies regarding neural encoding during whisking will require biomechanical modelling to decipher the exact relationship between changes in whisker shape and forces/moments at the whisker base. This, in turn, will aid to identify the underlying

mechanical inputs entering the system during whisking.

5.3.2 Active whisker contacts

Although the barrel cortex has been extensively studied in anaesthetised animals, only in the last decade has the mechanosensory basis that drives barrel cortex activity started to be uncovered. So far, it has been shown that primary whisker neurons (PWN) activity can be predicted from an estimation of the bending moment (M_z) and its rate of change ($\dot{M}_z$) (Campagner et al., 2016; Severson et al., 2017), suggesting that the bending moment is encoded in the whisker system. From recordings in the cortex in awake, behaving animals, some evidence of the coding of this variable has been collected using 2D whisker imaging (O'Connor, Peron, et al., 2010; Hires et al., 2015; Peron et al., 2015; J. Yu et al., 2016). However, no study has explicitly tested how well the barrel cortex activity is predicted from 3D mechanical inputs or their rate of change, specifically, the possibility that other mechanical inputs different to the bending moment can drive barrel cortex activity has not been assessed so far.

Chapter 3 showed that the rate of change of the total bending moment ($\dot{M}_b$) could be encoded in the barrel cortex during active touch. However, this is not the only mechanical variable affecting the base of the whisker. The predictions from this variable and another mechanical candidate, the twisting moment, were compared, suggesting that in addition to the bending moment, the twisting moment could also drive cortical activity. Further investigation is necessary to determine the effect of these variables on the neural activity. For this, an experimental setup that promotes a diverse set of active touches, in particular, that helps to decorrelate torsion from curvature is necessary. For example, using multiple pole location in the anterior-posterior axis would promote touches with different whisker orientation at touch onset, thereby promoting touches with different bending/torsion ratios.

In Chapter 3, the nonlinear transformation of these variables predicted the cortical activity better than touch for some units, implying that these variables are the mechanical basis underlying touch, therefore, the cortical responses to touch previously observed (see Chapter 3, Figure 3.4).

The cortical activity studied throughout this thesis was obtained using electrophysiological, extracellular recordings in awake, behaving mice. Although extracellular recordings have had a pivotal role in understanding neural activity, they have some limitations with respect to intracellular recordings. First, intracellular recordings allow the recoding of subthreshold events, such as synaptic potentials, which provide information about intracellular changes. For instance, they can track changes in cell excitability, which cannot be captured by extracellular recordings. Second, as intracellular recordings record activity from a single cell, they guarantee the correspondence between neural activity and the identity of the cell. However, in extracellular recordings, changes in electrophysiological properties need to be spike-sorted, in other words, to establish which spikes correspond to which cell. These two limitations of extracellular recordings can, in turn, limit the questions that can be asked about recorded neural activity. In this case, given that the barrel cortex activity is sparse, subthreshold events could provide more information about the encoding of mechanical variables through monitoring of subthreshold neural activity. Moreover, single- and multi-unit activity was observed in this study. The multi-unit activity could contain electrophysiological changes from different neurons, which potentially could be sensitive to different mechanical variables, hence, the combined activity of these neurons could yield inaccurate results in the modelling.

Throughout this study, the model applied to describe the moments on the whisker base was a quasi-static model, such models have been widely used to describe the mechanical inputs that enter the follicle (Birdwell et al., 2007; O'Connor, Clack, et al., 2010; Campagner et al., 2016; Severson et al., 2017; Hires et al., 2015; Campagner et al., 2019). However, the main assumption of this model limits the scenarios that can be characterised. The main limitation is the lack of dynamic effects over the mechanical variables, for example, the effects of friction during whisker contacts cannot be incorporated into this analysis. This limits the mechanical analysis of some experimental conditions, such as comparing mechanical inputs when the whiskers contact different textures. As each surface presents particular frictional properties, curvatures and torsion could be compared for the same textures, but they are hardly comparable across different textures.

Another case that is out of the scope of the quasi-static model is slip-sticks events,

where due to friction, the whisker slips over a surface, then suddenly sticks out of the surface. In both situations (slip-sticks and different textures), descriptors of whisker shape (curvature and torsion) extracted from the tracker are an accurate representation of whisker geometry over time, but they are not necessarily linearly proportional to the bending and twisting moments. To accurately measure mechanical variables under these circumstances, biomechanical modelling in three dimensions that include frictional, torsion and dynamical effects is needed (Knutsen et al., 2008; Quist et al., 2014; Vaxenburg, Wyche, Svoboda, Efros, & Hires, 2018; Huet et al., 2015).

Slip-sticks events are commonly found during active whisker exploration, and they were present during the contacts described here. Nevertheless, because of their rare presence during the trials and short duration, they constituted a minuscule fraction of the time of the recordings.

5.4 Dynamical properties of neural code in the barrel cortex

While Chapter 3 showed that mechanical inputs can drive activity in the barrel cortex, the model used to predict neural activity from sensory inputs assumes that the rules to encode these variables are static. The accuracy of this during active somatosensation was tested in Chapter 4. In a more general way, the effects of the changes in the encoding rules of sensory variables are also known as adaptation of neural activity (Weber & Fairhall, 2019; A. Fairhall, 2014). This phenomenon has been long observed across sensory modalities and species (see (Weber et al., 2019) for review).

Neural adaptation can produce profound repercussions in computational, perceptual and behavioural terms (Maravall et al., 2007; Wang et al., 2010; Ollerenshaw et al., 2014; Weber et al., 2019). However, it has been largely characterised in experimental setups with high control over the stimulus, such as in anaesthetised animals or applying passive stimulus. This is inaccurate for an active sense like the somatosensory system, where the animals can actively control their sensory inputs.

In Chapter 4, the method developed in Chapter 2 was used to produce an exhaustive description of the whisker shape and movement during a tactile detection

task. This characterisation enabled the identification of the physical inputs that modulate barrel cortex activity while mice performed the task, showing that within trials both neural activity and whisking behaviour adapted over time. This study not only provides evidence that neural adaptation is an observable phenomenon during active somatosensation but the paradigm described can also further characterise the sensory adaptation during active sensation. More specifically, extensions of this paradigm could quantify adaptation effects in a wide range of behavioural tasks and comprehend how animals exploit sensory adaptation to gather information about the environment in each scenario. This paradigm could also be extended to study specific contextual modulations of neural activity, for instance, differences in internal states of the brain, such as engagement in the task.

As the neural activity analysed here corresponded to extracellular recordings, it is still unknown how neural adaptation can change subthreshold neural activity in awake, behaving animals. Intracellular recordings in the barrel cortex during a behavioural task would shed light on the mechanisms that give rise to the extracellular effects of sensory adaptation.

Only a few studies had shown evidence of adaptation effects during active sensation, most of which have shown small differences in neural responses to repetitive active touch as a sign that neural activity would be relatively unaffected by neural adaptation. Nevertheless, none of these studied explicitly test how the mechanical inputs, which drive neural activity, evolve together with neural activity. For instance, Castro-Alamancos (2004) applied electrical stimulation of the whisker pad to show that adaptation effects are more prominent during quiescent states. Crochet et al. (2011), Crochet & Petersen (2006) and Yamashita et al. (2013) measured whisker position during active touch as an approximation of touch strength and while Hires et al. (2015) approximated the bending moment during active touch, they did not test if the neural changes were a cause of the changes in whisker behaviour or a change in the encoding properties.

In conclusion, a novel method was developed to describe whisker kinematic and shape in 3D from awake, behaving animals, which allowed the characterisation of 3D mechanical inputs and their encoding in the barrel cortex during a tactile detection

task, as well as the assessment of the extent of sensory adaptation during active somatosensation. Taken together, these results show that a comprehensive analysis of sensorimotor behaviour is vital to understand neural activity and shed light on the dynamic computations performed in the barrel cortex in awake, behaving animals.

5.5 Elucidating the neural code of the barrel cortex during active sensation

As discussed in Chapter 3 and 4, elucidating the neural code in the barrel cortex during active sensation is challenging for several reasons. Here I describe general points to consider when addressing this topic, the main obstacles to overcome and suggestions of how to tackle them.

Challenges for these studies come from two main sources: the difficulties of analysing sensory inputs to the system in awake, behaving mice, and the particular encoding properties of a central circuit like the barrel cortex.

In contrast to experimental paradigms where animals are anaesthetised and sensory stimuli are highly controlled, researchers have little control over whisker stimulation in awake, behaving animals. Therefore, several experimental paradigms designed to understand neural encoding properties during anaesthetised conditions cannot be extrapolated to active sensation. For instance, classical studies of adaptation in anaesthetised animals rely on the assumption that each stimulus presentation within a train of repetitive stimuli presents the same features (Simons, 1978, 1985; Khatri et al., 2004; Katz et al., 2006; Wang et al., 2010; Martin-Cortecero & Nuñez, 2014; Musall et al., 2014). It is virtually impossible that behaving animals produce a train of stimuli as this one during a single trial, and even more unlikely to produce them repetitively across multiple trials. Therefore, new paradigms and analytical methods need to be designed to fit the experimental conditions.

Another challenge of studying sensory inputs during active whisking behaviour is the correlation between the variables, described as multicollinearity. In behaving animals, motor variables are correlated, for example, whisking frequency with running speed (Sofroniew et al., 2014), roll angle and horizontal curvature (Knutsen et al., 2008), etc. This presents a complex scenario for elucidating the neural encoding

properties, not only in the whisker system but for neural circuits in general. First, multicollinearity hinders the identification of the variables encoded in neural circuits, for example, under certain experimental conditions whisker kinematics and mechanics are highly correlated (Bush et al., 2016). Under these circumstances, neurons that encode exclusively mechanical variables seem to be tuned to both mechanical and kinematical variables as a result of the correlation between the variables. Identifying the primary driver of the neural activity is challenging for typical neural modelling methods, which do not consider the high degrees of correlation between the variables. To address this problem, either modelling methods need to be adjusted to these specific conditions, or experimental conditions need to be carefully planned to avoid this phenomenon as much as possible. For example, as shown in (Campagner et al., 2016), primary drivers of PWN activity could be identified by using multiple pole location to decorrelate changes in the curvature from changes in whisker angle during touch.

Stimulus encoding in the barrel cortex differs from encoding in previous stages of the sensory pathway. While neurons in the periphery fire during contacts and non-contact whisking, more central circuits are more selective to whisker contacts than self-motion. Specifically, thalamocortical circuits filter self-motion signals out, so that neurons in layer 4 of the barrel cortex show a marked response to touch instead of self-motion (J. Yu et al., 2016; Gutnisky et al., 2017). In a more general aspect, this exemplifies how different the inputs to barrel cortex and peripheral neurons are, in turn, highlighting the transformation of the sensory input throughout the sensory pathway and how it can affect the modelling of central areas such as the barrel cortex. To accurately describe neural activity in the barrel cortex, information about the representation of the sensory inputs in previous stages is required. In the particular case of the encoding of bending and twisting moments in the barrel cortex, previous studies suggest that the bending moment and its derivatives drive the activity of PWN (Campagner et al., 2016; Bush et al., 2016; Severson et al., 2017). However, there is little information regarding the representation of this variable in downstream areas before the cortex (J. Yu et al., 2016). This leaves a gap in the encoding properties between PWN and the barrel cortex, which is more evident in the case of the twisting moment, the representation of which in the periphery has not been previously analysed.

Computational models could aid to describe the transformation of the sensory

inputs before arriving at the cortex and predict barrel cortex responses. For instance, in the case of using a GLM, allowing nonlinearities, quadratic terms or using a chain of GLMs to represent multiple stages could potentially help (Pillow et al., 2008). For all these strategies, the complexity, and in turn, the number of parameters to be fitted are restricted by the number of spikes of the recordings. In the case of cortical neurons, this is a limiting factor considering the sparsity of the neural activity in awake recordings (A. L. Barth & Poulet, 2012).

A final point to consider is that in awake, behaving animals, neurons in the barrel cortex not only code whisker-relative information but its neural dynamics are modulated by motor parameters such as locomotion (Ayaz et al., 2019) and body parts movements (Musall et al., 2019). Furthermore, some studies have shown that part of the activity of the barrel cortex reflects internal states such as behavioural choice and arousal (H. Yang et al., 2015; Kwon et al., 2016; Shimaoka, Harris, & Carandini, 2018). The activity related to all these variables obscures the encoding properties of whisker-related sensory inputs such as the mechanical variables at the whisker base. Fortunately, some of these internal states can be inferred from observable features of the animal, for example, changes in arousal states can be measured as changes in pupil dilation (Shimaoka et al., 2018). Capturing and analysing this variable during behavioural tasks could aid to differentiate the influence of the sensory and arousal components.

5.6 Future work

The results of this thesis raise new questions for future investigation and offer new tools and methodologies to address them. To define which sensory variables are encoded in barrel cortex during active somatosensation and how this encoding takes place, three long term goals should be achieved. First, to produce a 3D biomechanical model that clearly establishes the mechanical inputs that enter the whisker system during active somatosensation and how to measure them, in other words, this model should incorporate all relevant whisker behaviours, such as whisking, touch and slip-stick events. Second, to describe the encoding of sensory variables in subcortical areas during active sensation. Third, to describe the encoding of sensory variables in the

barrel cortex. The following paragraphs outline the possible steps and considerations to achieve these goals.

A method was developed in this thesis that offers a complete kinematic description of the whisker base and estimates the moments exerted on the whisker base in awake, behaving animals. This method should be extended to estimate the three forces exerted on the whisker in addition to the moments to understand the mechanosensory basis of somatosensation. This could be achieved via two approaches. First, the simplest one, it is to consider a quasi-static model of whisker contacts and approximate the forces from the geometry of the whisker (Pammer et al., 2013). Second, the more realistic is to integrate static and dynamic effects to model the forces and moments during active somatosensation in 3D (Knutsen et al., 2008; Quist et al., 2014; Vaxenburg et al., 2018; Huet et al., 2015), thereby improve the description of the forces and moments during touch but also help to understand the mechanics of non-contact whisking.

To understand how the mechanical variables are encoded throughout the whisker system, it is fundamental to establish a relationship between the mechanical variables and neural activity at each stage of the ascending pathway. To this end, experimental and computational aspects need to be considered.

Within the behavioural aspects, the aim of the task influences whisking behaviour and in turn the mechanical variables at the whisker base. Additionally, different behavioural tasks present different degrees of difficulty for the animal, varying not only the mechanical variables but also the internal states, such as attention and arousal. Although each task can provide valuable insights regarding animals' strategies to solve the task and how mechanical variables are encoded in that specific situation, it is elemental to compare sensory encoding across behavioural tasks for a complete map of the variables and their encoding.

In computational aspects, the region studied in the whisker system is key. While each stage of the pathway can receive information regarding the same variable, transformations to the variables (or the code itself) can be performed at each stage. These transformations can be static, affecting the representations of the inputs at each stage, for instance, coding temporal patterns of the variables instead of the pure magnitude. Also, some dynamic transformations can affect the neural encoding, for instance, the

different extent of adaptation effects. For these reasons, it is vital to study the encoding properties of mechanical variables in awake, behaving animals across stages of the whisker system.

Reference list

Adibi, M., McDonald, J. S., Clifford, C. W., & Arabzadeh, E. (2013). Adaptation improves neural coding efficiency despite increasing correlations in variability. *Journal of Neuroscience*, *33*, 2108–2120.

Adrian, E. D. (1928). *The basis of sensation.* New York, NY, US: W W Norton & Co.

Ahissar, E., Sosnik, R., Bagdasarian, K., & Haidarliu, S. (2001). Temporal frequency of whisker movement. II. Laminar organization of cortical representations. *Journal of Neurophysiology*, *86*, 354–367.

Ahissar, E., Sosnik, R., & Haidarliu, S. (2000). Transformation from temporal to rate coding in a somatosensory thalamocortical pathway. *Nature*, *406*, 302–306.

Ahl, A. S. (1986). The role of vibrissae in behavior: A status review. *Veterinary Research Communications*, *10*, 245–268.

Ahrens, M. B., Linden, J. F., & Sahani, M. (2008). Nonlinearities and contextual influences in auditory cortical responses modeled with multilinear spectrotemporal methods. *Journal of Neuroscience*, *28*, 1929–1942.

Ahrens, M. B., Paninski, L., & Sahani, M. (2008). Inferring input nonlinearities in neural encoding models. *Network: Computation in Neural Systems*, *19*, 35–67.

Arabzadeh, E., Petersen, R. S., & Diamond, M. E. (2003). Encoding of whisker vibration by rat barrel cortex neurons: Implications for texture discrimination. *Journal of Neuroscience*, *23*.

Arabzadeh, E., Zorzin, E., & Diamond, M. E. (2005). Neuronal encoding of texture in the whisker sensory pathway. *PLoS Biology*, *3*, e17.

Auffret, M., Ravano, V. L., Rossi, G. M., Hankov, N., Petersen, M. F., & Petersen, C. C. (2018). Optogenetic stimulation of cortex to map evoked whisker movements in awake head-restrained mice. *Neuroscience*, *368*, 199–213.

Axelrad, H., Verley, R., & Farkas, E. (1976). Responses evoked in mouse and rat SI cortex by vibrissa stimulation. *Neuroscience Letters*, *3*, 265–274.

Ayaz, A., Stäuble, A., Hamada, M., Wulf, M.-A., Saleem, A. B., & Helmchen, F. (2019). Layer-specific integration of locomotion and sensory information in mouse barrel cortex. *Nature Communications*, *10*, 2585.

Azouz, R., & Gray, C. M. (2000). Dynamic spike threshold reveals a mechanism for synaptic coincidence detection in cortical neurons in vivo. *Proceedings of the National Academy of Sciences*, *97*, 8110–8115.

Bale, M. R., Campagner, D., Erskine, A., & Petersen, R. S. (2015). Microsecond-scale timing precision in rodent trigeminal primary afferents. *Journal of Neuroscience*, *35*, 5935–5940.

Bale, M. R., Davies, K., Freeman, O. J., Ince, R. A., & Petersen, R. S. (2013). Low-dimensional sensory feature representation by trigeminal primary afferents. *Journal of Neuroscience*, *33*, 12003–12012.

Bale, M. R., & Maravall, M. (2018). Organization of sensory feature selectivity in the whisker system. *Neuroscience*, *368*, 70–80.

Bale, M. R., & Petersen, R. S. (2009). Transformation in the neural code for whisker deflection direction along the lemniscal pathway. *Journal of Neurophysiology*, *102*, 2771–2780.

Barth, A. L., & Poulet, J. F. A. (2012). Experimental evidence for sparse firing in the neocortex. *Trends in Neurosciences*, *35*, 345–355.

Barth, F. G., Humphrey, J. A. C., & Srinivasan, M. V. (2013). *Frontiers in sensing: From biology to engineering.*

Benjamin, A., Fernandes, H., Tomlinson, T., Ramkumar, P., VerSteeg, C., Chowdhury, R., ... Kording, K. P. (2017). Modern machine learning outperforms GLMs at predicting spikes. *bioRxiv*, 111450.

Berg, R. W. (2002). Rhythmic whisking by rat: retraction as well as protraction of the vibrissae is under active muscular control. *Journal of Neurophysiology*, *89*, 104–117.

Bermejo, R., Houben, D., & Zeigler, H. P. (1998). Optoelectronic monitoring of individual whisker movements in rats. *Journal of Neuroscience Methods*, *83*, 89–96.

Bermejo, R., Vyas, A., & Zeigler, H. P. (2002). Topography of rodent whisking - I. Two-dimensional monitoring of whisker movements. *Somatosensory and Motor Research*, *19*, 341–346.

Birdwell, J. A., Solomon, J. H., Thajchayapong, M., Taylor, M. a., Cheely, M., Towal, R. B., ... Hartmann, M. J. Z. (2007). Biomechanical models for radial distance determination by the rat vibrissal system. *Journal of Neurophysiology*, *98*, 2439–2455.

Blythe Towal, R., Quist, B. W., Solomon, J. H., & Hartmann, M. J. (2012). Active sensing: Head and vibrissal velocity during exploratory behaviors of the rat. In *Frontiers in sensing: From biology to engineering* (pp. 209–224). Vienna: Springer Vienna.

Bosman, L. W. J., Houweling, A. R., Owens, C. B., Tanke, N., Shevchouk, O. T., Rahmati, N., ... De Zeeuw, C. I. (2011). Anatomical pathways involved in generating and sensing rhythmic whisker movements. *Frontiers in Integrative Neuroscience*, *5*, 53.

Boubenec, Y., Shulz, D. E., & Debrégeas, G. (2012). Whisker encoding of mechanical events during active tactile exploration. *Frontiers in Behavioral Neuroscience*, *6*, 1–40.

Brown, A. E. X., & de Bivort, B. (2018). Ethology as a physical science. *Nature Physics*, *14*, 653–657.

Bush, N. E., Schroeder, C. L., Hobbs, J. A., Yang, A. E., Huet, L. A., Solla, S. A., & Hartmann, M. J. (2016). Decoupling kinematics and mechanics reveals coding properties of trigeminal ganglion neurons in the rat vibrissal system. *eLife*, *5*, e13969.

Calabrese, A., Schumacher, J. W., Schneider, D. M., Paninski, L., & Woolley, S. M. (2011). A generalized linear model for estimating spectrotemporal receptive fields from responses to natural sounds. *PLoS ONE*, *6*, e16104.

Campagner, D., Evans, M. H., Bale, M. R., Erskine, A., & Petersen, R. S. (2016). Prediction of primary somatosensory neuron activity during active tactile exploration. *eLife*, *5*, e10696.

Campagner, D., Evans, M. H., Chlebikova, K., Colins-Rodriguez, A., Loft, M. S., Fox, S., ... Petersen, R. S. (2019). Prediction of choice from competing

mechanosensory and choice-memory cues during active tactile decision making. *Journal of Neuroscience*, *39*, 3921–3933.

Campagner, D., Evans, M. H., Loft, M. S., & Petersen, R. S. (2018). What the whiskers tell the brain. *Neuroscience*, *368*, 95–108.

Carvell, G., & Simons, D. (1990). Biometric analyses of vibrissal tactile discrimination in the rat. *Journal of Neuroscience*, *10*.

Carvell, G. E., & Simons, D. J. (1995). Task- and subject-related differences in sensorimotor behavior during active touch. *Somatosensory & Motor Research*, *12*, 1–9.

Castro-Alamancos, M. A. (2004). Absence of rapid sensory adaptation in neocortex during information processing states. *Neuron*, *41*, 455–464.

Cheung, J., Maire, P., Kim, J., Sy, J., & Hires, S. A. (2019). The sensorimotor basis of whisker-guided anteroposterior object localization in head-fixed mice. *Current Biology*, *29*, 3029–3040.e4.

Chung, S., Li, X., & Nelson, S. B. (2002). Short-term depression at thalamocortical synapses contributes to rapid adaptation of cortical sensory responses in vivo. *Neuron*, *34*, 437–446.

Clack, N. G., O'Connor, D. H., Huber, D., Petreanu, L., Hires, A., Peron, S., ... Myers, E. W. (2012). Automated tracking of whiskers in videos of head fixed rodents. *PLoS Computational Biology*, *8*, e1002591.

Clarke, W. B., & Bowsher, D. (1962). Terminal distribution of primary afferent trigeminal fibers in the rat. *Experimental neurology*, *6*, 372–383.

Constanti, A., & Brown, D. (1981). M-currents in voltage-clamped mammalian sympathetic neurones. *Neuroscience letters*, *24*, 289–294.

Crochet, S., & Petersen, C. C. (2006). Correlating whisker behavior with membrane potential in barrel cortex of awake mice. *Nature Neuroscience*, *9*, 608–610.

Crochet, S., Poulet, J. F. A., Kremer, Y., & Petersen, C. C. H. (2011). Synaptic mechanisms underlying sparse coding of active touch. *Neuron*, *69*, 1160–75.

Diamond, M. E., & Arabzadeh, E. (2013). Whisker sensory system - From receptor to decision. *Progress in Neurobiology*, *103*, 28–40.

Diamond, M. E., Von Heimendahl, M., Knutsen, P. M., Kleinfeld, D., & Ahissar, E. (2008). 'where'and'what'in the whisker sensorimotor system. *Nature Reviews*

Neuroscience, *9*(8), 601–612.

Díaz-Quesada, M., & Maravall, M. (2008). Intrinsic mechanisms for adaptive gain rescaling in barrel cortex. *Journal of Neuroscience*, *28*, 696–710.

Dörfl, J. (1982). The musculature of the mystacial vibrissae of the white mouse. *Journal of Anatomy*, *135*, 147–54.

Ebara, S., Kumamoto, K., Matsuura, T., Mazurkiewicz, J. E., & Rice, F. L. (2002). Similarities and differences in the innervation of mystacial vibrissal follicle-sinus complexes in the rat and cat: A confocal microscopic study. *Journal of Comparative Neurology*, *449*, 103–119.

Ego-Stengel, V., Mello E Souza, T., Jacob, V., & Shulz, D. E. (2005). Spatiotemporal characteristics of neuronal sensory integration in the barrel cortex of the rat. *Journal of Neurophysiology*, *93*, 1450–1467.

Ellenbroek, B., & Youn, J. (2016). Rodent models in neuroscience research: Is it a rat race? *DMM Disease Models and Mechanisms*, *9*, 1079–1087.

Erchova, I. A., Lebedev, M. A., & Diamond, M. E. (2002). Somatosensory cortical neuronal population activity across states of anaesthesia. *European Journal of Neuroscience*, *15*, 744–752.

Estebanez, L., Bertherat, J., Shulz, D. E., Bourdieu, L., & Léger, J.-F. (2016). A radial map of multi-whisker correlation selectivity in the rat barrel cortex. *Nature Communications*, *7*, 13528.

Etnier, S. A. (2003). Twisting and bending of biological beams: Distribution of biological beams in a stiffness mechanospace. *Biological Bulletin*, *205*, 36–46.

Evans, M. H., Loft, M. S., Campagner, D., Petersen, R. S., Evans, M. H., Loft, M. S., ... Petersen, R. S. (2019). Sensing the environment with whiskers. In *Oxford research encyclopedia of neuroscience.*

Ewert, T. A. S., Vahle-Hinz, C., & Engel, A. K. (2008). High-frequency whisker vibration is encoded by phase-locked responses of neurons in the rat's barrel cortex. *Journal of Neuroscience*, *28*, 5359–5368.

Fairhall, A. (2014). Adaptation and Natural Stimulus Statistics. In M. S. Gazzaniga & G. R. Mangun (Eds.), *The cognitive neurosciences* (Fifth Edit ed., pp. 283–293). MIT Press.

Fairhall, A. L., Lewen, G. D., Bialek, W., & De Ruyter van Steveninck, R. R. (2001).

Efficiency and ambiguity in an adaptive neural code. *Nature*, *412*, 1–6.

Fanselow, E. E., & Nicolelis, M. A. (1999). Behavioral modulation of tactile responses in the rat somatosensory system. *Journal of Neuroscience*, *19*, 7603–7616.

Furuta, T., Bush, N. E., Yang, A. E.-T., Ebara, S., Miyazaki, N., Murata, K., ... Hartmann, M. J. (2020). The cellular and mechanical basis for response characteristics of identified primary afferents in the rat vibrissal system. *Current Biology*, *30*, 815–826.e5.

Ganmor, E., Katz, Y., & Lampl, I. (2010). Intensity-dependent adaptation of cortical and thalamic neurons is controlled by brainstem circuits of the sensory pathway. *Neuron*, *66*, 273–286.

Gibson, J. M., & Welker, W. I. (1983). Quantitative studies of stimulus coding in first-order vibrissa afferents of rats. 2. Adaptation and coding of stimulus parameters. *Somatosensory & Motor Research*, *1*, 95–117.

Gillespie, D., Yap, M. H., Hewitt, B. M., Driscoll, H., Simanaviciute, U., Hodson-Tole, E. F., & Grant, R. A. (2019). Description and validation of the locowhisk system: Quantifying rodent exploratory, sensory and motor behaviours. *Journal of Neuroscience Methods*, *328*, 108440.

Goble, A. K., & Hollins, M. (1993). Vibrotactile adaptation enhances amplitude discrimination. *Journal of the Acoustical Society of America*, *93*, 418–424.

Goldstein, H., Poole, C. P., & Safko, J. L. (2002). *Classical mechanics*. Addison Wesley.

Grant, R. A., Mitchinson, B., Fox, C. W., & Prescott, T. J. (2009). Active touch sensing in the rat: anticipatory and regulatory control of whisker movements during surface exploration. *Journal of Neurophysiology*, *101*, 862–874.

Guo, Z. V., Li, N., Huber, D., Ophir, E., Gutnisky, D., Ting, J. T., ... Svoboda, K. (2014). Flow of cortical activity underlying a tactile decision in mice. *Neuron*, *81*, 179–194.

Gustafson, J. W., & Felbain-Keramidas, S. L. (1977). Behavioral and neural approaches to the function of the mystacial vibrissae. *Psychological bulletin*, *84*, 477–488.

Gutnisky, D. A., Yu, J., Hires, S. A., To, M. S., Bale, M. R., Svoboda, K., & Golomb, D. (2017). Mechanisms underlying a thalamocortical transformation during

active tactile sensation. *PLoS Computational Biology*, *13*.

Gyory, G., Rankov, V., Gordon, G., Perkon, I., Mitchinson, B., Grant, R., & Prescott, T. (2010). an algorithm for automatic tracking of rat whiskers. *Proc Int Workshop on Visual observation and Analysis of Animal and Insect Behavior (VAIB) , Istanbul, in conjunction with ICPR 2010*, 1–4.

Haidarliu, S., Bagdasarian, K., Shinde, N., & Ahissar, E. (2017). muscular basis of whisker torsion in mice and rats. *The Anatomical Record*, *300*, 1643–1653.

Hartmann, M. (2016). Vibrissa Mechanical Properties. In *Scholarpedia of touch* (pp. 591–614). Paris: Atlantis Press.

Hartmann, M. J. Z. (2011). A night in the life of a rat: Vibrissal mechanics and tactile exploration. *Annals of the New York Academy of Sciences*, *1225*, 110–118.

Hewitt, B. M., Yap, M. H., Hodson-Tole, E. F., Kennerley, A. J., Sharp, P. S., & Grant, R. A. (2018). A novel automated rodent tracker (ART), demonstrated in a mouse model of amyotrophic lateral sclerosis. *Journal of Neuroscience Methods*, *300*, 147–156.

Hill, D. N., Bermejo, R., Zeigler, H. P., & Kleinfeld, D. (2008). Biomechanics of the vibrissa motor plant in rat: rhythmic whisking consists of triphasic neuromuscular activity. *Journal of Neuroscience*, *28*, 3438–3455.

Himmelheber, A. M., Sarter, M., & Bruno, J. P. (2000). Increases in cortical acetylcholine release during sustained attention performance in rats. *Cognitive Brain Research*, *9*, 313–325.

Hires, S. A., Gutnisky, D. A., Yu, J., O'Connor, D. H., & Svoboda, K. (2015). Low-noise encoding of active touch by layer 4 in the somatosensory cortex. *eLife*, *4*, e06619.

Huet, L. A., & Hartmann, M. J. (2016). Simulations of a Vibrissa Slipping along a Straight Edge and an Analysis of Frictional Effects during Whisking. *IEEE transactions on haptics*, *9*, 158.

Huet, L. A., Rudnicki, J. W., & Hartmann, M. J. (2017). Tactile sensing with whiskers of various shapes: determining the three-dimensional location of object contact based on mechanical signals at the whisker base. *Soft Robotics*, *4*, 88–102.

Huet, L. A., Schroeder, C. L., & Hartmann, M. J. (2015). Tactile signals transmitted by the vibrissa during active whisking behavior. *Journal of Neurophysiology*,

113, 3511–3518.

Ibrahim, L., & Wright, E. A. (1975). The growth of rats and mice vibrissae under normal and some abnormal conditions. *Journal of Embryology and Experimental Morphology*, *33*, 831–44.

Isett, B. R., Feasel, S. H., Lane, M. A., & Feldman, D. E. (2018). Slip-based coding of local shape and texture in mouse S1. *Neuron*, *97*, 418–433.e5.

Jadhav, S. P., & Feldman, D. E. (2010). Texture coding in the whisker system. *Current Opinion in Neurobiology*, *20*, 313–318.

Jadhav, S. P., Wolfe, J., & Feldman, D. E. (2009). Sparse temporal coding of elementary tactile features during active whisker sensation. *Nature neuroscience*, *12*, 792–800.

Jones, L. M. (2004). Precise temporal responses in whisker trigeminal neurons. *Journal of Neurophysiology*, *92*, 665–668.

Jun, J. J., Mitelut, C., Lai, C., Gratiy, S. L., Anastassiou, C. A., & Harris, T. D. (2017). Real-time spike sorting platform for high-density extracellular probes with ground-truth validation and drift correction. *bioRxiv*.

Katz, Y., Heiss, J. E., & Lampl, I. (2006). Cross-whisker adaptation of neurons in the rat barrel cortex. *Journal of Neuroscience*, *26*, 13363–13372.

Khatri, V., Bermejo, R., Brumberg, J. C., Keller, A., & Zeigler, H. P. (2009). Whisking in air: Encoding of kinematics by trigeminal ganglion neurons in awake rats. *Journal of Neurophysiology*, *101*, 1836–1846.

Khatri, V., Bruno, R. M., & Simons, D. J. (2009). Stimulus-specific and stimulus-nonspecific firing synchrony and its modulation by sensory adaptation in the whisker-to-barrel pathway. *Journal of Neurophysiology*, *101*, 2328–2338.

Khatri, V., Hartings, J. A., & Simons, D. J. (2004). Adaptation in thalamic barreloid and cortical barrel neurons to periodic whisker deflections varying in frequency and velocity. *Journal of Neurophysiology*, *92*, 3244–3254.

Khatri, V., & Simons, D. J. (2007). Angularly nonspecific response suppression in rat barrel cortex. *Cerebral Cortex*, *17*, 599–609.

Kleinfeld, D., Ahissar, E., & Diamond, M. E. (2006). Active sensation: insights from the rodent vibrissa sensorimotor system. *Current Opinion in Neurobiology*, *16*, 435–444.

Knutsen, P. M., Biess, A., & Ahissar, E. (2008). Vibrissal kinematics in 3d: tight coupling of azimuth, elevation, and torsion across different whisking modes. *Neuron*, *59*, 35–42.

Knutsen, P. M., Derdikman, D., & Ahissar, E. (2005). Tracking whisker and head movements in unrestrained behaving rodents. *Journal of Neurophysiology*, *93*, 2294–2301.

Kremer, Y., Léger, J. F., Goodman, D., Brette, R., & Bourdieu, L. (2011). Late emergence of the vibrissa direction selectivity map in the rat barrel cortex. *Journal of Neuroscience*, *31*, 10689–10700.

Krupa, D. J., Matell, M. S., Brisben, A. J., Oliveira, L. M., & Nicolelis, M. A. (2001). Behavioral properties of the trigeminal somatosensory system in rats performing whisker-dependent tactile discriminations. *Journal of Neuroscience*, *21*, 5752–5763.

Kwon, S. E., Yang, H., Minamisawa, G., & O'Connor, D. H. (2016). Sensory and decision-related activity propagate in a cortical feedback loop during touch perception. *Nature Neuroscience*, *19*, 1243–1249.

Laboy-Juárez, K. J., Langberg, T., Ahn, S., & Feldman, D. E. (2019). Elementary motion sequence detectors in whisker somatosensory cortex. *Nature Neuroscience*, *22*, 1438–1449.

Lampl, I., & Katz, Y. (2017). Neuronal adaptation in the somatosensory system of rodents. *Neuroscience*, *343*, 66–76.

Leiser, S. C., & Moxon, K. A. (2006). Relationship between physiological response type (ra and sa) and vibrissal receptive field of neurons within the rat trigeminal ganglion. *Journal of Neurophysiology*, *95*, 3129–3145.

Leiser, S. C., & Moxon, K. A. (2007). Responses of trigeminal ganglion neurons during natural whisking behaviors in the awake rat. *Neuron*, *53*, 117–133.

Li, D., & Tian, J. (2013). An accurate calibration method for a camera with telecentric lenses. *Optics and Lasers in Engineering*, *51*, 538–541.

Lichtenstein, S. H., Carvell, G. E., & Simons, D. J. (1990). Responses of rat trigeminal ganglion neurons to movements of vibrissae in different directions. *Somatosensory & Motor Research*, *7*, 47–65.

Lottem, E., & Azouz, R. (2011). A unifying framework underlying mechanotransduction in the somatosensory system. *Journal of Neuroscience*, *31*, 8520–8532.

Lottem, E., Gugig, E., & Azouz, R. (2015). Parallel coding schemes of whisker velocity in the rat's somatosensory system. *Journal of Neurophysiology*, *113*, 1784–1799.

Lucianna, F. A., Albarracín, A. L., Vrech, S. M., Farfán, F. D., & Felice, C. J. (2016). The mathematical whisker: A review of numerical models of the rat's vibrissa biomechanics. *Journal of Biomechanics*, *49*, 2007–2014.

Ma, P. M. (1991). The barrelettes—architectonic vibrissal representations in the brainstem trigeminal complex of the mouse. I. Normal structural organization. *Journal of Comparative Neurology*, *309*, 161–199.

Maravall, M., Alenda, A., Bale, M. R., & Petersen, R. S. (2013). Transformation of adaptation and gain rescaling along the whisker sensory pathway. *PLoS ONE*, *8*, e82418.

Maravall, M., & Diamond, M. E. (2014). Algorithms of whisker-mediated touch perception. *Current Opinion in Neurobiology*, *25*, 176–186.

Maravall, M., Petersen, R. S., Fairhall, A. L., Arabzadeh, E., & Diamond, M. E. (2007). Shifts in coding properties and maintenance of information transmission during adaptation in barrel cortex. *PLoS Biology*, *5*, 0323–0334.

Marsh, D. (2006). *Applied Geometry for Computer Graphics and CAD* (Second ed.). London: Springer London.

Martin-Cortecero, J., & Nuñez, A. (2014). Tactile response adaptation to whisker stimulation in the lemniscal somatosensory pathway of rats. *Brain Research*, *1591*, 27–37.

Mathis, A., Mamidanna, P., Cury, K. M., Abe, T., Murthy, V. N., Mathis, M. W., & Bethge, M. (2018). DeepLabCut: markerless pose estimation of user-defined body parts with deep learning. *Nature Neuroscience*, *21*, 1281–1289.

Mehta, S. B., Whitmer, D., Figueroa, R., Williams, B. A., & Kleinfeld, D. (2007). Active spatial perception in the vibrissa scanning sensorimotor system. *PLoS Biology*, *5*, 0309–0322.

Melaragno, H. P., & Montagna, W. (1953). The tactile hair follicles in the mouse. *The Anatomical Record*, *115*, 129–149.

Mitchinson, B., Gurney, K. N., Redgrave, P., Melhuish, C., Pipe, A. G., Pearson, M., ... Prescott, T. J. (2004). Empirically inspired simulated electro-mechanical model of the rat mystacial follicle-sinus complex. *Proceedings of the Royal Society B: Biological Sciences*, *271*, 2509–2516.

Mitchinson, B., Martin, C. J., Grant, R. A., & Prescott, T. J. (2007). Feedback control in active sensing: Rat exploratory whisking is modulated by environmental contact. *Proceedings of the Royal Society B: Biological Sciences*, *274*, 1035–1041.

Mitchinson, B., & Prescott, T. J. (2013). Whisker movements reveal spatial attention: a unified computational model of active sensing control in the rat. *PLoS Computational Biology*, *9*, e1003236.

Moore, J. D., Mercer Lindsay, N., Deschênes, M., & Kleinfeld, D. (2015). Vibrissa self-motion and touch are reliably encoded along the same somatosensory pathway from brainstem through thalamus. *PLoS Biology*, *13*, e1002253.

Morita, T., Kang, H., Wolfe, J., Jadhav, S. P., & Feldman, D. E. (2011). Psychometric curve and behavioral strategies for whisker-based texture discrimination in rats. *PLoS ONE*, *6*, e20437.

Musall, S., Haiss, F., Weber, B., & von der Behrens, W. (2017). Deviant Processing in the Primary Somatosensory Cortex. *Cerebral cortex*, *27*, 863–876.

Musall, S., Kaufman, M. T., Juavinett, A. L., Gluf, S., & Churchland, A. K. (2019). Single-trial neural dynamics are dominated by richly varied movements. *Nature Neuroscience*, *22*, 1677–1686.

Musall, S., von der Behrens, W., Mayrhofer, J. M., Weber, B., Helmchen, F., & Haiss, F. (2014). Tactile frequency discrimination is enhanced by circumventing neocortical adaptation. *Nature Neuroscience*, *17*, 1567–1573.

Nashaat, M. A., Oraby, H., Peña, L. B., Dominiak, S., Larkum, M. E., & Sachdev, R. N. (2017). Pixying behavior: a versatile real-time and post hoc automated optical tracking method for freely moving and head fixed animals. *Eneuro*, *4*(1).

Neimark, M. A., Andermann, M. L., Hopfield, J. J., & Moore, C. I. (2003). Vibrissa resonance as a transduction mechanism for tactile encoding. *Journal of Neuroscience*, *23*, 6499–6509.

Nicolelis, M. A., & Chapin, J. K. (1994). Spatiotemporal structure of somatosensory

responses of many-neuron ensembles in the rat ventral posterior medial nucleus of the thalamus. *Journal of Neuroscience*, *14*, 3511–3532.

Nuñez, A., Domínguez, S., Buño, W., & Fernández de Sevilla, D. (2012). Cholinergic-mediated response enhancement in barrel cortex layer V pyramidal neurons. *Journal of Neurophysiology*, *108*, 1656–1668.

O'Connor, D. H., Clack, N. G., Huber, D., Komiyama, T., Myers, E. W., & Svoboda, K. (2010). Vibrissa-based object localization in head-fixed mice. *Journal of Neuroscience*, *30*, 1947–1967.

O'Connor, D. H., Hires, S. A., Guo, Z. V., Li, N., Yu, J., Sun, Q. Q., ... Svoboda, K. (2013). Neural coding during active somatosensation revealed using illusory touch. *Nature Neuroscience*, *16*, 958–965.

O'Connor, D. H., Peron, S. P., Huber, D., & Svoboda, K. (2010). Neural activity in barrel cortex underlying vibrissa-based object localization in mice. *Neuron*, *67*, 1048–1061.

Ollerenshaw, D., Zheng, H., Millard, D., Wang, Q., & Stanley, G. (2014). The adaptive trade-off between detection and discrimination in cortical representations and behavior. *Neuron*, *81*, 1152–1164.

Pammer, L., O'Connor, D. H., Hires, S. A., Clack, N. G., Huber, D., Myers, E. W., & Svoboda, K. (2013). The mechanical variables underlying object localization along the axis of the whisker. *Journal of Neuroscience*, *33*, 6726–6741.

Park, I. M., Meister, M. L., Huk, A. C., & Pillow, J. W. (2014). Encoding and decoding in parietal cortex during sensorimotor decision-making. *Nature Neuroscience*, *17*, 1395–1403.

Pasquet, M. O., Tihy, M., Gourgeon, A., Pompili, M. N., Godsil, B. P., Léna, C., & Dugué, G. P. (2016). Wireless inertial measurement of head kinematics in freely-moving rats. *Scientific Reports*, *6*, 35689.

Perkon, I., Kosir, A., Itskov, P. M., Tasic, J., Diamond, M. E., Perkon, I., ... Diamond, M. E. (2011). Unsupervised quantification of whisking and head movement in freely moving rodents. *Journal of Neurophysiology*, 1950–1962.

Peron, S. P., Freeman, J., Iyer, V., Guo, C., & Svoboda, K. (2015). A cellular resolution map of barrel cortex activity during tactile behavior. *Neuron*, *86*, 783–799.

Petersen, C. C. (2007). The functional organization of the barrel cortex. *Neuron*, *56*, 339–355.

Petersen, C. C. (2019). Sensorimotor processing in the rodent barrel cortex. *Nature Reviews Neuroscience*, *20*, 533–546.

Petersen, R. S., Brambilla, M., Bale, M. R., Alenda, A., Panzeri, S., Montemurro, M. A., & Maravall, M. (2008). Diverse and temporally precise kinetic feature selectivity in the vpm thalamic nucleus. *Neuron*, *60*, 890–903.

Petersen, R. S., Colins Rodriguez, A., Evans, M. H., Campagner, D., & Loft, M. S. (2020). A system for tracking whisker kinematics and whisker shape in three dimensions. *PLoS Computational Biology*, *16*, e1007402.

Petreanu, L., Mao, T., Sternson, S. M., & Svoboda, K. (2009). The subcellular organization of neocortical excitatory connections. *Nature*, *457*, 1142–1145.

Pillow, J. W., Shlens, J., Paninski, L., Sher, A., Litke, A. M., Chichilnisky, E. J., & Simoncelli, E. P. (2008). Spatio-temporal correlations and visual signalling in a complete neuronal population. *Nature*, *454*, 995–999.

Pinto, D. J., Brumberg, J. C., & Simons, D. J. (2000). Circuit dynamics and coding strategies in rodent somatosensory cortex. *Journal of Neurophysiology*, *83*.

Prescott, T. J., & Dürr, V. (2016). Introduction: The World of Touch. In *Scholarpedia of touch* (pp. 1–28). Atlantis Press, Paris.

Prescott, T. J., Mitchinson, B., & Grant, R. A. (2016). Vibrissal Behavior and Function. In *Scholarpedia of touch* (pp. 103–116). Paris: Atlantis Press.

Quist, B. W., & Hartmann, M. J. (2012). Mechanical signals at the base of a rat vibrissa: The effect of intrinsic vibrissa curvature and implications for tactile exploration. *Journal of Neurophysiology*, *107*, 2298–2312.

Quist, B. W., Seghete, V., Huet, L. A., Murphey, T. D., & Hartmann, M. J. Z. (2014). Modeling forces and moments at the base of a rat vibrissa during noncontact whisking and whisking against an object. *Journal of Neuroscience*, *34*, 9828–9844.

Ramirez, A., Pnevmatikakis, E. A., Merel, J., Paninski, L., Miller, K. D., & Bruno, R. M. (2014). Spatiotemporal receptive fields of barrel cortex revealed by reverse correlation of synaptic input. *Nature Neuroscience*, *17*, 866–875.

Roy, S., Bryant, J. L., Cao, Y., & Heck, D. H. (2011). High-precision, three-dimensional tracking of mouse whisker movements with optical motion capture technology. *Frontiers in Behavioral Neuroscience*, *5*, 27.

Sachdev, R. N. S., Ebner, F. F., & Wilson, C. J. (2004). Effect of subthreshold up and down states on the whisker-evoked response in somatosensory cortex. *Journal of Neurophysiology*, *92*, 3511–3521.

Sanchez-Vives, M. V., Nowak, L. G., & McCormick, D. A. (2000). Cellular mechanisms of long-lasting adaptation in visual cortical neurons in vitro. *Journal of Neuroscience*, *20*, 4286–4299.

Severson, K. S., Xu, D., Van de Loo, M., Bai, L., Ginty, D. D., & O'Connor, D. H. (2017). Active touch and self-motion encoding by merkel cell-associated afferents. *Neuron*, *94*, 666–676.e9.

Shimaoka, D., Harris, K. D., & Carandini, M. (2018). Effects of arousal on mouse sensory cortex depend on modality. *Cell Reports*, *22*, 3160–3167.

Simons, D. J. (1978). Response properties of vibrissa units in rat SI somatosensory neocortex. *Journal of Neurophysiology*, *41*, 798–820.

Simons, D. J. (1985). Temporal and spatial integration in the rat SI vibrissa cortex. *Journal of Neurophysiology*, *54*, 615–635.

Simons, D. J., & Carvell, G. E. (1989). Thalamocortical response transformation in the rat vibrissa/barrel system. *Journal of Neurophysiology*, *61*, 311–330.

Sofroniew, N. J., Cohen, J. D., Lee, A. K., & Svoboda, K. (2014). Natural whisker-guided behavior by head-fixed mice in tactile virtual reality. *Journal of Neuroscience*, *34*, 9537–9550.

Storchi, R., Bale, M. R., Biella, G. E. M., & Petersen, R. S. (2012). Comparison of latency and rate coding for the direction of whisker deflection in the subcortical somatosensory pathway. *Journal of Neurophysiology*, *108*, 1810–1821.

Stüttgen, M. C., Rüter, J., & Schwarz, C. (2006). Two psychophysical channels of whisker deflection in rats align with two neuronal classes of primary afferents. *Journal of Neuroscience*, *26*, 7933–7941.

Szwed, M., Bagdasarian, K., Blumenfeld, B., Barak, O., Derdikman, D., & Ahissar, E. (2006). Responses of trigeminal ganglion neurons to the radial distance of contact during active vibrissal touch. *Journal of Neurophysiology*, *95*, 791–802.

Timofeeva, E., Mérette, C., Émond, C., Lavallée, P., & Deschênes, M. (2003). A map of angular tuning preference in thalamic barreloids. *Journal of Neuroscience*, *23*, 10717–10723.

Tinbergen, N. (1951). *The study of instinct.* New York, NY, US: Clarendon Press/Oxford University Press.

Tonomura, S., Ebara, S., Bagdasarian, K., Uta, D., Ahissar, E., Meir, I., ... Kumamoto, K. (2015). Structure-function correlations of rat trigeminal primary neurons: Emphasis on club-like endings, a vibrissal mechanoreceptor. *Proceedings of the Japan Academy Series B: Physical and Biological Sciences*, *91*, 560–576.

Torvik, A. (1956). Afferent connections to the sensory trigeminal nuclei, the nucleus of the solitary tract and adjacent structures. An experimental study in the rat. *The Journal of Comparative Neurology*, *106*, 51–141.

Towal, R. B., & Hartmann, M. J. (2006). Right-left asymmetries in the whisking behavior of rats anticipate head movements. *Journal of Neuroscience*, *26*, 8838–8846.

Towal, R. B., Quist, B. W., Gopal, V., Solomon, J. H., & Hartmann, M. J. (2011). The morphology of the rat vibrissal array: A model for quantifying spatiotemporal patterns of whisker-object contact. *PLoS Computational Biology*, *7*, e1001120.

Van Der Loos, H. (1976). Barreloids in mouse somatosensory thalamus. *Neuroscience Letters*, *2*, 1–6.

Van Der Loos, H., Dörfl, J., & Welker, E. (1984). Variation in pattern of mystacial vibrissae in mice: A quantitative study of ICR stock and several inbred strains. *Journal of Heredity*, *75*, 327–336.

Vanzella, W., Grion, N., Bertolini, D., Perissinotto, A., Gigante, M., & Zoccolan, D. F. (2019). A passive, camera-based head-tracking system for real-time, three-dimensional estimation of head position and orientation in rodents. *Journal of Neurophysiology*, *122*, 2220–2242.

Vaxenburg, R., Wyche, I., Svoboda, K., Efros, A. L., & Hires, S. A. (2018). Dynamic cues for whisker-based object localization: An analytical solution to vibration during active whisker touch. *PLOS Computational Biology*, *14*, e1006032.

Veinante, P., & Deschênes, M. (1999). Single- and multi-whisker channels in the

ascending projections from the principal trigeminal nucleus in the rat. *Journal of Neuroscience*, *19*, 5085–5095.

Vincent, S. B. (1912). *The functions of the vibrissae in the behavior of the white rat...* (Vol. 1) (No. 5). University of Chicago.

Voges, D., Carl, K., Klauer, G. J., Uhlig, R., Schilling, C., Behn, C., & Witte, H. (2012). Structural characterization of the whisker system of the rat. *IEEE Sensors Journal*, *12*, 332–339.

Voigts, J., Sakmann, B., & Celike, T. (2008). Unsupervised whisker tracking in unrestrained behaving animals. *Journal of Neurophysiology*, *100*, 504–515.

Wallach, A., Bagdasarian, K., & Ahissar, E. (2016). On-going computation of whisking phase by mechanoreceptors. *Nature Neuroscience*, *19*, 487–493.

Wang, Q., Webber, R. M., & Stanley, G. B. (2010). Thalamic synchrony and the adaptive gating of information flow to cortex. *Nature Neuroscience*, *13*, 1534–1543.

Webber, R. M., & Stanley, G. B. (2004). Nonlinear encoding of tactile patterns in the barrel cortex. *Journal of Neurophysiology*, *91*, 2010–2022.

Weber, A. I., & Fairhall, A. L. (2019). The role of adaptation in neural coding. *Current Opinion in Neurobiology*, *58*, 135–140.

Weber, A. I., Krishnamurthy, K., & Fairhall, A. L. (2019). Coding principles in adaptation. *Annual Review of Vision Science*, *5*, 427–449.

Welker, C., & Woolsey, T. A. (1974). Structure of layer IV in the somatosensory neocortex of the rat: Description and comparison with the mouse. *Journal of Comparative Neurology*, *158*, 437–453.

Welker, E., Armstrong-James, M., Van der Loos, H., & Kraftsik, R. (1993). The mode of activation of a barrel column: response properties of single units in the somatosensory cortex of the mouse upon whisker deflection. *European Journal of Neuroscience*, *5*, 691–712.

Welker, W. (1964). Analysis of sniffing of the albino rat 1. *Behaviour*, *22*(3-4), 223–244.

Whitmire, C. J., & Stanley, G. B. (2016). *Rapid sensory adaptation redux: A circuit perspective* (Vol. 92).

Wolfe, J., Hill, D. N., Pahlavan, S., Drew, P. J., Kleinfeld, D., & Feldman, D. E.

(2008). Texture coding in the rat whisker system: Slip-stick versus differential resonance. *PLoS Biology*, *6*, 1661–1677.

Wolfe, J., Mende, C., & Brecht, M. (2011). Social facial touch in rats. *Behavioral Neuroscience*, *125*, 900–910.

Woolsey, T. A., & Van der Loos, H. (1970). The structural organization of layer IV in the somatosensory region (S I) of mouse cerebral cortex: The description of a cortical field composed of discrete cytoarchitectonic units. *Brain Research*, *17*, 205–242.

Yamashita, T., Pala, A., Pedrido, L., Kremer, Y., Welker, E., & Petersen, C. C. (2013). Membrane potential dynamics of neocortical projection neurons driving target-specific signals. *Neuron*, *80*, 1477–1490.

Yan, W., Kan, Q., Kergrene, K., Kang, G., Feng, X. Q., & Rajan, R. (2013). A truncated conical beam model for analysis of the vibration of rat whiskers. *Journal of Biomechanics*, *46*, 1987–1995.

Yang, A. E., & Hartmann, M. J. (2016). Whisking kinematics enables object localization in head-centered coordinates based on tactile information from a single vibrissa. *Frontiers in Behavioral Neuroscience*, *10*, 1–15.

Yang, H., Kwon, S. E., Severson, K. S., & O'Connor, D. H. (2015). Origins of choice-related activity in mouse somatosensory cortex. *Nature Neuroscience*, *19*, 127–134.

Yu, C., Derdikman, D., Haidarliu, S., & Ahissar, E. (2006). Parallel thalamic pathways for whisking and touch signals in the rat. *PLoS Biology*, *4*, e124.

Yu, J., Gutnisky, D. A., Hires, S. A., & Svoboda, K. (2016). Layer 4 fast-spiking interneurons filter thalamocortical signals during active somatosensation. *Nature Neuroscience*, *19*, 1647–1657.

Yu, Y. S., Bush, N. E., & Hartmann, M. J. (2019). Whisker vibrations and the activity of trigeminal primary afferents in response to airflow. *Journal of Neuroscience*, *39*, 5881–5896.

Yu, Y. S. W., Graff, M. M., Bresee, C. S., Man, Y. B., & Hartmann, M. J. Z. (2016). Whiskers aid anemotaxis in rats. *Science Advances*, *2*, e1600716.

Zuo, Y., & Diamond, M. E. (2019). Rats Generate Vibrissal Sensory Evidence until Boundary Crossing Triggers a Decision. *Current Biology*, *29*, 1415–1424.e5.

Zuo, Y., Perkon, I., & Diamond, M. E. (2011). Whisking and whisker kinematics during a texture classification task. *Philosophical Transactions of the Royal Society B: Biological Sciences*, *366*, 3058–3069.